Aus dem Institut für Experimentelle Schmerzforschung
der Medizinischen Fakultät Mannheim
(Direktor: Prof. Dr. med. Martin Schmelz)

Modulation of neuronal excitability in ex-vivo and in-vitro systems

Inauguraldissertation
zur Erlangung des Doctor scientiarum humanarum (Dr. sc. hum.)
der
Medizinischen Fakultät Mannheim
der Ruprecht-Karls-Universität
zu
Heidelberg

vorgelegt von
Julius Pakalniškis

aus
Šiauliai
2019

Dekan: Prof. Dr. med. Sergij Goerdt
Referent: Prof. Dr. med. Martin Schmelz

TABLE OF CONTENTS

Page

ABBREVIATIONS

A-CAP – A-fibre compound action potential

AUC – area under the curve

C-CAP – C-fibre compound action potential

Ca^{2+} - calcium ion

Cl^- - chloride ion

CTX – conotoxin

DMSO – dimethyl sulfoxide

DNA – deoxyribonucleic acid

HEPES – 4-(2-hydroxyethyl)-1-piperazineethanesulfonic acid

K^+ - potassium ion

Li^+ - lithium ion

Mg^{2+} - magnesium ion

mRNA – messenger RNA

Na^+ - sodium ion

Na_V – voltage-sensitive sodium channels

PBS – phosphate-buffered saline

RNA – ribonucleic acid

TRPM8 – transient receptor potential cation channel subfamily M member 8

TRPV1 – transient receptor potential cation channel subfamily V member 1

TTX – tetrodotoxin

1   <u>INTRODUCTION</u>

1.1 Nociception

The pain sensation is crucial for organisms to survive. Nociceptors – primary sensory neurons specialized to detect intense, potentially harmful stimuli – are specifically equipped to encode the level of threat and signal it to the spinal cord (Sherrington, 1906). These cells therefore represent the first line of defence against any potentially threatening and damaging environmental inputs (Woolf and Ma, 2007). Intense chemical, mechanical or thermal (heat and cold) stimuli can activate nociceptors that relay signals to the spinal cord to generate reflex responses, but also lead to information being sent to the brain where it is evaluated and integrated into an aversive, painful sensation.

The nociceptive system has three main implications related to the level of integration in the human body: detection/encoding (peripheral nervous system), reflex generation (spinal cord) and perception (central nervous system). Modulation of sensitivity in all three systems can contribute to chronic pain states (Meacham et al., 2017) and crucially, hyper-excitability in the peripheral nervous system can sensitize spinal and finally central processing reflecting their interdependence. Stimulus detection in nociceptors can be increased or decreased in pathophysiological conditions (for example mutations) and result either in hypersensitivity, spontaneous activity and pain or in loss of function with lack of pain sensations (Bennett et al., 2019). Both increased and absence of pain syndromes have a severe impact on the quality of life (Cox et al., 2006; Salvatierra et al., 2018).

1.1.1 Peripheral nerve fibre classes

Peripheral afferent nerve fibres transduce stimuli at their sensory endings where action potentials are generated and conducted along their axons to the spinal cord. Different nerve fibre classes were initially defined based on the conduction velocity of their axons in peripheral nerves. Joseph Erlanger and Herbert Spencer Gasser classified fibres from cutaneous nerves in the cat into classes according to their conduction velocity. They found four different groups of fibres: Aα-fibres conducting at 120m.s^{-1}, Aβ-fibres conducting slightly slower at around 70 m.s^{-1}, Aδ-fibres at around 30 m.s^{-1} and finally slow C-fibres conducting at around 1 m.s^{-1} (figure 1 and table 1) (Kandel et al., 2013).
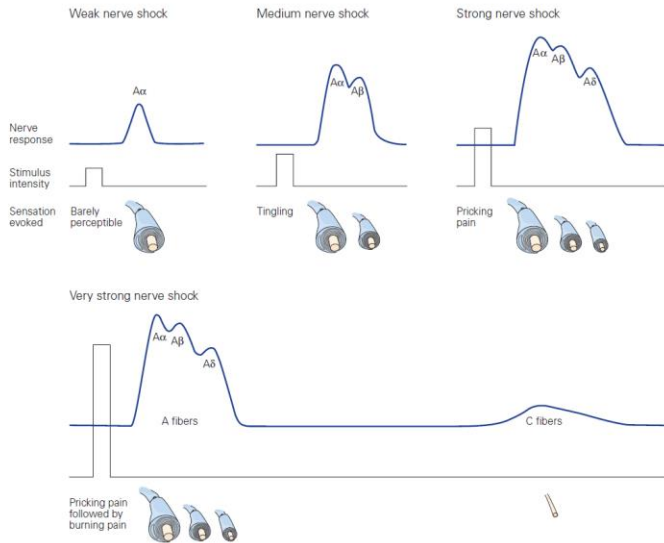
Fig.1: Identification of different fibre classes by conduction speed from compound action potential recording. Rectangular electrical stimuli activate different classes of fibres in peripheral nerve at increasing stimulus amplitudes. Axons of different conduction speeds produce deflections at different time delays. Adapted from (Kandel et al., 2013)

Larger diameter and thicker myelination are the basis for faster conduction in axons. It is important to note that axons with a similar conduction velocity are also segregated in terms of their function (table shown below).

	Fibre class	Diameter (µm)	Conduction velocity (m/s)	Functional significance
myelinated (20%)	A α	15	50-90	afferent and efferent muscle innervation
	A β	8	30-70	low threshold mechanosensors (skin)
	A γ	5	15-30	*efferent muscle innervation*
	A δ	<3	5-20	mechano-nociceptors, heat nociceptors
				cold receptors
unmyelinated (80%)	**C**	1	0.5-2	**polymodal & „silent" nociceptors**
				pruriceptors
				warm receptors
				C-touch fibres (social touch)
				sympathetic efferent vasoconstrictors, sudomotors, piloerectors

Table 1: summary of structural and functional characteristics of peripheral nerve fibres classes based on the classification of Erlanger & Gasser

1.1.2 Markers and function of nociceptors

Nociceptors are mainly found among Aδ- and C-fibres although there are also reports on high threshold Aβ- fibres in humans (Nagi et al., 2019). Nociceptors are all activated by noxious stimuli , but based on their higher axonal conduction velocity, Aδ-fibres relay their information to the brain faster and in a more synchronized fashion as compared to C-fibres. Aδ-fibres therefore evoke a fast, sharp pain sensation that is followed by C-fibre mediated burning pain.
Nociceptors were initially classified according to their sensitivity to external stimuli (mechanical, cold, heat and etc.) resulting in a complex scheme of functional nociceptor classes.

*	Unit type	Modality	Characteristics	Ref.
C (unmyelinated) nociceptors	**MECHANO-SENSITIVE nociceptors (CM)**			
	CMH (**C**-**m**echano-**h**eat)	Heat (> 42°) Mechanical (< 750 mN) Irritants (~60% MO/CAP~)	"polymodal nociceptors" 40-50% of human C-fibres Perhaps non-peptidergic	*(Schmidt et al., 1995; Serra et al., 2004; Serra et al., 1999; Weidner et al., 1999)*
	CM (**C**-**m**echano)	Mechanical (< 750 mN) Irritants (~35% MO+)	Heat: > 50°C ~ 10-20% of human C-fibres	*(Schmidt et al., 1995; Serra et al., 2004; Serra et al., 1999; Weidner et al., 1999)*
	CMHC (**C**-**m**echano-**h**eat-**c**old)	Cold (< 15°C) Heat (>40°C) Pressure (relatively high) Irritants (MO, menthol +)	<5% of human C-fibres; distal (i.e., ankle) > proximal (i.e., knee) recordings	*(Campero et al., 2009; Campero et al., 1996)*
	MECHANO-INSENSITIVE nociceptors (CMi)			
	CMiHi (**C**-**m**echano-**i**nsensitive-**h**eat-**i**ns.)	Irritants (~80% CAP+/ 30% MO+)	Long, intense discharge(>60") 5-15% of human C-fibres Presumably peptidergic	*(Schmidt et al., 1995; Serra et al., 2004; Serra et al., 1999; Weidner et al., 1999)*
	CH (**C**-**h**eat)	Heat (>45°C) Irritants (~30% MO/CAP+)	~8 % of human C-fibres Presumably peptidergic	*(Schmidt et al., 1995; Serra et al., 2004; Serra et al., 1999; Weidner et al., 1999)*
	[Mechano-insensitive] COLD NOCICEPTORS			
	CC2 ("bimodal")	Cold (0-30°C) Heat (35-48°C) Irritants (MO +)	only in distal (i.e., ankle) recordings	*(Campero et al., 2009; Campero et al., 2001; Campero et al., 1996; Yarnitsky and Ochoa, 1991)*
	CN (**C**old **n**ociceptors)	Cold (< 15°C) Irritants (MO +)	only in distal (i.e., ankle) recordings	*(Campero et al., 2009; Campero et al., 2001; Campero et al., 1996; Yarnitsky and Ochoa, 1991)*
Aδ- nociceptors (thinly myelinated)	**MECHANO-SENSITIVE nociceptors**			
	A-MH type 1 (**A**-**m**echano-**h**eat)	Heat (>53°C) Pressure; low Irritants (CHG; HIS?)	Hairy and glabrous skin; fast CV; wind-up; CAP negative; TRPV2-positive	*(Adriaensen et al., 1983; LaMotte and Thalhammer, 1982; Ringkamp et al., 2001; Treede et al., 1995)*
	A-MH type 2 (**A**-**m**echano-**h**eat)	Heat 43-47 Pressure; high (>22.5mN) Irritants (CAP; CHG; HIS?)	Hairy skin; slower CV; slowly adapting; TRPV1-positive	*(Adriaensen et al., 1983; LaMotte and Thalhammer, 1982; Ringkamp et al., 2001; Treede et al., 1995)*
	A-M (**A**-**m**echano)	Pressure; high Irritants (MC; CHG)	scarce; CAP negative; TRPV2-positive	*(Adriaensen et al., 1983; LaMotte and Thalhammer, 1982; Treede et al., 1995)*
	MECHANO-INSENSITIVE nociceptors			
	A-H type 1 (**A**-**h**eat)	Pressure > 100 mN Heat (> 53°C) Irritants (HIS?)		*(Ringkamp et al., 2011; Treede et al., 1998)*
	A-H type 2 (**A**-**h**eat)	Pressure > 100 mN Heat 43-48 Irritants (CAP; HIS)		*(Ringkamp et al., 2011; Treede et al., 1998)*
	A-MiHi (**A**-**m**echano-**i**nsensitive-**h**eat-**i**ns.)	Pressure > 100 mN Irritants (CAP, HIS)	Largest response to CAP	*(Ringkamp et al., 2001; Ringkamp et al., 2011; Treede et al., 1998)*

Table 2*: Common nociceptor classes identified in primate skin** (for C fibres, data are provided by human microneurography; for Ad fibres, data are provided by in vivo extracellular recordings in monkey). Abbreviations: CAP: capsaicin; CHG: cowhage; HIS: histamine; MC: methylene chloride; MO: mustard oil. M: mechano-sensitive; Mi: mechano-insensitive: H: heat sensitive; Hi: heat insensitive; C: cold sensitive; CC2: "bimodal" C fibres (respond to both innocuous and noxious cold,

respectively heat; CV, conduction velocity; TRPV, transient receptor potential, vanilloid family).*after Erlanger and Gasser. (table from habilitation PD Dr. Otilia Obreja (Obreja, 2013))

Recently, an alternative approach to classify neuronal populations has been successfully initiated. Analysis of single cell mRNA expression patterns of neurons (Haring et al., 2018; Usoskin et al., 2015; Zeisel et al., 2018) has provided data from a new perspective and suggests the existence of 10 to 14 subpopulations of sensory afferent neurons (Li et al., 2018; Li et al., 2016). However, the translation of functional classes to those defined by expression patterns has not yet been completed. It is obvious that expression of specific receptors could be used as marker for fibre functional class. For example, cold sensitive neurons should express the cold receptor TRPM8, and similarly heat sensitive neurons should express the TRPV1 receptor for heat and capsaicin. Cooling will activate TRPM8 channels and generate action potentials in cold sensitive fibres. Thus the chemical TRPM8 agonist menthol induces cold sensations upon contact with skin or mucosa. On other hand, the majority of nociceptors are polymodal (Perl, 1996; Wang et al., 2018). Polymodal sensory neurons can be activated by different modalities of stimuli (for example chemical, cold and mechanical) and this reflects the expression of multiple receptors in these cells that overlap with more specialized neurons. Furthermore, there is special class of mechano nociceptors that under normal conditions does not respond to mechanical stimuli. This class of nociceptor are called silent nociceptors. Half of the Aδ-fibres and around 30% of C-fibres nociceptors belong to this class (Meyer et al., 1991). Silent nociceptor neurons require initial activation by extracellular ligands such as inflammation mediators to render them sensitive to mechanical stimuli (Prato et al., 2017). It is currently unclear whether the expression pattern of mRNA found in the soma reflects the functional expression of sensory proteins at the sensory endings in such a manner that we will be able to translate the expression profiles of somata of primary afferent neurons into the functional classes that are based on their response profile to external stimuli.

1.2 Modulation of nociceptor excitability

Trauma can initiate a multitude of cellular events leading to inflammation that is linked to increased pain sensitivity ("hyperalgesia"; i.e., noxious stimuli evoke an aberrantly stronger pain sensation than normal and "allodynia"; i.e. non-noxious stimulation such as skin brushing evokes the sensation of pain) (Koltzenburg, 2000; Meyer, 1995). These clinical phenomena can result from peripheral or central sensitization. **Peripheral sensitization** is characterized by increased excitability of the injured primary afferent nociceptors that might even provoke spontaneous activity. **Secondary sensitization** implies involvement of the spinal secondary neurons, thereby enlarging the hyperalgesic area include the uninjured zone surrounding a site of injury.

The best studied example of peripheral sensitization is increased heat-sensitivity under inflammatory conditions such as acute application of noxious heat (Handwerker and Neher, 1976; LaMotte, 1984; Perl et al., 1976), or capsaicin (Szolcsanyi, 1977), or mustard oil (Schmelz et al., 1996; Schmidt et al., 1995) or different inflammatory mediators (Cesare and McNaughton, 1996; Davis et al., 1993; Martin et al., 1988) applied to the skin. This sensitization is linked to sensitization of the TRPV1 receptor. In contrast, sensitization of nociceptors to mechanical stimulation is less clear. Reduced mechanical thresholds were found upon acute nerve lesion (Shim et al., 2005) and administration of low pH (Steen and Reeh, 1993). The molecular mechanisms for mechanical transduction and thereby sensitization are not yet well established.

If one considers the time course of sensitization, acute processes are based on post-translational events such as phosphorylation/de-phosphorylation, modification of biophysical properties or trafficking of receptors modifying their expression at the cell surface (Pace et al., 2018; Reichling and Levine, 2009). The mechanisms leading to chronic sensitization involve activation of transcription factors, initiating gene expression and protein synthesis. In particular growth factors such as neurotrophins and cytokines govern this long-term modulation of nociceptor excitability (Mantyh, 2018; Price and Inyang, 2015). Such upregulation includes sensory transduction proteins such as TRPV1, but other targets include voltage dependent sodium channels (Schaefer et al., 2018; Zhang et al., 2019) which are involved in the initiation and conduction of action potentials.

It is important to note that translational and post-translational mechanisms contributing to sensitization occur in parallel in chronic pain conditions and interact: Thus, upregulation of sensory proteins such as TRPV1 will provide a more effective target for inflammatory mediators while post-translational sensitization of sodium channels, for example $Na_V1.8$, can enhance firing frequency (Tan et al., 2014; Xiao et al., 2019). Exemplifying this interaction, is a paradigm in which skin is conditioned with nerve growth factor to greatly enhance acute inflammatory hyperalgesia induced by UV-irradiation in human, even provoking some ongoing pain (Rukwied et al., 2014; Rukwied et al., 2013).

1.2.1 Voltage-sensitive sodium channels

Voltage-sensitive sodium channels (Na_V) are probably the most obvious candidates for axonal excitability modulation. These channels set activation thresholds for the generation of action potentials and also shape the encoding properties of afferent neurons. Sodium channels are integral membrane proteins that conduct sodium ions through the cell membrane. Na_V channels comprise pore-forming α-subunits

(~260kDa) that are associated with much smaller β-subunits (30-40kDa) (Catterall, 2000). The α-subunit forms the channel pore and contains four voltage sensors while the β-subunits modulate the channel's activity. There are ten members of the α-subunit family, nine of them ($Na_V1.1$-$Na_V1.9$) are voltage-sensitive and one is not (Na_x). Voltage-sensitive sodium channels are classified functionally based on their sensitivity to the bacterial toxin tetrodotoxin (TTX). $Na_V1.5$, $Na_V1.8$ and $Na_V1.9$ need much higher TTX concentrations to be blocked (low millimolar range) and are therefore classified as TTX resistant (TTX-R) whereas the remaining voltage-sensitive sodium channels ($Na_V1.1$-1.4, 1.6 and 1.7) are TTX-sensitive (TTX-S) being blocked in the low nanomolar range.

Every sodium channel α-subunit has its own gene (*SCN1A-SCN11A*) that show tissue dependent expression profiles. Specifically, α-subunits of voltage-sensitive sodium channels contain four domains (DI-DIV) and each domain contains six transmembrane segments (S1-S6) (fig. 2). S4 segments act as voltage sensors, while S5-S6 form the pore. The loop between S5 and S6 is responsible for filtering sodium ions. A functionally very important intracellular loop is located between DIII and DIV, which forms the inactivation unit. This unit limits action potential duration and terminates sodium current in a time and voltage dependent fashion. Recent investigations showed that individual nociceptors express up to six different voltage-sensitive sodium channels: $Na_V1.1$, $Na_V1.3$ and $Na_V1.6$-$Na_V1.9$ (Bennett et al., 2019).
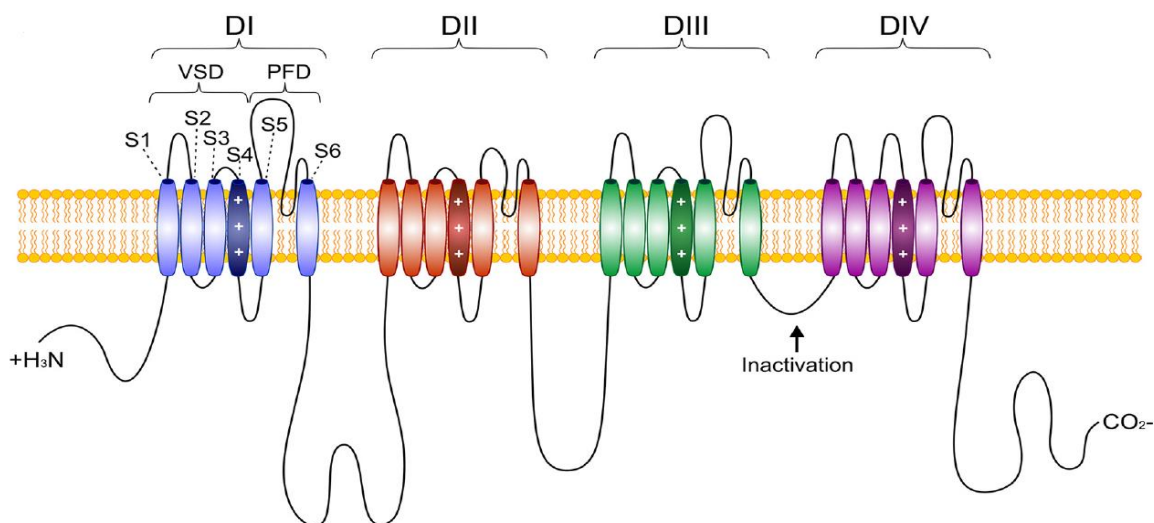
Fig. 2: Structure of voltage-sensitive sodium channel α-subunits. (Bennett et al., 2019)

$Na_V1.1$ channels were once thought to contribute little in the context of nociception. However, recent studies showed that $Na_V1.1$ channels are expressed in C-fibres (Osteen et al., 2016). Adding to that, selective $Na_V1.1$ activation in human skin caused pain and mechanical hypersensitivity (Osteen et al., 2016).

In peripheral sensory neurons, $Na_V1.3$ expression peaks in foetal stages, then declines to undetectable levels in adulthood (Waxman et al., 1994). However, $Na_V1.3$ expression increases substantially subsequent to injury (Bennett et al., 2019).

$Na_V1.6$ replaces foetal $Na_V1.2$ expression in adult A-fibres but is also found in some C-fibres (Black et al., 1996). $Na_V1.6$ interacts with ankyrin B and is strongly localized at nodes of Ranvier in myelinated fibres (Caldwell et al., 2000). A lot of experiments and clinical evidence have linked $Na_V1.6$ with neuropathic and inflammation pain (Bennett et al., 2019).

Na$_V$1.7 generates a TTX-sensitive current and is preferentially expressed in the periphery nervous system. mRNA of Na$_V$1.7 was detected in both A- and C-fibres (Black et al., 1996). On other hand, immunochemistry showed higher expression of Na$_V$1.7 in C-fibres than in A-fibres (Djouhri et al., 2003b). These channels are thought to trigger action potentials in C-fibres by their ability to amplify subthreshold depolarisation ("ramp current") (Bennett et al., 2019). Gain- and loss-of-function mutations of Na$_V$1.7 mutations lead respectively to chronic pain states (erythromelalgia and paroxysmal extreme pain disorder) (Choi et al., 2011; Waxman and Dib-Hajj, 2005; Yang et al., 2004) or the inability to sense pain (congenital insensitivity to pain, CIP) (Cox et al., 2010; Goldberg et al., 2007). Thus, this channel apparently has a crucial functional role in human nociception (Dib-Hajj et al., 2013; Dib-Hajj et al., 2008) suggesting that it is a very promising target for analgesic therapy.

Na$_V$1.8, as with Na$_V$1.7, is preferentially expressed in peripheral sensory neurons. Interestingly, Na$_V$1.8 current is not detectible in the foetal stage (Renganathan et al., 2002), only in adults, and expression of Na$_V$1.8 is reduced by aging (Wang et al., 2006). It is thought to provide the main part of the sodium current for the action potential, at least at the level of the somata (Djouhri et al., 2003a; Renganathan et al., 2001). Na$_V$1.8 is mainly found in nociceptive C-fibres (Jurcakova et al., 2018; Shields et al., 2012) and produces TTX-resistant current. Na$_V$1.8 is resistant to cooling (Zimmermann, 2007) and enriched in the distal part of axons (Klein et al., 2017; Zimmermann et al., 2007). Inflammatory mediators can slow its fast inactivation kinetics to provoke "resurgent currents" (Tan et al., 2014; Xiao et al., 2019) providing a mechanism for inflammatory and neuropathic pain.

Na$_V$1.9 is one of the least investigated voltage-sensitive sodium channels. This is probably, because of limitations in its heterologous expression in mammalian cells (Zhou et al., 2017) and limitations to isolate it in native neurons (Bennett et al., 2019). Na$_V$1.9 is mainly expressed in trigeminal and somatosensory nonpeptidergic dorsal root ganglia neurons. Excepting hair cells, there is no evidence that this channel is expressed in any other cells in the body (Bennett et al., 2019; Cai et al., 2015). Ultra-slow inactivation allows Na$_V$1.9 to generate very long (up to a few minutes) persistent currents supporting the idea that Na$_V$1.9 does not influence the shape of action potentials, but instead sets threshold. Na$_V$1.9 has a low activation threshold that is probably below the resting membrane potential in axons. It features a window current, such that this channel is constantly open at resting membrane potential. All these characteristics set Na$_V$1.9 channels apart from other voltage-sensitive sodium channels. There are some recent clinical investigations on chronic pain and/or itch patients suggesting a functional clinical role of Na$_V$1.9 in these pain and itch states (Huang et al., 2014; Huang et al., 2017; Kabata et al., 2018; Leipold et al., 2013; Salvatierra et al., 2018).

1.2.1.1 Inactivation mechanisms in voltage-sensitive sodium channels

Activation and inactivation of voltage-sensitive sodium channels has been conceptualized as two independent mechanisms that control the channel's open probability (Hodgkin and Huxley, 1952). Activation is governed by membrane potential that determines the open or closed state of the channel, whereas inactivation describes the switching of the channel from active to the inactive state. Sodium will only pass the channel in the open, non-inactivated state. Hodgkin and Huxley created a revolutionary mathematical model for which they were awarded the 1963 Nobel prize in Physiology or Medicine (Hodgkin and Huxley, 1952). Later it has become clear that rather than the H-H deterministic model there are Na$_V$ properties not foreseen by Hodgkin and Huxley, such as the resurgent current that require a

non-inactivated but nevertheless blocked-open state. Similarly, the transition from closed active to closed inactive ("closed state inactivation") was suggested by Hodgkin and Huxley, empirical verification was provided somewhat later by Bean (1981). Closed-state inactivation will not induce any sodium current and thus, it considerably reduces excitability of neurons (Armstrong, 2006).

Mechanistically, two kinetics can be differentiated: fast and slow inactivation, based on the time that the channel needs to recover from inactivation (Ulbricht, 2005). Only short rectangular electrical stimuli were used in early experiments that only allow investigating fast inactivation. Later, this inactivation was found to be more bound to open-state inactivation and that the Na_V α-subunit´s intracellular DIII-DIV loop is crucial for its functioning (Kellenberger et al., 1997; Patton et al., 1992; Vassilev et al., 1988; West et al., 1992). Classical literature describing fast inactivation as physical block of sodium channel pores by a so-called inactivation body (DIII-DIV loop). Recent findings support the idea that sodium channels are not physically blocked by fast inactivation but rather that inactivation is associated with an allosteric alteration in the channel requiring the DIII-DIV loop for its full functioning (Shen et al., 2019; Yan et al., 2017). Slow ramp electrical currents were used as stimulation paradigm for sodium channels slightly later. Because of that, slow inactivation - activated by slow ramps currents - was found after fast inactivation. Slow inactivation takes from few seconds to up to a minute to recover while fast inactivation lasts less than few seconds (Ulbricht, 2005). It was found that slow inactivation is based on an allosteric block by channel conformations related to the EEDD ring in the external part of the sodium channel pore (Tikhonov and Zhorov, 2007). Interestingly, mutations that limit or eliminate fast inactivation do not have an effect on slow inactivation (Featherstone et al., 1996; Vedantham and Cannon, 1998). This confirmed that fast and slow inactivation are independent. Importantly, slow inactivation is more related to closed-state than to open-state inactivation. In summary, slow inactivation can be induced by slow ramps currents and closed-state inactivation while fast inactivation with rapid currents and open-state inactivation. All of this suggests that slow ramp currents can push sodium channels from close-active state into close-inactive state and keep it in this phase for a long period of time compared to fast inactivation. Concerning sodium channel subtypes, $Na_V1.7$ takes a long time to transition into closed state inactivation and can thus deliver a ramp current (Cummins et al, 1998) but Nav1.7 is also more prone to enter slow inactivation than $Na_V1.8$ during cooling (Zimmermann et al., 2007).

1.2.2 Single fibre vs. compound action potential recordings in C-fibres

Excitability of neurons can be investigated on a single fibre level or in nerves containing several thousand axons. Single cell recordings allow for exact functional classification and are essential to investigate different functional classes of C-fibres (Ackerley and Watkins, 2018; Reeh, 1988; Schmelz et al., 2000; Serra et al., 1999). These studies mainly rely on classic extracellular recordings (Wooten et al., 2014) and there have only been a few attempts to functionally classify primary afferents while performing intracellular recordings in the dorsal root ganglia neurons, in-vivo (Acosta et al., 2012; Gao et al., 2012; Li et al., 2016). The major drawback of single fibre recordings is their comparatively low yield. When investigating nerve fascicles rather than single units the action potentials of the single fibres will summate to a compound action potential. Based on the differences in conduction velocity, A- and C-fibres can be easily separated in time. The variability of axonal conduction velocity between individual C-fibres (0.2 -1.5 m/s) causes dispersion of the compound action potential, in particular for longer recording distances leading to a loss of synchronicity

(Ritchie and Straub, 1956). The key advantage of the recording of compound action potentials is the simultaneous assessment of a multitude of axons enormously facilitating pharmacological studies. On the other hand, the information on different functional populations of C-fibres is lost in this approach.

1.2.3 Excitability testing in neurons

Neuronal excitability changes will not only change activation thresholds, but also conduction velocity and amplitude of the compound action potential. The key parameter of excitability is the electrical threshold, i.e. minimal electric current stimulus amplitude required to evoke an action potential. Electrical threshold is quantified by increasing the amplitude and/or duration of stimulus. Most commonly, electrical stimuli are applied as short rectangular or ramp (triangular) currents (0.1 – 1 ms). Reduced electrical thresholds indicate hyperexcitable axons. The reduction can be based on depolarized membrane potential such that less charge is required to trigger an action potential. On the other hand, stronger depolarization will reduce the number of sodium channels available for activation by their inactivation, thus the electrical thresholds will not allow for absolute measurement of membrane potential. Hyperpolarization can increase the number of available Na_V by reducing closed-state inactivation and thereby reducing electrical threshold and increasing excitability. On other hand, hyperpolarization is pushing resting membrane potential away from action potential triggering threshold thereby increasing electrical threshold. In summary, electrically induced compound action potentials of C-fibres is a fast and robust approach to quantify changes of axonal excitability in a large number of single neurons simultaneously. Information about specific subpopulations or absolute measures of membrane potential or currents is not possible with this method.

1.3 Spontaneous activity of nociceptors and chronic pain

Spontaneous ongoing pain is the most common symptom in peripheral neuropathic pain and it is often combined with mechanically evoked hyperalgesia (Scadding and Koltzenburg, 2006). Hyper-excitability of primary nociceptive neurons has been supposed to be the most important factor in the generation and maintenance of chronic neuropathic pain in humans (Scadding and Koltzenburg, 2006). This hyper-excitability can lead to ectopic activity and sensitization (Costigan et al., 2009). Pathophysiologic mechanisms of neuropathic pain have been investigated extensively in experimental animal models based on nerve injury (Bennett et al., 2003), or subsequent to non-traumatic disease (Bennett, 2010; Wallace et al., 2007). In humans single fibre recordings with microneurograpy have not only revealed that neuronal and axonal hyper-excitability are linked to sensory symptoms such as pain or paresthesia in patients (Bostock et al., 2005; Burchiel and Baumann, 2004; Campero et al., 2010; Campero et al., 1998; Cline et al., 1989; Jorum et al., 2007; Mackel et al., 1994; Nordin et al., 1984; Nystrom and Hagbarth, 1981; Ochoa et al., 2005; Orstavik et al., 2006; Orstavik et al., 2003; Serra et al., 2009), but have also identified a higher incidence of spontaneous activity in C-nociceptors in patients with painful neuropathy as compared to non-painful neuropathy (Kleggetveit et al., 2012), indicating a causal role of this nociceptive input for ongoing clinical pain. The back-translation of these clinical results into experimental models is problematic as mainly evoked pain behaviour (Serra, 2010) is assessed in animal models rather than spontaneous pain behaviour which more clinically relevant (Mogil, 2009).

1.3.1 Peripheral and central mechanisms of chronic pain

It is obvious that chronic pain can be maintained by peripheral nociceptive input such as that occurring following a peripheral nerve injury, but can also arise without any peripheral pathology such as after a thalamic stroke (Millan, 1999). There has been a controversial debate about the relative contribution of the peripheral and central nervous system to chronic pain states. On one hand it is held that even for peripheral nerve injuries only the initial pain is due to primary nociceptor discharge whereas chronic pain states are linked to maladaptive central changes (Flor et al., 2006). On the other hand, even in clearly defined central neuropathic pain conditions, such as thalamic infarction a role of peripheral nociceptive input has been suggested (Haroutounian et al., 2018; Meacham et al., 2017). Fortunately, integrated concepts for mechanisms contributing to chronic pain have been developed that consider posit central sensitization processes that are induced and maintained by long term nociceptive input and also include the biopsychosocial model of pain (Andrasik et al., 2005) that focuses on the central interactions at high cognitive and emotional levels. Conceptually, pain is based on highly complex interactions between peripheral and central neuronal activity on one hand and a multitude of facilitatory and inhibitory external factors. Therefore, current therapeutical concepts often combine pharmacological and psychological elements with physical therapy resulting in a multimodal pain therapy (Enax-Krumova et al., 2017). As patients with pain cannot wait until the mechanisms of chronic pain have been completely understood, it is obvious that the treatment has to be more pragmatic. On the other hand, it is also required to focus on certain aspects in the development of chronic pain to clarify and specify their molecular mechanisms. In this respect the origin and maintenance of ongoing activity in nociceptors is of particular interest.

1.3.2 Spontaneous activity in nociceptors

As described above, there is evidence that spontaneous activity in peripheral nociceptors is higher in those patients with neuropathy that also suffer from pain (Kleggetveit et al., 2012). It might appear straight forward to provoke ongoing activity in nociceptors, however, although nocicpetors are activated by a multitude of chemical mediators they notoriously adapt and desensitize upon tonic noxious stimulation: even using a mixture of various inflammatory mediators (histamine, serotonin, bradykinin, prostaglandin E2) activity subsides after about 5 min of application and can be prolonged only be acidification (Steen et al., 1995b). Even using membrane depolarization to induce action potential firing in nociceptive dorsal root ganglion neurons still did not prevent adaptation of the response (Blair and Bean, 2003). Thus, there appears to be a disconnection between the apparent ongoing activity of nociceptors in patients with chronic pain and the degree of adaptation observed in healthy nociceptors. Recently, transcutaneous electrical stimulation using a 4 Hz sine wave profile has been shown to preferentially activate C-nociceptors in mouse, pig and human (Jonas et al., 2018a). Interestingly, repetitive stimulation for 1 minute resulted in a massive adaptation in healthy volunteers, but this adaptation did not occur at painful sites in patients with neuropathic pain (Jonas et al., 2018a) indicating that perhaps it is a lack of inhibitory mechanisms normally supporting adaptation that contributes to chronic pain states. Unfortunately, experimental models that would allow investigating spontaneous activity in nociceptors are lacking. Recently, application of an extracellular solution with a low potassium concentration has been shown to induce ongoing activity in cutaneous nociceptors for more than 1 h in an ex-vivo skin nerve preparation of the mouse (Diskin et al. submitted). Although such a stimulus is outside the normal physiological range, to our knowledge this is the first model to induce acute ongoing discharge in healthy nociceptors experimentally.

1.4 Aim of thesis

In this thesis, two major questions were targeted: first, how does the application of low extracellular potassium, that induces ongoing nociceptor activity at the sensory endings of skin nociceptors, change the excitability of C-axons and which molecular mechanisms are involved. Secondly, what are the mechanisms that allow activation of C-axons when stimulated by slow depolarizing ramp stimuli (4 Hz sinusoidal) and can this test be used to investigate hypersensitivity in experimental neuropathy models. Within the graduate school, rats were injected with cisplatin to induce acute kidney injury, but this treatment is also associated with neuropathy and neuropathic pain. Peripheral nerves of these rats were investigated for signs of hyper-excitability using the above-mentioned newly developed stimulation paradigms. Ideally, our investigation would uncover mechanisms that can induce ongoing activity in nociceptors and provide specific test protocols such that these mechanisms could both be analysed in experimental animal models, but may also be explored as targets for future pain therapy in people.

2 MATERIAL AND METHODS

2.1 Physiological solution

All experiments were done in physiological solution (in mM): NaCl 118, KCl 3.2, HEPES 6, Na gluconate 20, $CaCl_2$ 1.5, $MgCl_2$ 1.0, D-glucose 5.55. Solution pH was calibrated to 7.4 by NaOH 1M solution. Recipes for solutions with different potassium and sodium concentrations were generated in respect to normal physiological solution. Different potassium concentration solutions were compensated by NaCl. Solutions with lower sodium concentrations had NaCl changed into LiCl or choline chloride to keep osmolarity constant.

2.2 Chemicals

Reagents:

Chemical	Company	Catalogue number
• Sodium chloride	Sigma-Aldrich	S7653
• Potassium chloride	Sigma-Aldrich	P9333
• HEPES	Sigma-Aldrich	H3375
• D-Gluconic acid sodium salt	Sigma-Aldrich	G9005
• D-(+)-Glucose	Sigma-Aldrich	G8270
• Calcium chloride solution	Fluka Analytics	21114
• Magnesium chloride solution	Fluka Analytics	63020
• Lithium chloride	Merck	105679
• Choline chloride	Sigma-Aldrich	C7527
• Sodium hydroxide	Sigma-Aldrich	S8045
• Dulbecco's PBS	Sigma-Aldrich	D8662
• DMSO	Sigma-Aldrich	D5879

Drugs:

Chemical	Company	Catalogue number
• Tetrodotoxin (with citrate)	Alomone labs	T-550
• μ-Conotoxin PIIIA	Alomone labs	STC-400
• (1R,2S,5R)-(-)-Menthol	Sigma-Aldrich	M2780
• Icilin	Sigma-Aldrich	I9532
• ZD7288 hydrate	Sigma-Aldrich	Z3777
• Ouabain octahydrate	Sigma-Aldrich	O3125
• Narcoren	Merial GmbH	
• Sevoflurane	Abbott	

Others chemicals:

- Weißes Vaselin Lichtenstein DAB   Zentiva Pharma GmbH

Physiological solution without glucose was kept in a fridge until the start of experiments. (-)-menthol 1M and icilin 10mM in DMSO stock solutions were kept at room temperature. Tetrodotoxin (TTX) 10mM and μ-conotoxin PIIIA (CTX) 1mM PBS stock solutions were kept at -20°C in a freezer. Ouabain 10mM distilled water stock solution was kept at room temperature. ZD7288 10μM DMSO solution was kept in a fridge at 4°C.

2.3 Devices

Compound action potential recording
Devices:

Device	Model	Company
• Stimulator	A395	World Precision Instruments
• Humbug	HumBug	Quest Scientific
• Differential Amplifier	NL104A	Digitimer
• Digitizer	PXIe	National Instruments

Single fibre recordings from sensory neuron terminals
Devices:

Device	Model	Company
• Stimulator	A395	World Precision Instruments
• Differential Amplifier	NL104A	Digitimer
• Band-Pass Filter	NL125, NL126	Digitimer
• Digitizer	micro 1401	CED
• Micropipette puller	P-77	Sutter Instrument co.

2.4 Animals

Three different animals' species were used in this thesis: mouse, rat and guinea pig. The majority of experiments were done in mice because of genetic modifications available in these animals. I got the opportunity to work with mice that are lacking $Na_V1.9$ [gift from Prof. Reeh, Erlangen] and rats that received cisplatin injections [Prof. Gretz laboratory]. Cisplatin-induced neuropathic pain is well known experimental model. I used guinea pig eyes for single fibre recordings from sensory nerve terminals because this method was established in these animals. On the other hand, literature confirms that single fibre recordings in cornea are also possible in mice and rats, but with a lower success rate.

2.4.1 Mice

C57BL/6N (Charles River Laboratories) mice of both sex, ranging in age between 2-24 months and weight 23-34 g were used in experiments. Animals were housed in cages at 12-hour light-dark cycle and were supplied by food and water ad libitum. Mice were killed by cervical dislocation, in some cases decapitation. Some animals were anaesthetized by Sevoflurane gas before procedures.

$NaV1.9^{-/-}$ (KO) mouse line was generated by Mohammed A. Nassar. Mice were genotyped from C57BL/6 line and back-crossed for more than 9 generations to purify the line. $NaV1.9^{-/-}$ mice were kept in same environment as wild-type (WT) and were killed by cervical dislocation.

2.4.2 Rats

Cisplatin neuropathic rat model was generated by Prof. Gretz group. Sprague Dawley (200g) male rats got single intraperitoneal administration of cisplatin at the dose of 7 mg*kg^{-1}. The control group received the same volume of sterile saline. Animals were housed in cages at 12-hour light-dark cycle and were supplied by food and water ad libitum. Rats were sacrificed on day 15 after cisplatin injection by perfusion under anaesthesia.

2.4.3 Guinea pig

Duncan-Hartley female guinea pigs 3-4 week old weighting 350±70 g were used in experiments. Animals were kept together in a cage under 12-hour light-dark cycle and were supplied by food and water ad libitum. Animals got intraperitoneal injection of 1 ml pentobarbital (Narcoren) overdose and were checked for pain response before decapitation.

2.5 Compound action potential recording

Compound action potential (CAP) recordings were done for excitability testing in mice and rats nerves and investigating zeroK solution induces ongoing activity in mouse nerve. In the mouse sural and in rat saphenous nerves were used in CAP recordings.

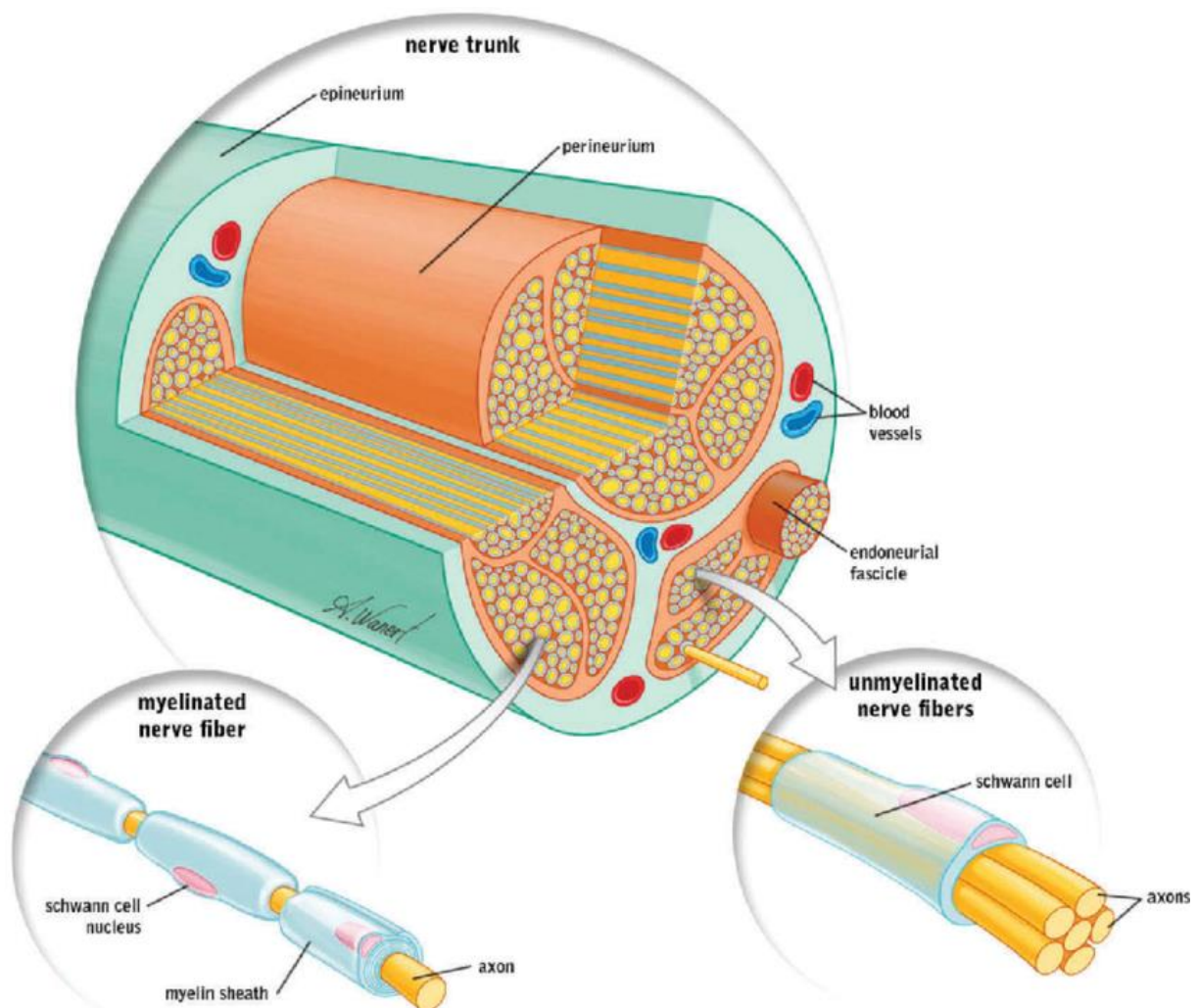### 2.5.1 Histological structure of the nerve

Fig. 3: Histological nerve structure. (Ilfeld et al., 2016)

Within a peripheral nerve axons are organized in cable-like fascicles. The nerve is protected by three sheets: endoneurium, perineurium and epineurium (fig.3). The endoneurium ensheaths a bunch of axons and this way generates one fascicle. The perineurium groups a few endoneurium fascicles and generates a perineurium

fascicle. The epineurium is the outer sheet of a peripheral nerve containing all perineurium fascicles and blood vessels.

A peripheral nerve contains myelinated A-fibres and unmyelinated C-fibres ensheathed in glia cells (fig.3). These Schwann cells form the myelin sheath of single A-fibres. In contrast, several C-fibres are ensheathed by non-myelinating Schwann cells. This group of C-fibres surrounded by Schwann cells is called Remak bundle. Remak bundles in rat sciatic nerve contain approximately 2.1 axons on average (Murinson and Griffin, 2004). However, they can contain up to 20 axons when assessed more proximal close to the spine. This number drops to one or a few axons per Remak bundle at the distal end of the nerve in mouse and rats, or humans (Ebenezer et al., 2007; Murinson and Griffin, 2004).

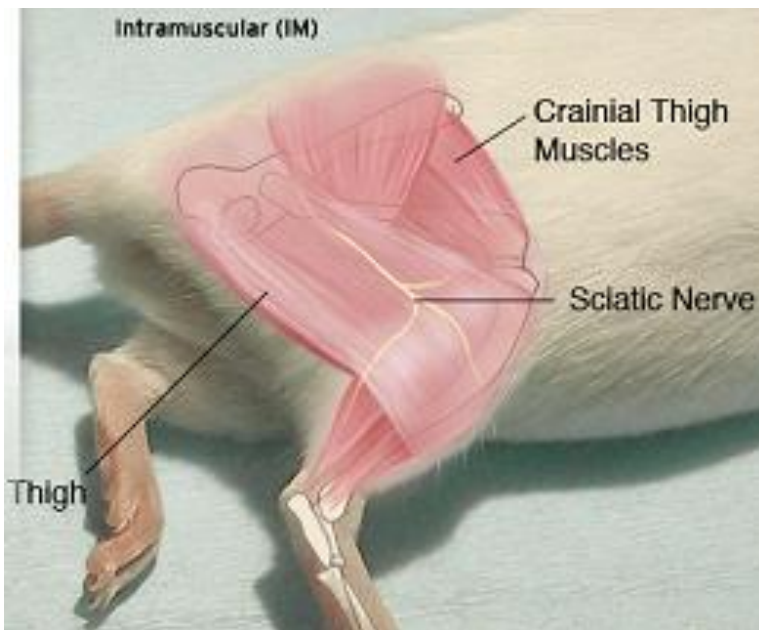## 2.5.2 Anatomical structure of the mouse sural nerve

Fig. 4: Hind mouse leg with marked sciatic nerve trifurcation. The sural nerve fuses with sciatic nerve on proximal part and innervated pawn on distal part. (Picture taken and modified from https://theodora.com/rodent_laboratory/injections.html)

The sural nerve is a sensory nerve that comes out of sciatic nerve which is the biggest and longest peripheral nerve in mammals and can easily be located in dorsal thigh area (fig.4). Axons of this nerve are formed by spinal nerves of the lumbar segments 3 to 5 (L3-L5) in mice. This can be different between species, for example, it is L4-L6 in rats, or L4-S3 in humans. Mouse sciatic nerve is mainly supplied by L3 and L4 spinal nerves, L5 spinal nerve contributes the smallest amount of axons. In some cases, L5 spinal nerve is not fusing into the sciatic nerve at all (Rigaud et al., 2008). Main function of sciatic nerve is innervation of the foot and entire lower leg (except for its inner side). The sciatic nerve has a characteristic trifurcation on its distal part where it splits into three different nerves: common peroneal nerve, tibial and sural nerve. Sensory innervation of the mouse paw is provided by these three nerves. The sural nerve is emerging from deeper tissue near the sciatic nerve trifurcation to the superficial leg muscles and it is located very superficially in its distal part (Fig. 4). This nerve is a nearly pure sensory nerve and it has only few branches. Thus, simple preparation procedure, few branching points and purely sensory are

main characteristics ideally suited for excitability testing in the electrophysiological investigations.

2.5.3 Anatomical structure of the rat saphenous nerve

The saphenous nerve is the largest terminal cutaneous branch of the femoral nerve and innervates the anteromedial, medial and posteromedial surface of the leg. The femoral nerve is the largest branch of the lumbar plexus. It contains spinal nerves from segments L2-L4 and has sensory and motor function. The saphenous nerve is a nearly pure sensory nerve, only 4% of axons are motor-neurons, and contains spinal nerves from segments L3-L4 in humans and rats. This nerve together with sural nerve is most commonly used for peripheral pain models.

2.5.4 Nerve preparation

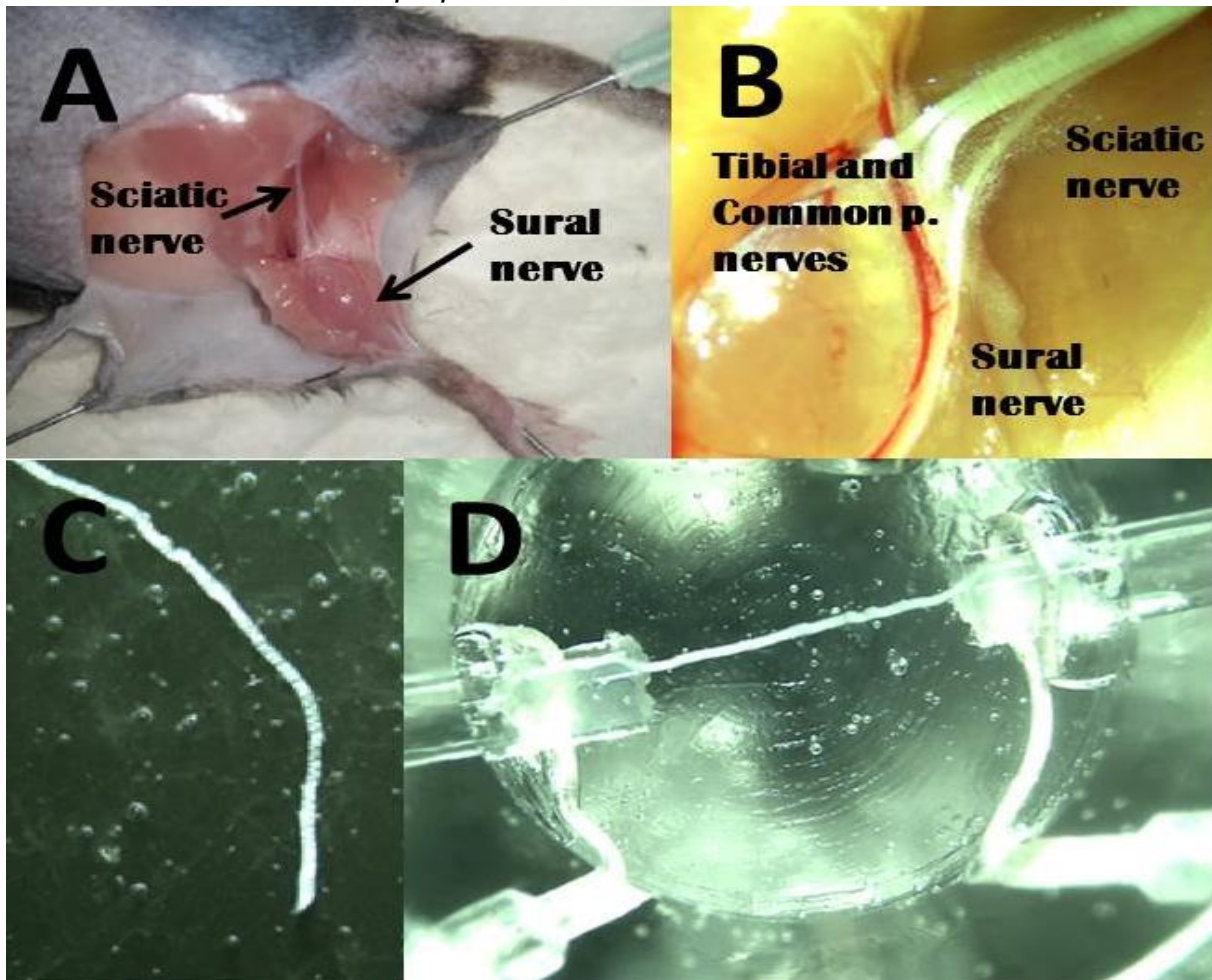#### 2.5.4.1 Mouse sural nerve preparation

Fig. 5: Sciatic nerve trifurcation and cleaned sural nerve in the dish and bath. Sural nerve was cut near the sciatic nerve trifurcation (A&B), cleaned (C) and placed into the recording chamber (D).

Mice were killed by cervical dislocation. Some animals were anaesthetized by Savoflurane gas before they were sacrificed. Hind legs of the mice were shaved and cleaned by water or 70% alcohol solution. Animals were fixated on a plastic surface and attached to the surface by using needles. A small cut was performed in the skin in thigh area and prolonged along the leg to proximal and distal directions (fig.4). The

sural nerve is easily found on top of muscles at distal part, this anatomical feature allowed to track the nerve proximally and dissect it from the surrounding tissue. The sural nerve was cut at the proximal part with a small part of the sciatic nerve near the trifurcation in the popliteal fossa area (fig.5 A&B). The distal part at the foot was cut near the Achilles tendon. The nerve was placed in physiological solution with glucose and cleaned from epi- and perineurium under a microscope using scissors (fig.5 C). The cleaned nerve was truncated up to 12 mm in length to fit the bath dimension (fig.5 D).

2.5.4.2 Rat saphenous nerve preparation
The inner side of the sacrificed rat's hind limb was shaved and cleaned with water or 70% alcohol solution. A small cut was done in the shaved area and prolonged between groin and knee. The saphenous nerve can easily be identified on the superficial muscle surface (fig.6). The nerve was dissected from surrounded tissue and cut out at a length of approximately 2-3 cm. The saphenous nerve was placed in physiological solution and cleaned under a microscope.
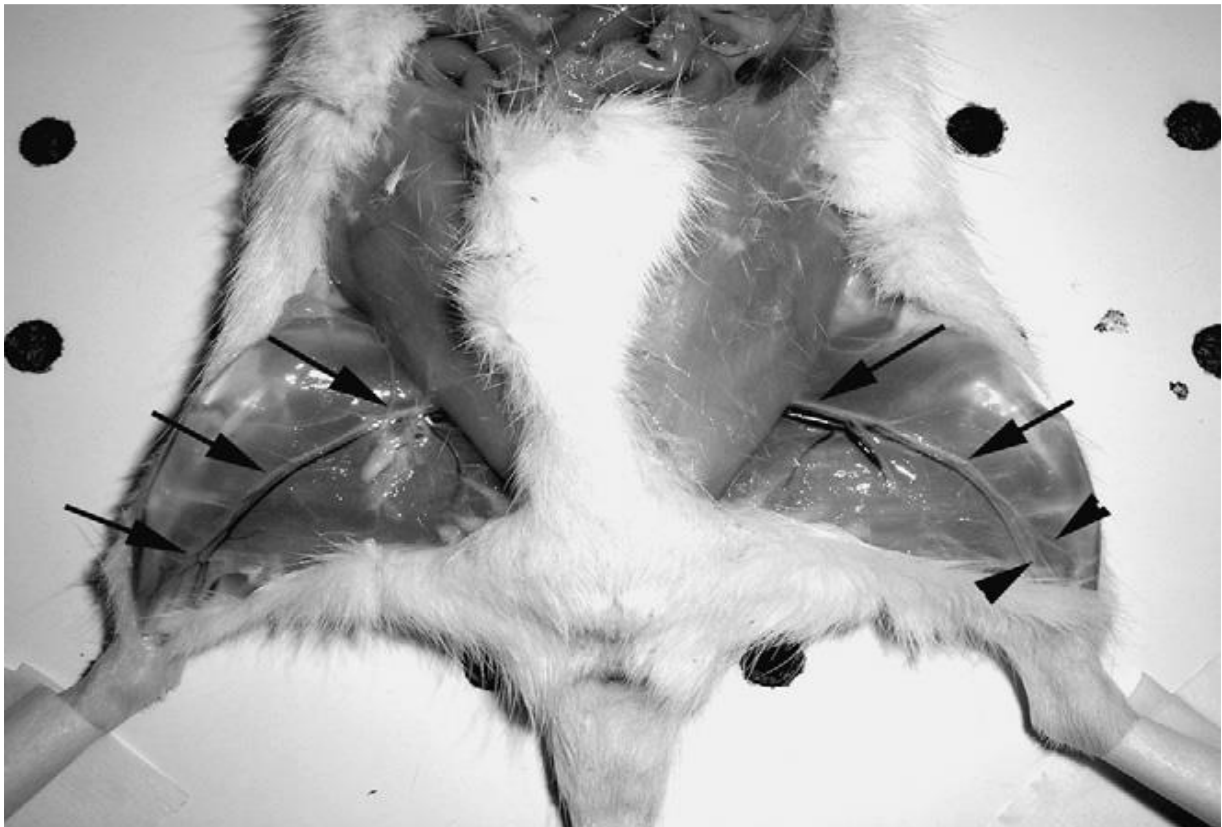

Fig. 6: Rats saphenous nerves (marked by arrows). (Campos et al., 2008)
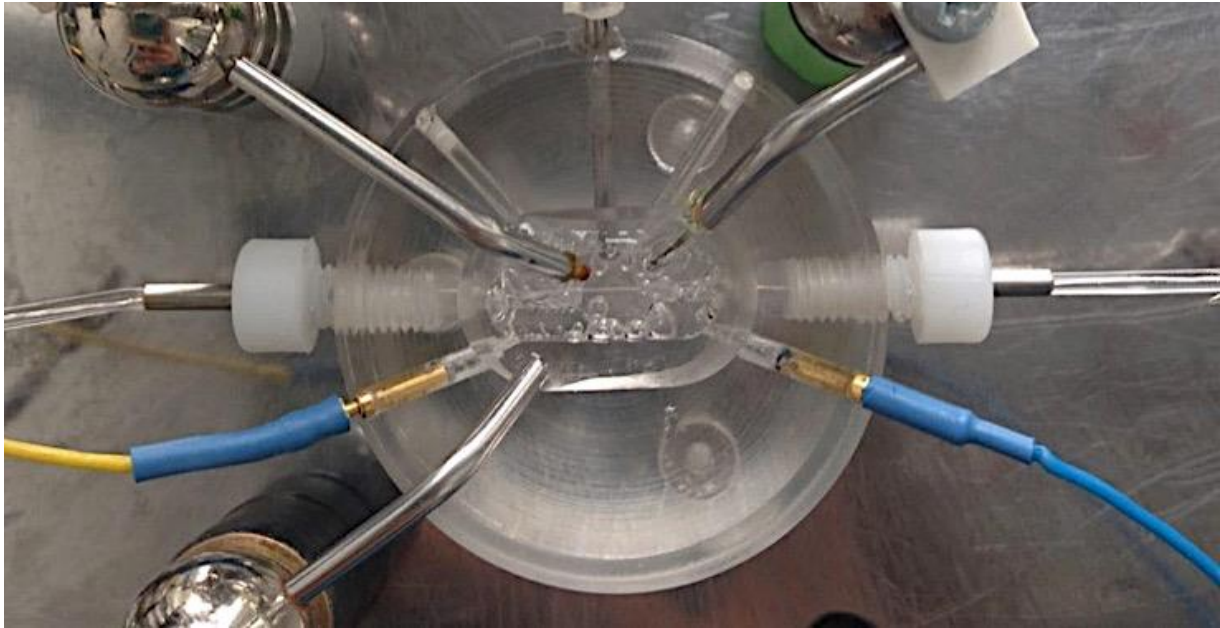
2.5.5 Set up

Fig. 7: Custom-made organ bath.

The cleaned nerve was placed in a custom-made organ bath (volume ca. 2ml) with physiological solution (fig.7). The nerve was fixed between two suction electrodes using petroleum jelly to generate mechanical stability and high electrical resistance. The distance between suction electrodes was modulated between 5-10 mm based on nerve's length. The custom-made organ bath was perfused continuously with physiological solution at a flow rate of 10ml*min^{-1}. The physiological solution was bubbled continuously with oxygen. The temperature of the solution was measured by a thermistor sensor placed in the organ bath and was controlled by an inline Peltier device. A constant current electrical stimulator was delivering electrical stimulation via a silver wire inside the stimulating suction electrode, which served as the anode, and a second silver wire, wound around the suction pipette, which served as the cathode. Other suction electrode with silver wire wrapped around served as recording electrodes. Signal recording was done over the sealing resistance amplified 5,000 times by a differential amplifier and filtered from 50/60 Hz noise frequency by a "Hum Bug".

2.5.6 Recording protocols and analysis

2.5.6.1 QTRAC program working principle

Compound action potential recordings and electrical stimulations were controlled by QTRAC software (Institute of Neurology, London, UK). The program is working in loops. Loops are split time intervals of identical duration, which can be set by function "SI" (stimulus interval). Thus, when 3 intervals are defined and SI is set to "2", then loop duration is 6 s. Stimulation parameters for each these time intervals (channels) are set individually and repeated sequentially in the same order in loops. The user can change amount of channels any time by using function "SC" (select channels). Functions that were used in this project are listed in table 3.

Command	Description
Test High (TH)	Stimulus intensity by adding number as it intensity in percent of max stimulator intensity for example supra-maximal test stimulus TH=100
Window Start (WS)	Starting point on X scale for tracking window
Windows Width (WW)	Length of tracking window
MV	Averaging function for shape of signal
Display X (DX), Display Y (DY), DA, DAA	Function to adjust x and y scales (DX and DY), do automatically for set units (DA) or for all units in program interface (DAA)
Display Channel (DC)	Visible channel, others channels are still tracked
Select Channel (SC)	Turning ON channels, others channels are not tracked
MH, ML	High (MH) and low (ML) pass filters
Test Width (TW)	Length of stimulus
Test Start (TS)	Starting position of stimulus
Test Period (TP)	Period of stimulus
Starting traces grabbing (GS)	Starting and stopping grabbing shapes of signal for saving
Stop/Start Stimulus (SS)	Stops or Starts stimulation
File save (FS), File close (FC)	Comments to save and close QTRAC program

Table 3: QTRAC functions

Stimulus intensity can be set by using function "TH" and adding number as stimulus intensity in %. Supra-maximal rectangular stimulus was defined as TH=100 function which is interpreted as stimulus of maximal amplitude defined by the stimulator. The input of the stimulator has a range ±10V, whereas the computer output has a range of ±5V. Thus, the computer will sent its maximum of 5 V for a stimulus intensity of 100%. The 5 V signal is interpreted as 50 µA current (50% of the maximum stimulus output of 100 µA) by stimulator.

2.5.6.2 Monitored units
The electrical stimulus is inducing synchronized activity of axons resulting in a compound action potential. The QTRAC program is tracking the shape of signal and is monitoring units in a time window to be defined by the user (fig.8). The program allows tracking different compound action potentials by setting the window in different time position, for example A-fibres CAP (A-CAP) or C-fibre CAP (C-CAP). Importantly, the baseline signal is calculated from the readings before the stimulus and set to 0 µV on the y scale. Other values that are monitored by the program:

- Peak, P (amplitude) - difference between biggest and smallest values inside the window.
- Latency, L (delay) – time delay between start of stimulus and 50% of up-rising positive amplitude.
- Non-conditioned current – stimulus amplitude to evoke 40% of supra-maximal rectangular stimulus induced C-CAP amplitude (Peak, P).
- Conditioned current – same as non-condition just there is supra-maximal rectangular conditioning stimulus 30 ms before the actual stimulation.
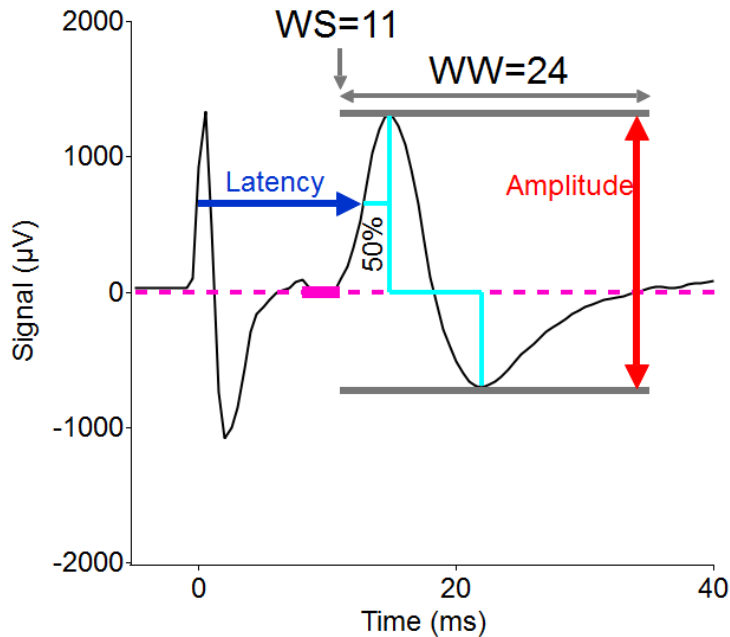
Fig. 8: QTRAC monitored units. All units were measured inside the window set by the user [commands: start of window (WS) and window width (WW)]. Amplitude was measured as distance between maximum and minimum in the window, latency as time delay between start of stimulus and 50% of positive amplitude.

2.5.6.3 Protocol for sinusoidal stimulation

The stimulator delivered two types of stimulation profiles: 1 ms duration constant current rectangular stimulus once per 2 s or 125 ms duration half sine ware constant current sinusoidal shape stimulus once per 8 s. The only varying stimulus parameters was stimulus amplitude. Stimulation protocol was established as a step by step increase in stimulus amplitude from 0 µA up to supra-maximal 50 µA for rectangular and 20 µA for sinusoidal stimulus at 20, 26 and 32°C. The same protocol was repeated after adding 1 mM (-)-menthol or 10 µM icilin into physiological solution. Supra-maximal rectangular stimulus was used as reference to check any long lasting damage on nerve's C-CAP signal.

2.5.6.4 Protocol for long latency C-CAP evoked by sine wave

Long latency C-CAP evoked by weak sinusoidal stimulus protocol was done in 20°C. Stimulus amplitude was increased step by step from 0 µA up to supra-maximal 50 µA for rectangular and 20 µA for sinusoidal stimulus. The perfusion pump was stopped and CTX stock solution was injected directly into the organ bath. CTX (20 µM) was used to block A-CAP and extract pure C-CAP from the signal thereby increasing the quality of latency measurements. Same step by step increase stimulus amplitude protocol was repeated after CTX injection. Weak sinusoidal stimuli were applied with different intensities to assess the threshold of sine wave stimulation evoking the first detectable C-CAP. TTX stock solution was injected directly into the organ bath to separate TTX-R C-CAP from TTX-S C-CAP. Both stimulation protocols were repeated after TTX (10 µM) application.

2.5.6.5 Mathematical analysis of sine wave stimulation

Compound action potential signals induced by rectangular stimuli were filtered by a 800 Hz low pass, the sigmoidal stimulus by a 30-1200Hz bandpass filter. C-CAP signal was separated from A-CAP by conduction delay and shape. C-CAP amplitudes evoked by different stimulus intensities (I_S) were fitted into a sigmoidal function as stimulus-response curve (fig.9):

$$s(x) = base + max/[1 + \exp((xhalf - x)/rate)]$$

s(x) – amplitude of signal, *x* – stimuli intensity, *max* – maximal C-CAP amplitude value, *base* – amplitude of noise level (it was set to 0), *rate* represents slope of sigmoidal curve, *xhalf* – strength of signal to generate half-maximal C-CAP amplitude.
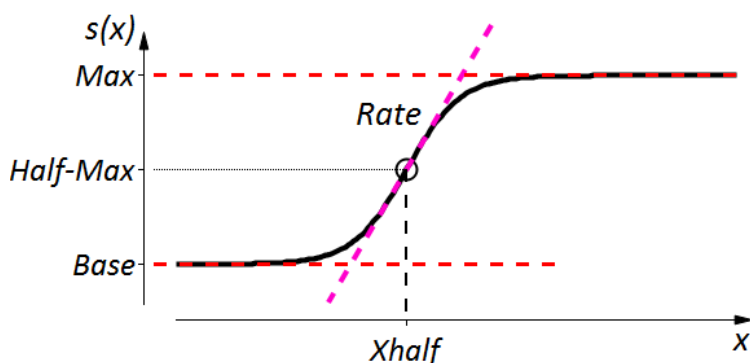

Fig. 9: Sigmoidal function

Max, *xhalf* and *rate* values of sigmoidal fit were collected in all three temperatures (20°C, 26°C, 32°C), before and after adding (-)-menthol (1 mM) or icilin (10 µM). Few experiments showed that *max* value is not representable for biggest possible signal's amplitude. In that case, *max* value was calculated from raw signal's shape.

The supra-maximal 50 µA amplitude rectangular stimulus was assumed to induce the maximum C-CAP and its latency $t_{L(R)}$ represents the conduction delay that axons need to conduct action potentials signal from the stimulation to the recording site. C-CAP latency $t_{L(S)}$ evoked by sinusoidal stimulus contains this conduction delay $t_{L(R)}$, but also the latency between start of the stimulus and the initiation of the action potentials "initiation latency" t_I (fig.10). Thus, sine wave evoked C-CAP latency $t_{L(S)}$ was corrected by subtracting conduction delay $t_{L(R)}$. Corrected sinusoidal stimulus evoked C-CAP latency t_I (initiation latency) was used to calculate the current that was delivered by sine wave stimulus at that moment of action potential generation and accordingly the charge delivered up to the C-CAP initiation moment.

Initiation current represents the current intensity of the sine wave stimulus at the moment that action potentials were initiated and was calculated using function:

$$I_I = A \cdot sin(2\pi f \cdot t_I) \, , \, t_I = t_{L(S)} - t_{L(R)}$$

I_I - current at C-CAP activation moment, *A* - stimulus amplitude, *f* - sine wave frequency (4Hz), t_I – initiation latency (corrected latency).

The charge (integrated current over time) delivered by the rectangular stimulus was calculated as stimulus amplitude (I_S) multiplied by the 1 ms stimulus duration. Charge values for rectangular stimulus were fitted into sigmoidal function and charge to activate half-maximal C-CAP amplitude was used for comparisons. The sinusoidal stimulus evoked C-CAP at a latency consisting of the conduction delay and the time required to accumulate sufficient charge for the action potential generation. Thus, sinusoidal stimulus evoked C-CAP latency was corrected by subtracting the C-CAP

latency induced by the 50 µA amplitude rectangular stimulus representing the conduction delay. Corrected sine wave induced C-CAP latency t_I (initiation moment) was used to calculate the charge (fig.10). The function used to calculate the charge delivered by sinusoidal stimulus until initiating C-action potentials was

$$q_{sine} = \int_0^{\Delta t} A \cdot \sin(2\pi f \cdot t_I), \ t_I = t_{L(S)} - t_{L(R)}$$

q_{sine} - a charge delivered by sine wave stimulus up to C-CAP initiation moment, A - stimulus amplitude, f - sine wave frequency (4Hz), t_I – initiation latency (corrected latency).
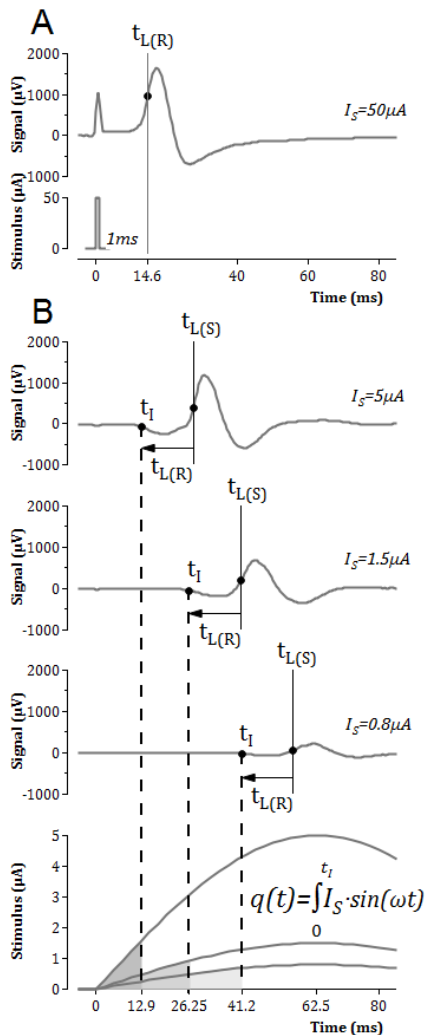

Fig. 10: Specimen to illustrate calculations. Rectangular constant current stimulation is used to evoke a supra-maximal C-fibre compound action potential (C-CAP; **A**). The latency to onset of the C-CAP is defined as the delay between stimulus onset and the first positive-going signal crossing a threshold of 50% of the peak positive C-CAP amplitude and is illustrated in response to constant current rectangular stimulation (A, latency $t_{L(R)}$) and sine wave stimulation (**B**, latency $t_{L(S)}$). Charge is calculated from the time integral of stimulus current, which represents the product of stimulus amplitude and duration for rectangular stimuli, and the integral (Formula here) for sine wave stimulate (B lower panel). To estimate the time of initiation of the C-CAP, defined as the initiation latency t_I (B), the latency to rectangular stimulation was subtracted from the sine wave latency. The charge to CAP initiation was determined over the period from stimulus onset (t=0) to t_I.S

Weak sinusoidal stimulus evoked A-CAPs and C-CAPs that partly overlapped. Therefore, C-CAP latency measurements were less robust. Thus, CAPs recorded

following sinusoidal stimulation less than 2.5 µA were ignored. Average charge was calculated for sinusoidal stimulus current in the interval 2.5 - 20µA.

Area under the curve (AUC) was calculated only from supra-maximal stimulus evoked C-CAP shapes. C-CAP signal was cut out from CAP signal and baseline, as a straight line connecting start and end C-CAP points, was compensated before calculating AUC.

2.5.6.6 Protocol for stimulation with zeroK solution

ZeroK solution was investigated using a protocol that had supra-maximal, conditioned and non-conditioned 1 ms duration rectangular stimuli. Conditioned and non-conditioned stimuli were evoking 40% of supra-maximal rectangular stimulus induced C-CAP amplitude. Stimuli were applied once per 2 s. All experiments were done at two temperatures: 26°C and 32°C. Excitability index was calculated as difference between non-conditioned and conditioned current normalized into non-condition current and expressed as %:

$$Excitability = \frac{(conditioned\ current) - (non-conditioned\ current)}{(non-conditioned\ current)} \cdot 100\%$$

Sine wave excitability testing was done at 20°C and 26°C in 1.6 mM and 3.2 mM potassium concentration. Stimulus-response curve was generated and analysed as described before.

2.5.6.7 Protocol for excitability testing in cisplatin rats

The protocol investigating nerves from the rats that had been injected with cisplatin included excitability index and sinusoidal stimulus excitability tested at 26°C and 32°C.

2.6 Single fibre recording from sensory neuron terminals

Single fibre recordings were done only in guinea pigs. This method was described before (Brock and Cunnane, 1995).

2.6.1 Innervation of cornea

The cornea is part of the optical system in the eye that is generating a focussed image on the retina. It is obviously translucent and consists of a 5-7 layers of stratified squamous epithelial cells on the Bowmans layer and the stroma that does not contain blood vessels. Based on the change of the refractory index (air vs. cornea) the cornea contributes the largest part of total refraction. The sensory innervation of the cornea derives from the trigeminal nerve and is the most dense in the human body.

Moreover, the eye has short and long ciliary nerves that innervate eye and its muscles (fig.11). The long ciliary nerve comes out of nasociliary nerve while the short ciliary nerve from ciliary ganglion. Both of these nerves have mainly sensory function. However, the long ciliary nerve also contains sympathetic fibres, while the short ciliary nerve has sympathetic and parasympathetic nerve fibres. The ciliary nerves reaches the eye close to the optical nerve, splits and without going into deeper eye layers reaches cornea. Axons enter the cornea along the limbus from where the terminals axons spread and innervate different part of eye.
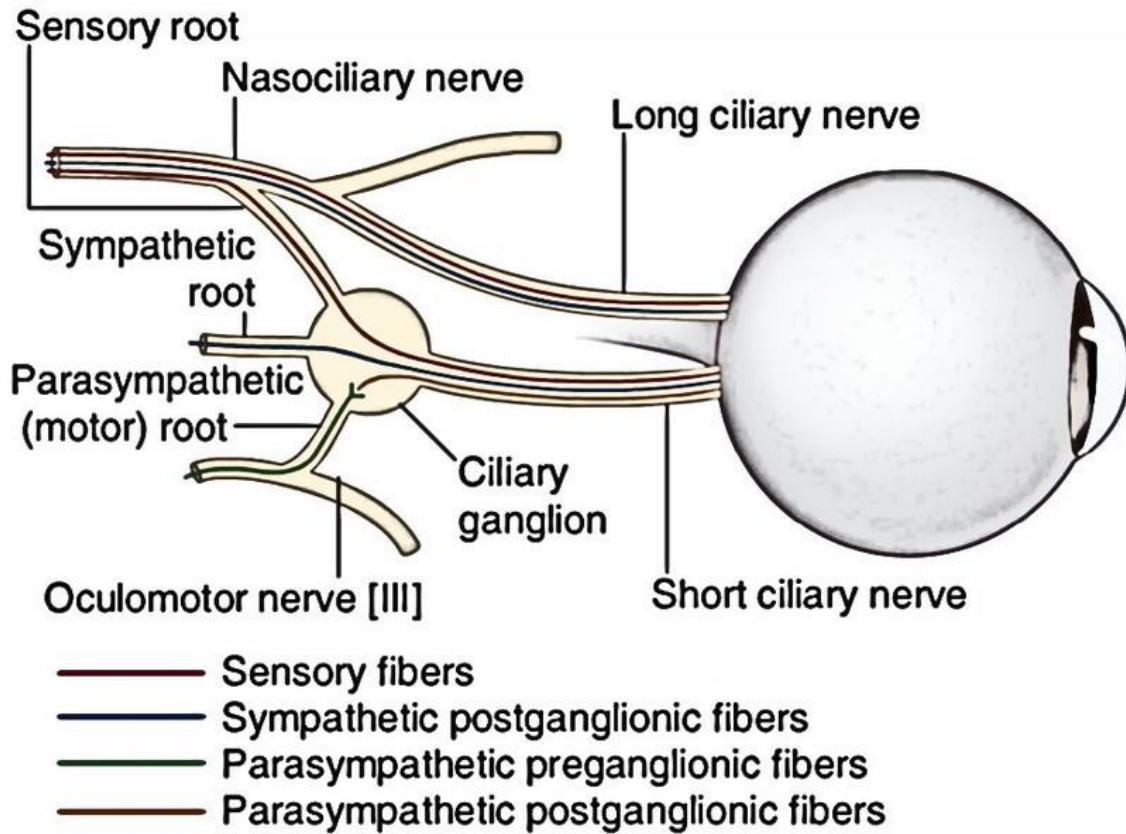
Fig. 11: Anatomical structure of ciliary nerves. (Took and adapted from: https://www.earthslab.com/anatomy/nerves-of-the-orbit/).

Cornea innervating sensory axons are following deeper corneal layers to approach the basal layer where they change direction into a path parallel to the cornea surface. From there they deploy terminal sensory endings to the cornea surface in a perpendicular angle and reach the uppermost layers of the epithelium hardly covered by any tissue (fig.12). There are three types of sensory afferents in the cornea: mechanoreceptors, cold sensitive and polymodal fibres. Histological investigations showed that of these types of fibres are distributed over the entire corneal surface.
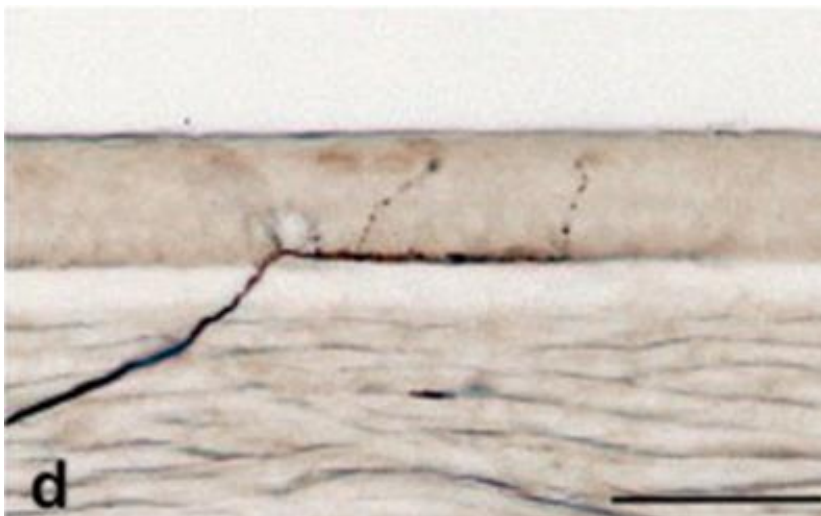

Fig. 12: Terminals of unmyelinated sensory fibre in the cornea (scale 50 µm)

2.6.2 Animal preparation

The heads of guinea were cut and cleaned from skin. Interparietal and parietal skull parts were removed using bone rongeur forceps. Brains were slightly lifted in the frontal part by a spoon and optical tracts were cut after the chiasm. Brains were removed using a spoon. All procedure was performed with repetitive application of physiological solution with glucose. Eyes were dissected from surrounding connection tissue and muscles. Frontal and sphenoid bones were removed by using bone rongeur forceps to free the optic nerves. Eyes with optical nerves were taken out, placed into physiological solution. Electrical ciliary nerve stimulation activate muscles what would generate noise level. Ciliary nerves are on the top of eye surface and be damaged easily. Because of that, some tissue, except muscles, was left on guinea pig eye.

2.6.3 Set up

The cleaned eye was place in an organ bath with a small ring in bottom that was connected to a syringe. Using negative pressure via a syringe the eye fixed. Optic and ciliary nerves were sucked inside a suction electrode that had a silver wire inside. The organ bath was constantly perfused at $4ml*min^{-1}$ flow of physiological solution with glucose and oxygen. The recording glass electrode was filled with physiological solution and was placed on the cornea surface (fig.13). The organ bath had a silver wire inside which served as cathode recording electrode.

During stimulation charge was applied via the stimulation suction electrode. The recording suction electrode was placed on the cornea surface to generate a seal used for recording via a differential amplifier. The signal was amplified 5,000 times amplified, filtered by low-pass 5 kHz filter and digitized.
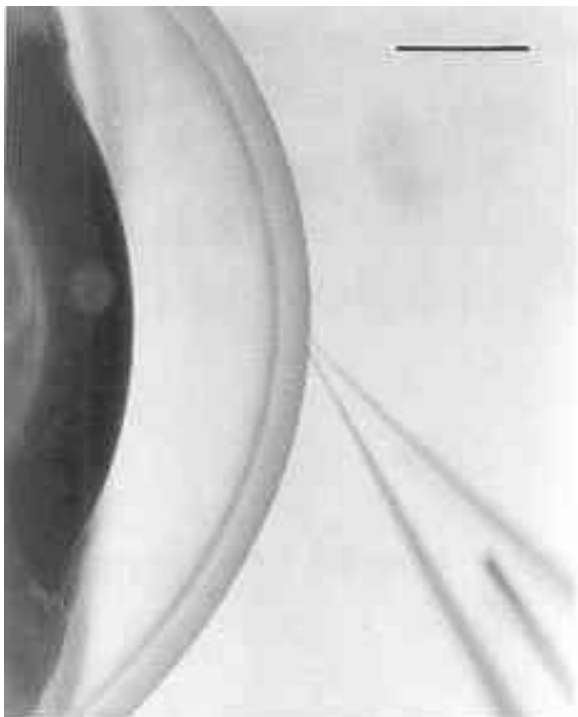

Fig. 13: Recording electrode on cornea surface (scale 500 µm)

2.6.4 Recording protocols and analysis

2.6.4.1 Recordings from terminals
Electrical stimulation and recording was controlled by custom script in Spike2 (CED, Cambridge, UK) for single fibre recordings from sensory nerve terminals in the cornea. Cold receptors have ongoing activity. Because of that electrical stimulation was not needed to investigate these terminals. Sensitivity to temperature was checked by heating from 32-33°C for 1 min and then cooling for 2min. Effect of zeroK on terminals was performed by switching physiological solution to zeroK for at least 1 hr and then switched back to control solution.

2.6.4.2 Statistical analysis of signal recorded in cornea
One minute intervals were analysed as baseline before switching to zeroK solution, then after 15 min and 1 hr of stimulation with zeroK. Occurrence of action potentials was detected and the impulse generation profile was calculated including the interval between action potentials:

$$T(t_n) = t_{n+1} - t_n$$

T – period (time different) between impulses, n – number of impulse.
Spiking probability profiles were generated by plotting impulses generated in specific period in a histogram with 1 min bins:

$$P(T) = n_T/n$$

P – spike generation probability, T – period of impulse generation, n_T– amount of impulses in specific period interval, n – amount of impulses generated in 1min time interval.

2.7 Potassium concentration measurement in extracellular solution

Potassium and other electrolytes measurements was done using blood gas analyser (ABL90 FLEX, Radiometer Medical ApS, Danmark). This device is measuring electrolytes concentrations in 65 µl of blood or other solution using selective permeable membrane and electrodes. Thereby we checked if zeroK solution is washing out potassium ions from axons. Clean sural and sciatic nerves were collected and kept in 0.25 mL eppendorf tubes filled by zeroK solution for 1 hr at room temperature. Solution was collected inside glass pipettes and delivered to blood gas analyser for assessment of ion concentrations.

2.8 Statistics

Fitting, averaging, filtering and others mathematical modifications were done by Igor Pro 7 (WaveMatrics, OR, USA). Impulse detection in recordings from cornea was performed with Spike2 (CED, Cambridge, UK). Multifactorial repeat measures ANOVA and t-tests were done with Statistica 7.1 (StatSoft, Hamburg, Germany).
Bonferroni post-hoc tests were used in multifactorial repeat measures ANOVA to locate significant differences. P values less than 0.05 were deemed statistically significant.

3   RESULTS

3.1   Determinants of axonal C-fibre excitability

C-fibre excitability can be described by different parameters and factors such as electrical threshold, stimulus shape and etc. Traditionally, rectangular electrical stimuli are used whereas no data exist on sinusoidal stimulation. Therefore, initially rectangular stimuli were compared to the sinusoidal stimulation profile.

3.1.1   Temperature effects

Temperature is modulating different factors in neuronal activity, such as conduction speed, action potential duration and others. Thus, temperature effects on C-CAP amplitude and threshold were investigated for rectangular constant current stimulus and compared to the sinusoidal stimulus.

3.1.1.1 Effects on recorded amplitude

Maximal C-CAP amplitude evoked by supra-maximal 50 µA constant current rectangular stimuli at 20, 26 and 32°C was measured (fig.14 left). C-CAP maximal amplitude was depended on temperature. Cooling was increasing C-CAP amplitude induced by constant current rectangular stimulus (1-way repeat measures ANOVA, n=21, 20-26°C p=1, 20-32°C and 26-32°C p<0.01; Bonferroni post hoc). Average maximal amplitudes were 1105±476 µV at 20°C, 1071±432 µV at 26°C, 759±334 µV at 32°C (fig.14 right).
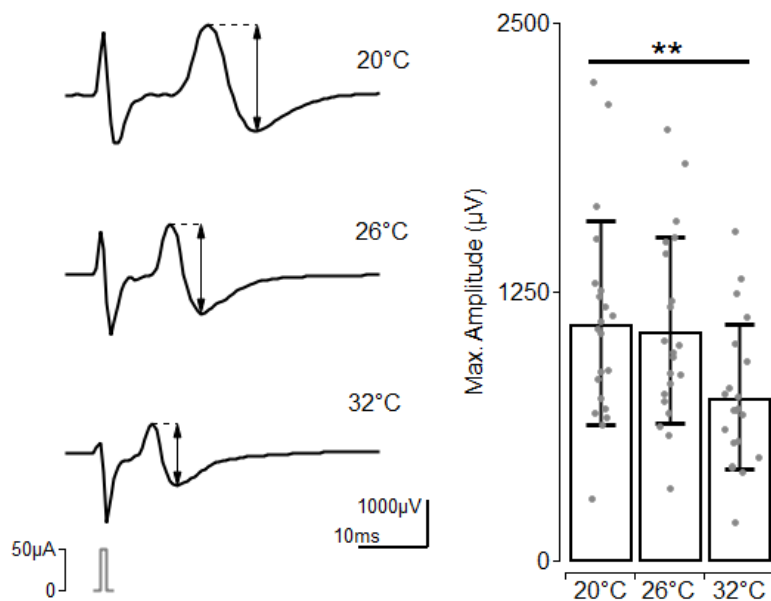

Fig. 14: Temperature effect on maximal C-CAP amplitude evoked by constant current rectangular stimulus. Specimen of CAP signal induced by supra-maximal constant current rectangular stimulus at 20, 26 and 32°C (left). Arrows marks amplitude of signal which is measured as distance between biggest positive and negative C-CAP peaks. Location and shape of supra-maximal rectangular stimulus is marked in bottom. Individual points, averages and standard deviation of pooled data of maximal C-CAP amplitude at different temperatures (right).

3.1.1.2 Effects on excitability

Excitability was tested as electrical stimulus strength to evoke 50% of maximal peak-peak C-CAP amplitude. Excitability testing for rectangular stimulus was done by generating stimulus-response curves at temperatures of 20, 26 and 32°C (fig.15 left). Stimulus amplitude to evoke half-maximal C-CAP amplitude was used to describe electrical threshold (fig.15 left). Amplitude of constant current rectangular stimulus to evoke half-maximal C-CAP amplitude was bigger at colder temperature (fig.15 right) (1-way repeat measures ANOVA, n=21, Bonferroni post hoc 20-26°C and 20-32°C $p < 0.01$, 26-32°C $p = 0.02$). Average current to evoke half-maximal C-CAP amplitude was 6.9±2.9 µA at 20°C, 5.4±1.5 µA at 26°C, 4.2±1.2 µA at 32°C.
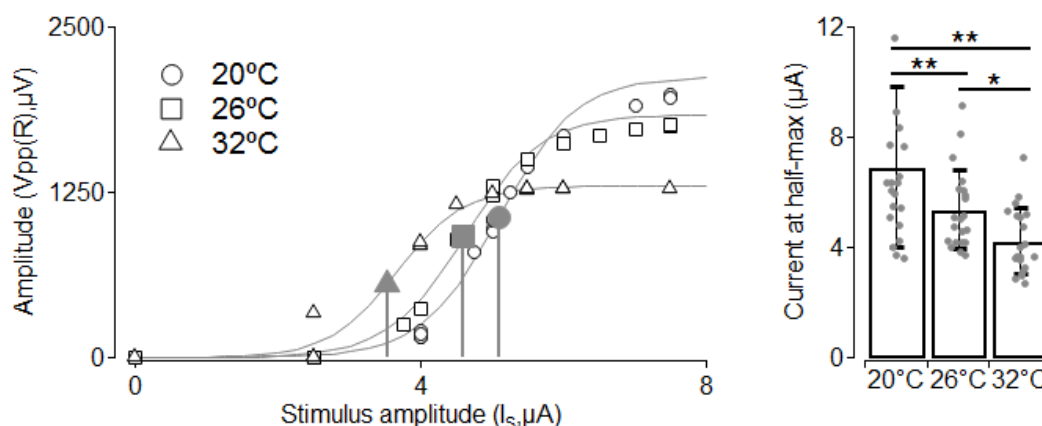

Fig. 15: Determination and quantification of the stimulus-response properties for electrical evoked C-CAP in mouse sural nerve to rectangular stimulus current profile. Stimulus-response curve were generated by giving different amplitude constant current rectangular stimulus and fit points into sigmoidal function (left). Half-maximum current levels for the C-CAP decreased with temperature (left, big grey marks). Pooled data of maximal C-CAP amplitude at different temperatures (right). * $p < 0.05$, ** $p < 0.01$, Bonferroni post hoc test.

3.1.2 Effects of stimulus shape

Electrical sinusoidal stimuli provide a slowly depolarizing current and represent a new paradigm for excitability testing. We compared the classic 1 ms duration rectangular pulse to 4 Hz sine wave stimuli and investigated its potentially different response to temperature changes.

3.1.2.1 Slow depolarizing stimulation

4 Hz sine wave stimuli evoked C-CAP at 20, 26 and 32°C (fig.16 left). Cooling increased maximal C-CAP amplitude evoked by constant current sinusoidal stimulus (fig. 16 right) (1-way repeat measures ANOVA, n=21, Bonferroni post hoc 20-26°C $p = 0.02$, 20-32°C and 26-32°C $p < 0.01$). The average maximal C-CAP amplitude evoked by sine wave stimulus was 853±323 µV at 20°C, 757±277 µV at 26°C, and 553±264 µV at 32°C.
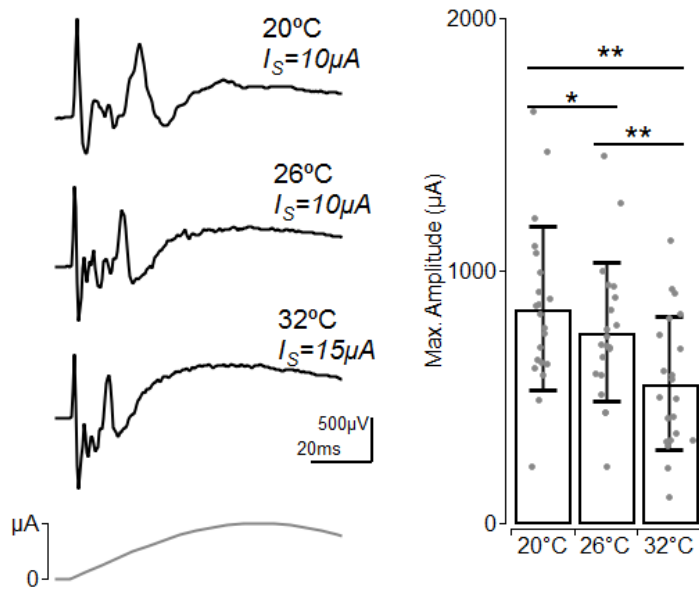
Fig. 16: Temperature effect on maximal C-CAP amplitude evoked by constant current sine wave stimulus. Constant current sine wave stimulus induced C-CAP 20, 26 and 32°C temperatures (left). Shape of stimulus is drawn in bottom. Pooled data of maximal C-CAP amplitude evoked by constant current sine wave stimulus at 20°C, 26°C and 32°C (right). * p<0.05, ** p<0.01, Bonferroni post hoc test.

Excitability testing for sine wave stimuli showed that cooling was shifting stimulus-response curve to the left, i.e. weaker currents were effective at lower temperatures (fig.17 left). It was opposite compared to rectangular stimuli (fig.15). Sine wave stimulus threshold to evoke half-maximal peak-peak C-CAP amplitude was smaller at 20°C than at 26°C or 32°C (fig.17 right) (1-way repeat measures ANOVA, n=21, Bonferroni post hoc all p<0.01). Average sinusoidal stimulus current to evoke half-maximal C-CAP amplitude was 3.1±1.5 µV at 20°C, 6.6±2.7 µV at 26°C and 12.9±3.7 µV at 32°C.
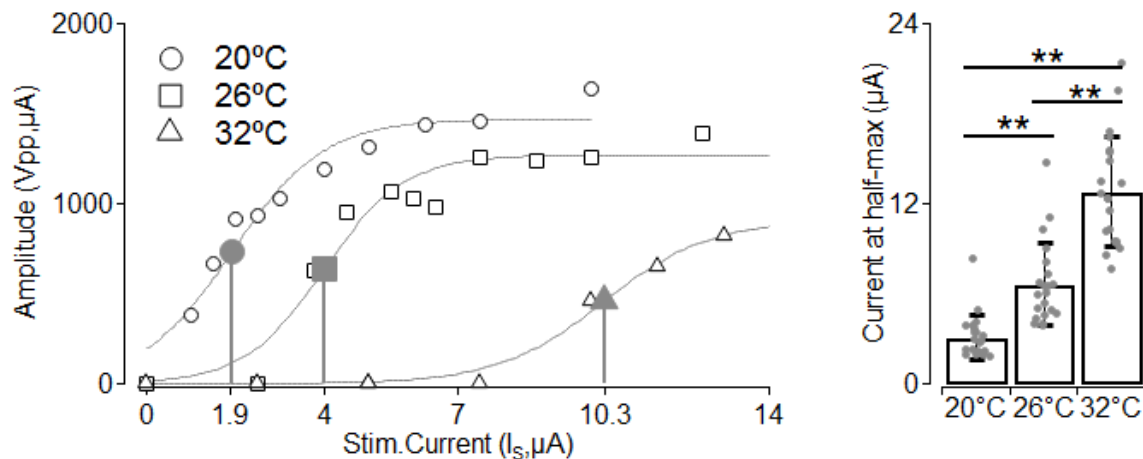

Fig. 17: Determination and quantification of the stimulus-response properties for electrical evoked C-CAP in mouse sural nerve to sine wave stimulus current profile. Stimulus-response curves for constant current sine wave stimulus at three different temperatures (left). Currents to induce half-maximal C-CAP amplitude are marked in grey. Pooled data of current at half-maximal C-CAP amplitude evoked by sine wave stimulus (right) (Repeat measures 1-way ANOVA, ** p<0.01, Bonferroni post hoc).

3.1.2.2 Comparison to standard rectangular pulses

Rectangular and sinusoidal constant current stimulus evoked C-CAP at 20, 26 and 32°C. In order to check if rectangular and sinusoidal stimulus evoked the same C-CAP amplitudes we analysed the ratio of maximal peak-peak C-CAP amplitudes at 20, 26 and 32°C by dividing sine wave evoked maximal C-CAP amplitude by rectangular induced maximal C-CAP amplitude. This ratio of maximal C-CAP amplitudes was smaller than 1 at all three temperatures (fig.18 left). Interestingly, cooling increased this ratio (1-way repeat measures ANOVA, n=21, Bonferroni post hoc 20-26°C p=0.06, 20-32°C p<0.05, 26-32°C p=1). Average ratio of peak C-CAP amplitudes was 0.79±0.12 at 20°C, 0.73±0.12 at 26°C, 0.72±0.13 at 32°C.

Excitability testing showed that cooling had opposite effect on stimulus current to evoke half-maximal C-CAP amplitude for rectangular and sine wave stimuli. The ratio of currents to evoke half-maximal C-CAP amplitudes between sine wave and rectangular stimuli was smaller than 1 at 20°C, but significantly increased at 26°C and 32°C (fig.18 right) (1-way repeat measures ANOVA, n=21, Bonferroni post hoc all p<0.01). Average ratio of currents at half-maximal C-CAP amplitude was 0.50±0.26 at 20°C, 1.24±0.33 at 26°C and 3.15±0.83 at 32°C (fig.18 right).
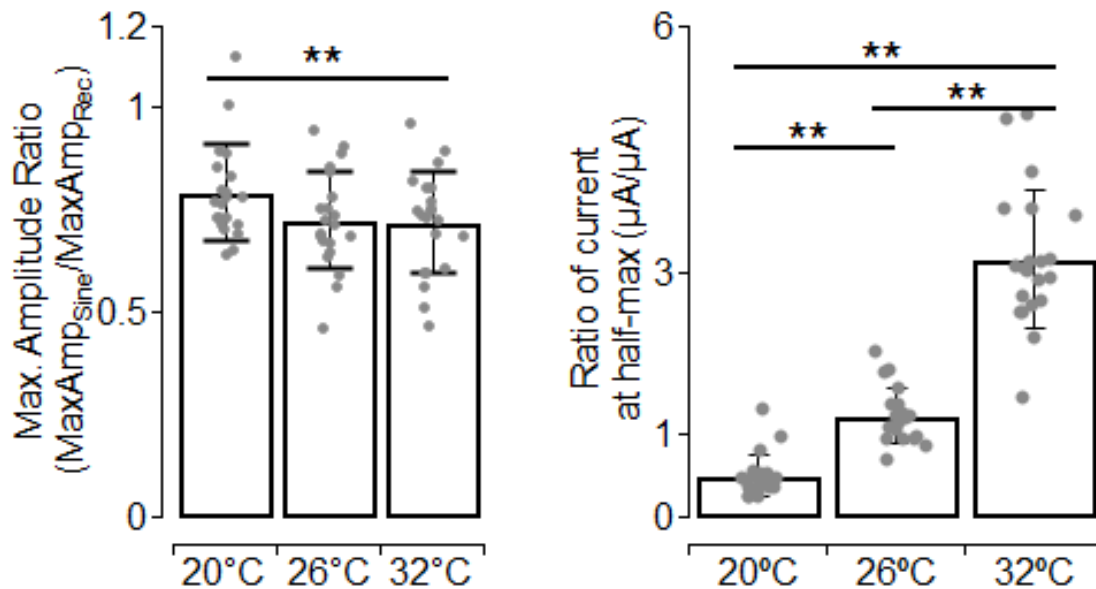

Fig. 18: Quantification of the ratio of rectangular and sine wave evoked C-CAP maximal amplitudes (left) and currents at half-max C-CAP amplitude (right). Maximum amplitudes of C-CAPs increased for sine wave stimulation at lower temperatures, but remained lower than for rectangular stimulation. In contrast, at lower temperatures half-maximum currents were lower for sine wave stimulation and higher at 32°C. Repeat measures 1-way ANOVA, * p<0.05, ** p<0.01, Bonferroni post hoc.

3.1.3 Differential effect of cooling on rectangular vs. sine wave stimulation

Excitability testing showed that cooling was increasing stimulus current for constant current rectangular stimulus, but decreased it for sinusoidal stimulation.

3.1.3.1 Cold receptors influence on stimulus current threshold

Cooling had opposite effect on stimulus current for rectangular and sinusoidal stimulation. This differential effect could have been caused by activation of cold receptors. Therefore, the excitability testing protocol was repeated on nerves after

applying agonists for the cold receptor TRMP8 ((-)-menthol 1 mM or icilin 10 µM) (fig.19). Application of (-)-menthol 1 mM did not generate significant changes for currents to evoke half-maximal C-CAP amplitude for both stimulus profiles (fig.19 A) (3-way repeat measure ANOVA, n=10, menthol factor p=0.215). Interestingly, icilin 10 µM significantly reduced current to evoke half-maximal C-CAP amplitude by sinusoidal stimulus at 26°C (3-way repeat measures ANOVA, n=11, Bonferroni post hoc p<0.05). On other hand, application of (-)-menthol 1 mM or icilin 10 µM did not change the diverting temperature effects on current at half-max for sine wave and rectangular stimuli (fig.19).
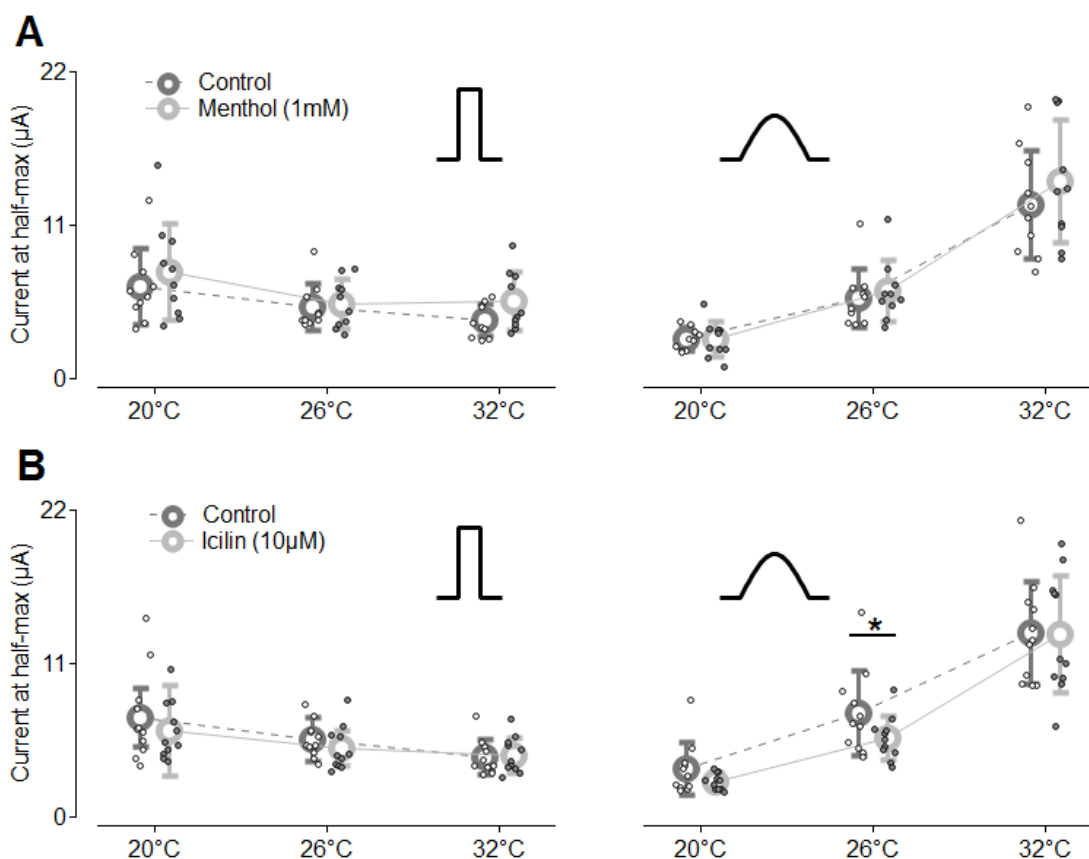

Fig. 19: Quantification of the effect of chemicals TRPM8 agonist (-)-menthol and icilin on current to evoke half-maximal C-CAP amplitude by rectangular (left) and sine wave (right) constant current stimulus. Pooled data comparing stimuli currents to evoke half-maximal C-CAP before (dark grey markers, A&B) and after menthol (1mM, light grey markers, A, n=10) or icilin (10µM, light grey markers, B, n=11). Repeat measures 2-way ANOVA, * p<0.05, Bonferroni post hoc.

3.1.3.2 Dependence of activation threshold on current, latency and charge

The latency between the start of stimulation to the time when 50% of the up-rising positive C-CAP amplitude is reached reflects the conduction delay and it obviously grossly independent of stimulus intensity for rectangular stimuli, but is increasing at lower temperatures (fig. 20 A&D left). Interestingly, there was strong sine wave evoked C-CAP latency modulation by stimulus intensity (fig.20 A&D right). The rectangular pulse is assumed to induce the local action potential immediately with the initial depolarization and the C-CAP latency is conduction delay needed to conduct the action potential to the recording site. When corrected for this C-CAP latency the

sine wave induced CAP shows a clear dependence on intensity (fig.20 B&E): the lower the stimulus amplitude the longer the corrected latency became. Moreover, modulation was more pronounced at colder temperature with latencies of up to 30 ms. Adding to that, all sinusoidal stimulus evoked C-CAP were induced in uprising phase of sine wave stimulus (fig.20 C&F).
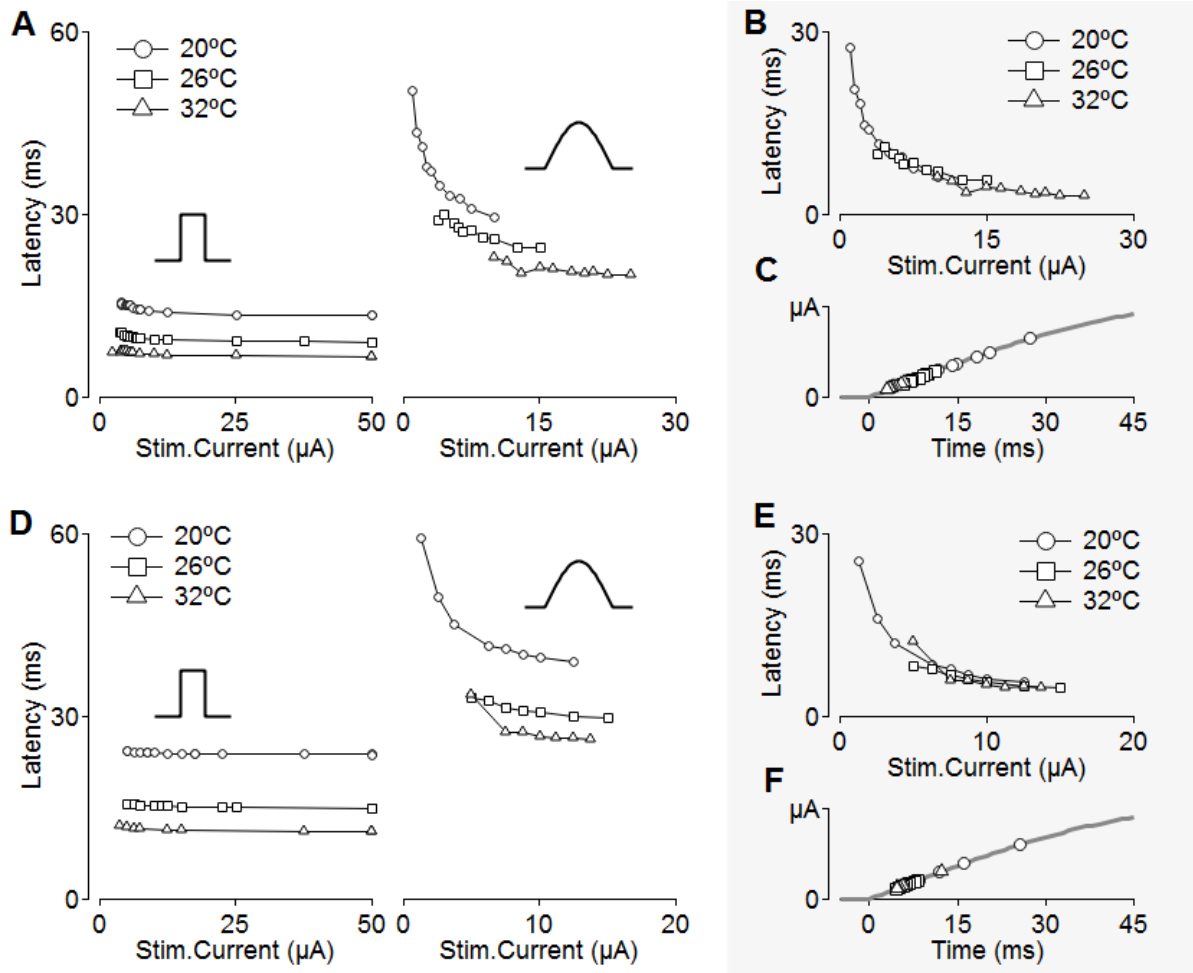

Fig. 20: Determination and quantification of the C-CAP latency in mouse sural nerve to rectangular and sine wave stimulus current profiles. Two specimen of C-CAP latency evoked in the same nerve by rectangular (A, left) and sine wave (A, right) constant current stimuli. Corrected latency (B) was calculated by subtracting conduction latency from sine wave C-CAP latency (A, right). Time of assumed induction of the local action potential is projected on the shape of the actual sine wave stimulus profile for the different temperatures (C). D,E,F: second specimen, stimulation identical to A, B, C.

The corrected latency allowed calculating the current that was applied when the local action potential was initiated by the sine wave stimulus. This threshold current initiating the local action potential was higher for shorter stimulation times (fig.21 left). Stronger stimuli triggered C-CAP at a shorter time, but with stronger currents (fig.21 right). At colder temperature higher currents were required (fig.21 left).
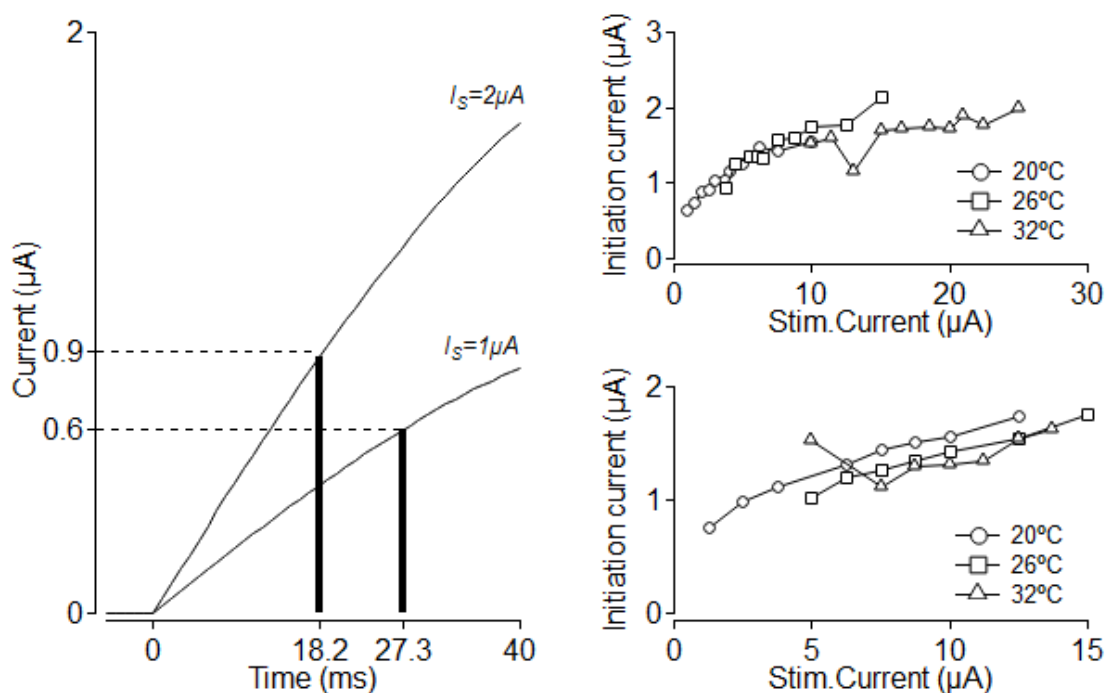
Fig. 21: Determination and quantification of the threshold current required to initiate local action potentials ("initiation current") in mouse sural nerve. Specimen of two different current calculations from the same nerve fascicle at 20°C (left). Two examples of current at C-CAP initiation moment (corrected latency) at 20°C, 26°C and 32°C (right).

Depending on the charge delivered by rectangular constant current stimuli the amplitude of the C-CAP increased. This relation was fitted with a sigmoidal function (fig. 22 C). Charge to evoke half-maximal C-CAP amplitude by rectangular stimuli increased by cooling (1-way repeat measures ANOVA, n=21, Bonferroni post hoc 20-26°C and 20-32°C p<0.01, 26-32°C p=0.02) (fig.22 E). Charge at half-max was 6.9±2.9 nC at 20°C, 5.4±1.5 nC at 26°C and 4.2±1.2 nC at 32°C for the rectangular stimulus.

The charge delivered by the sinusoidal stimuli to initiate local action potentials was calculated using the corrected latency. Interestingly, there was no correlation between stimulus amplitude and C-CAP amplitude; it rather appeared that a certain charge was required to initiate the local action potentials. This charge would be reached earlier for higher amplitude sine waves. Thus, we did not observe a correlation between C-CAP amplitude and charge (fig.22 D). On other hand average charge delivered by sinusoidal stimulus was depended on temperature (fig.22 F). Cooling was increasing charge values required to initiate action potentials by the sinusoidal stimulus (1-way repeat measures ANOVA, n=21, Bonferroni post hoc 20°C-26°C p=0.02, 20°C-32°C p<0.01, 26°C-32°C p=0.48). Average charge delivered by sine wave was 12.5±6.1 nC at 20°C, 9.5±4.3 nC at 26°C and 8.1±3.4 nC at 32°C.
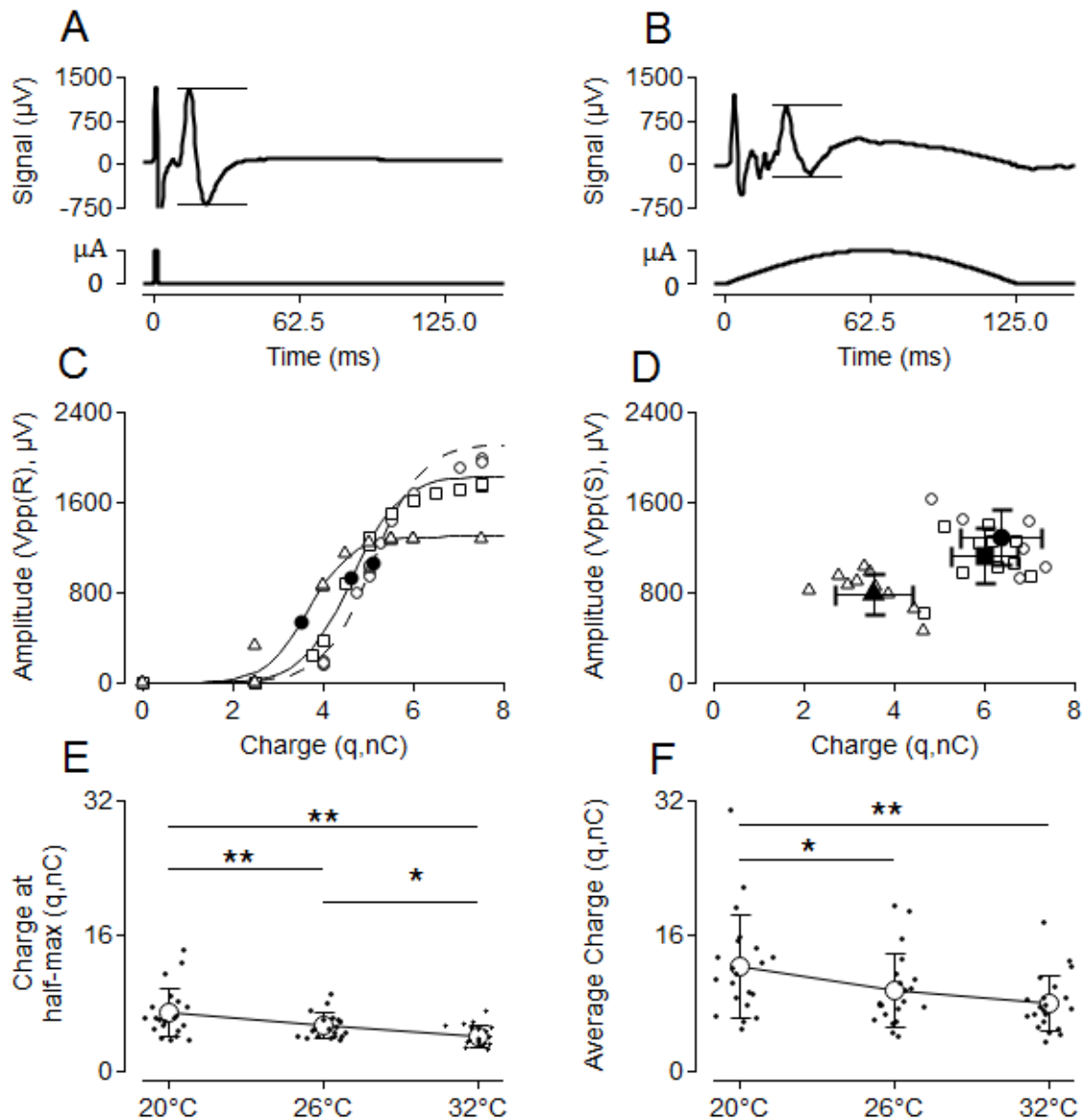
Fig. 22: Determination and quantification of the charge required for action potential initiation by rectangular and sine wave constant current stimulus in mouse sural nerve. Conduction delay was described as C-CAP latency induced by supra-maximal constant current rectangular stimulus (A) and it was used as correction for sine wave induced latency (B). For rectangular stimulation C-CAP amplitudes increase with delivered charge (sigmoidal fit) (C); charge required to evoke half-maximal C-CAP amplitude are marked by black dots, C). Charge that was delivered by sine wave stimulus up to C-CAP initiation moment (corrected latency) were averaged for stimuli amplitude in the interval [2.5, 20] µA (dark symbols, D). Pooled charge at half-maximal C-CAP amplitude for rectangular stimulus (E, n=21) and average charge for sine wave stimulus (F, n=21) are shown. Repeated measures ANOVA, Bonferoni post-hoc tests * p<0.05 and ** p<0.01.

The TRPM8-agonists (-)-menthol (1 mM) and icilin (10 µM) were used to check for any effects that the cooling might have exerted via activation of the cold sensitive channel TRPM8. Thus, charge values required to initiate action potentials by rectangular and sinusoidal stimuli were compared before and after stimulation. However, there were no significant effects of TRPM8 activation on charge threshold for both stimuli (3-way repeat measures ANOVA, n=10, menthol factor p=0.184, 3-way repeat measures ANOVA, n=11, icilin factor p=0.328) (fig. 23).
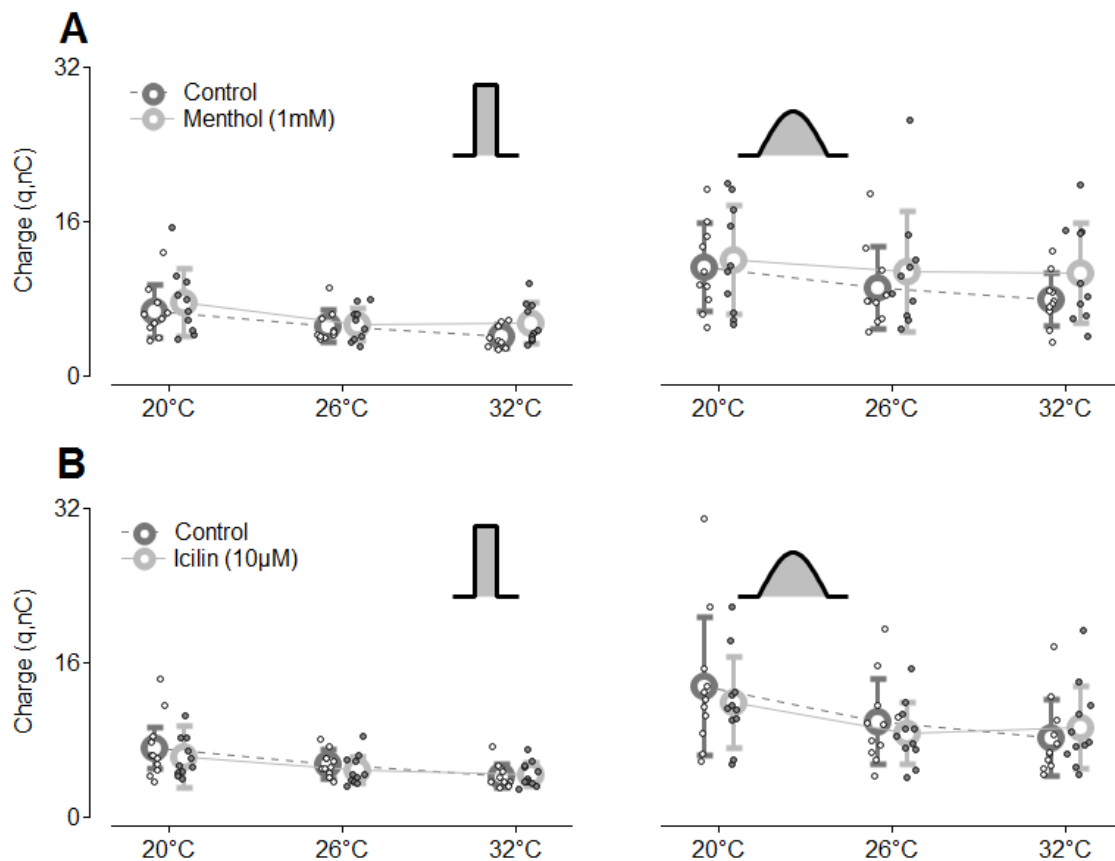

Fig. 23: Quantification of the effect of the TRPM8 agonists (-)-menthol and icilin on charge at half-maximal C-CAP amplitude evoked by rectangular (left) and average charge for sine wave (right) constant current stimulus. (-)-menthol (1mM, A) and icilin (10µM, B) were used to activate cold receptors TRPM8. TRPM8 activation did not change charge thresholds for either stimulus profile.

3.1.3.3 AUC values

Sine wave stimulus evoked C-CAP area under the curve (AUC) was similar to the one induced by rectangular pulses at 20°C, but smaller at 26°C and 32°C (fig.24 B). The ratio of AUC between rectangular and sine wave stimuli induced C-CAP showed that both stimulus profiles induced the same AUC at 20°C, but sine wave evoked C-CAP AUC was smaller at 26°C and 32°C (fig.24 C). Warming significantly reduced ratio values (1-way repeat measures ANOVA, n=21, Bonferroni post hoc 20-26°C and 20-32°C $p<0.01$, 26-32°C $p=1$). The average AUC ratio was 1.03 ± 0.10 at 20°C, 0.89 ± 0.13 at 26°C and 0.87 ± 0.12 at 32°C.
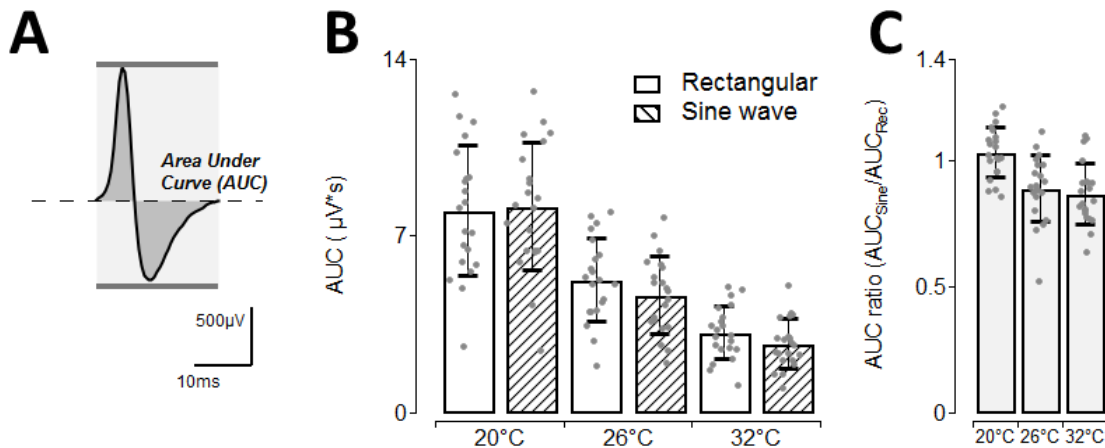
Fig. 24: Determination and quantification of C-CAP area under the curve (AUC) that was evoked by supra-maximal rectangular and sine wave constant current stimulus in mouse sural nerve. Area under the curve (AUC) was calculated according to the schematic view in (A). Pooled data of AUC induced by supra-maximal rectangular and sine wave constant current stimulus are shown for three different temperatures (B) and ratio between rectangular and sine wave induced C-CAP AUC are depicted for the three temperatures in (C).

3.1.3.4 Effects of TTX

CTX at 20 µM was used to block A-fibres and leave only C-fibres conducting thus producing a clearer C-CAP signal (fig. 25 A&C). Application of CTX at 20 µM did not change the maximal C-CAP amplitude (2-way repeat measures ANOVA, n=6, CTX factor p=0.107) or AUC (2-way repeat measures ANOVA, n=6, CTX factor p=0.782) for rectangular and sine wave stimulus at 20°C (fig. 25 B&D). In contrast, TTX at 10 µM nearly abolished the C-CAP signal.
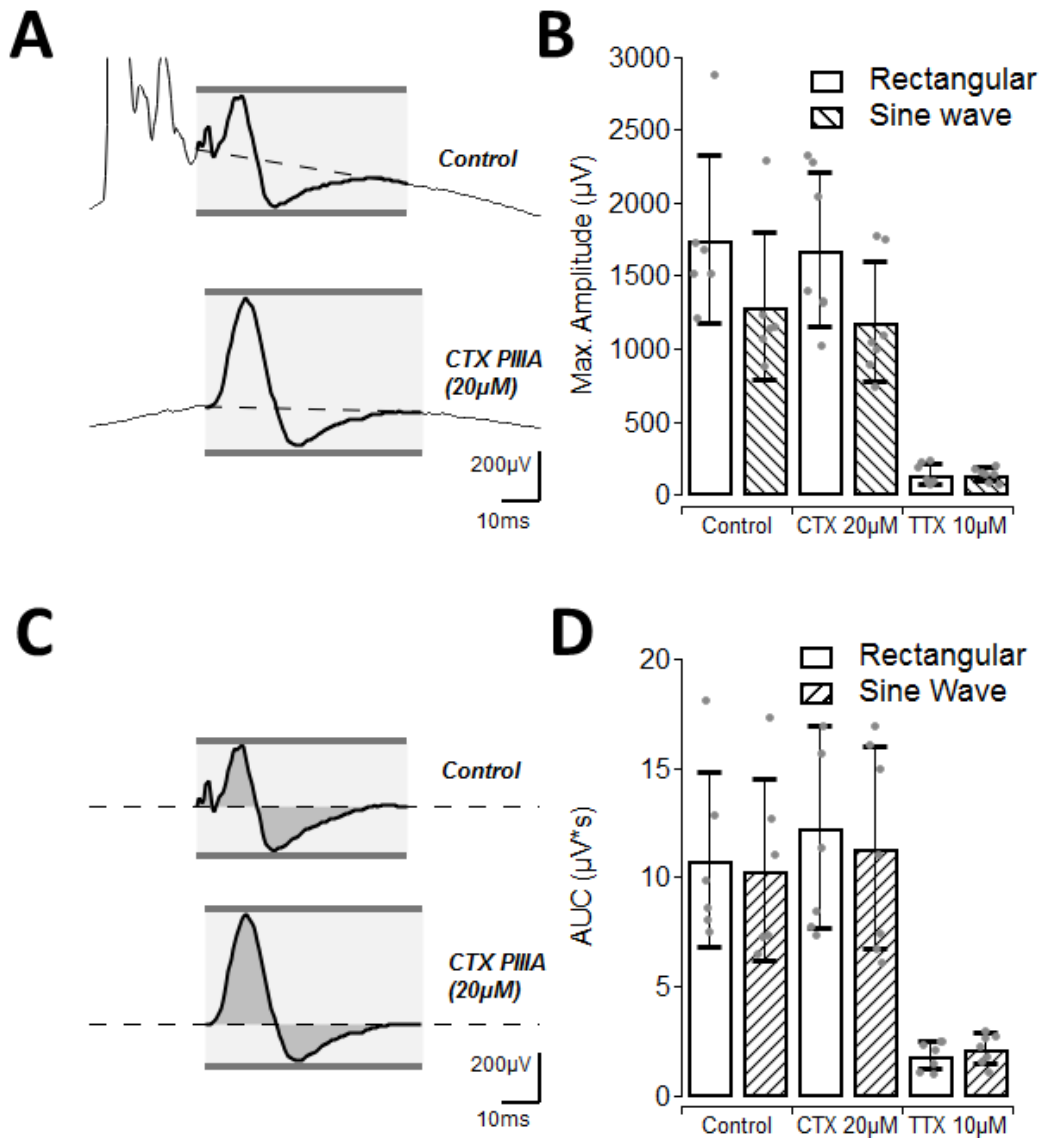
Fig. 25: Quantification of CTX and TTX effects on C-CAP maximal amplitude and area under the curve (AUC) that was evoked by supra-maximal rectangular and sine wave constant current stimulus in mouse sural nerve. Specimen of C-CAP before (D, top) and after CTX (20 µM, D, bottom). Dashed lines shows baseline that was removed before calculations. Pooled data of maximal C-CAP amplitude evoked by rectangular and sine wave stimulus in control situation, after treating with 20 µM CTX and 10 µM TTX.

TTX at 10 µM massively reduced the C-CAP amplitude and thus shifted the stimulus-response curve downward and to the right (fig.26 A). Moreover, it increased C-CAP latency (fig. 26 B). CTX (20 µM) improved signal noise ratio for the C-CAP signal and was used as control for investigating TTX 10 µM effect on long latency C-CAPs

induced by sine wave stimulation. Small amplitude C-CAPs were identified when reducing sine wave stimulus intensity (fig.26 C&D). Average corrected longest latency of C-CAPs was 51.2±10.6 ms after CTX (20 µM) and 50.4±9.3 ms after adding TTX (10 µM). Thus, blocking TTX-S channels did not change the time required to initiate C-action potentials (fig.26 H) (pair t-test, n=7, p=0.97), albeit stimulation intensity was increased.
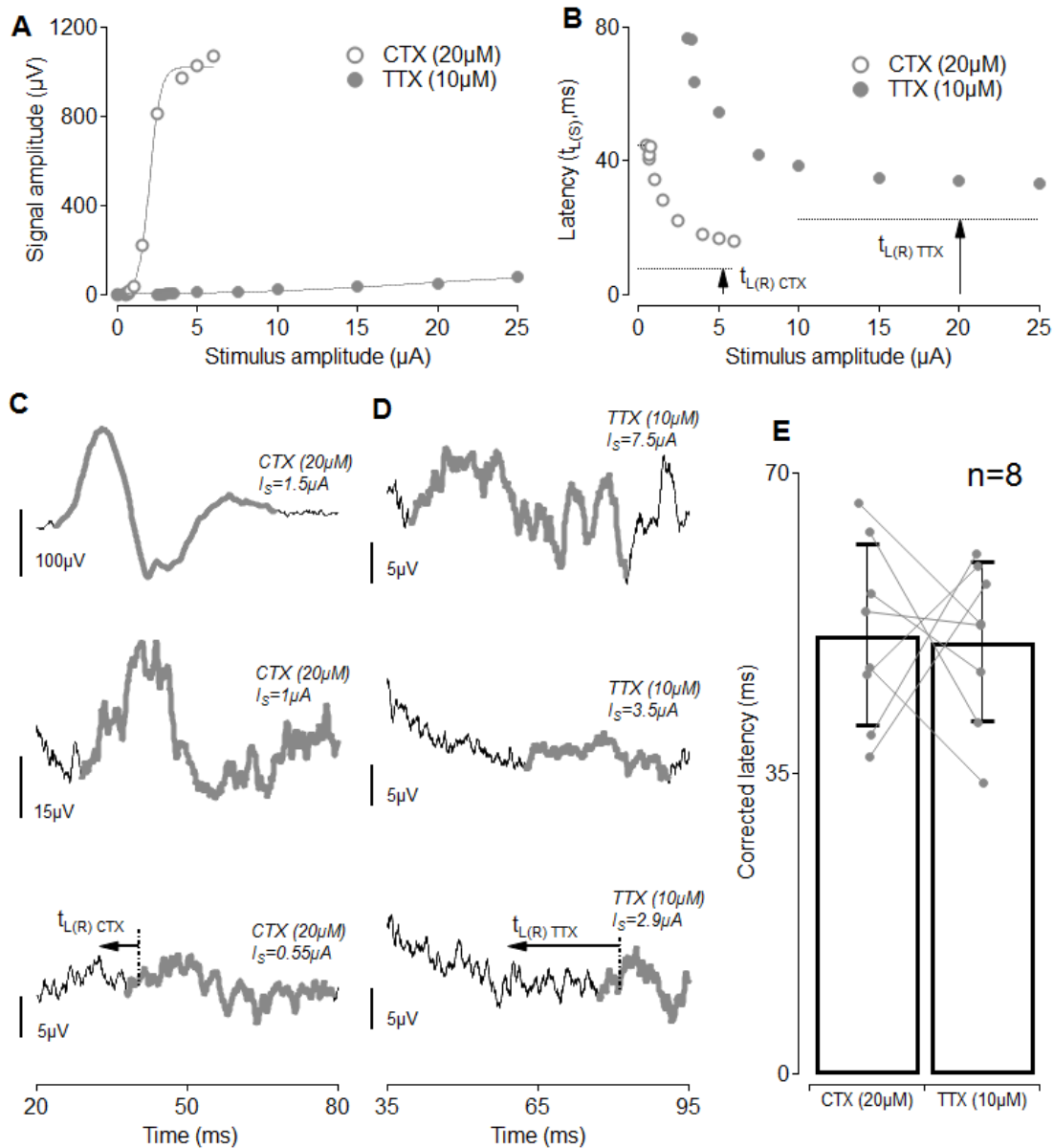
Fig. 26: Investigation of TTX (10 µM) effects on long latency C-CAPs evoked by sine wave stimuli at 20°C. Specimen of stimulus-response curves for amplitude (A) and latency (B) after treatment with CTX (20 µM, grey open circles, and TTX (20 µM, grey filled circles. Conduction delay was normalized by the C-CAP latency induced by rectangular pulses after CTX ($t_{L(R)\,CTX}$) and TTX ($t_{L(R)\,TTX}$) treatment (C,D lower panel). CTX (20 µM) completely blocked the A-CAP. Gradual reduction of sine wave stimulus intensity decreased C-CAP amplitude after treating with CTX (C) and TTX (D). At the stimulation threshold low amplitude C-CAPs at high latencies were recorded, but latencies did not differ between CTX and TTX treatment (E).

3.2 Depletion of extracellular potassium ions as model for spontaneous activity in nociceptors

In single fibre ex-vivo recordings in the skin-nerve preparation our group found that the application of solutions with low potassium concentration to nociceptive nerve endings induced ongoing activity in C-fibres (data not shown) that lasts for hours. We set out to investigate excitability changes induced by this stimulus using thresholds tracking. Thus, we replaced the potassium in our stimulation solutions ("zeroK") and assessed the time course of excitability changes in the axon.

3.2.1 Time course of zeroK-induced CAP changes

Using induced compound action potential recordings ongoing activity of axons cannot be directly assessed. On other hand, this method allows to investigate excitability changes of the axonal membrane that are supposed to underlie ongoing activity. Thus, we recorded the time course of excitability changes after application of extracellular solution with low potassium ion concentration.

3.2.1.1 Amplitude, latency and excitability changes following zeroK
Parameters that were monitored following stimulation with low potassium:
- Shape of C-CAP
- C-CAP amplitude
- C-CAP latency
- Excitability index (non-conditioned vs. conditioned current)

In addition, we systematically assessed the effects of temperature. Low potassium stimulation commenced when readings of the above listed parameters were stable. Excitability index was calculated directly after experiment and was used as one of parameter to check the quality of recording. Excitability index was calculated as ratio of non-conditioned / conditioned current in %.

Initially, low potassium was applied for 60 minutes. However, in many recordings C-CAP signal was completely lost by 30 min of zeroK. Therefore, the protocol was modified such that zeroK application was stopped when the C-CAP amplitude was reduced to noise level and perfusion was switched back to physiological solution.

The following changes were observed after zeroK application (fig.27):
- progressive drop in C-CAP amplitude
- increase in C-CAP latency
- rapid initial increase in conditioned current and excitability index
- slow gradual increase in non-conditioned current

All these changes were reversible by switching back solutions to normal potassium concentration ($[K^+]_e$= 3.2mM).
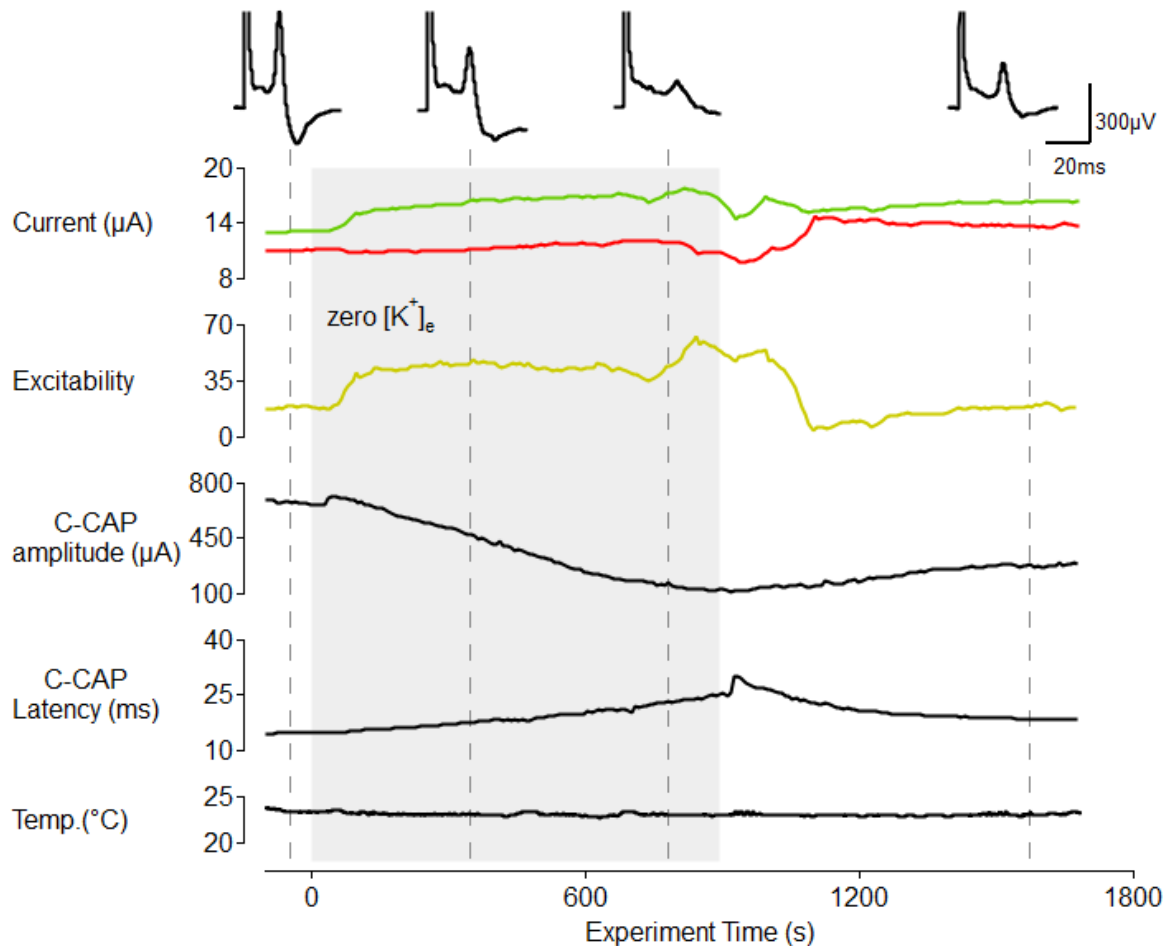
Fig. 27: Example of zeroK experiment. Physiological solution was switched to perfusion with zeroK (grey area) for about 15 minutes and back to normal (white area). Specimen of supra-maximal constant current rectangular stimulus evoked CAP (top panel) are shown on top – dashed lines indicate the time when they were recorded. Non-conditioned (red line) and conditioned currents (green line) required to induce 50% of the C-CAP were used to calculate the excitability index (dark yellow line). Time course of C-CAP amplitude and latency are shown in the lower traces.

Under control conditions, we observed a gradual decline of C-CAP amplitude during the 30 min observation period ($[K^+]_e$= 3.2mM). Upon stimulation with zeroK this reduction was massively facilitated (fig.28 A) ($p<0.01$, repeated measures 2-way ANOVA, n= 6, 7, 11, 9). On other hand, the kinetics was temperature independent ($p=0.822$, repeated measures 1-way ANOVA, n=11, 9). This progressive C-CAP amplitude reduction fitted well to a single exponential function. The time constant τ (time interval in which C-CAP lost 63% of its starting amplitude) was assessed for the two temperatures. Average C-CAP amplitude reduction time constant τ was 432.1±82.9 s at 26°C and 394.6.89±177.1 s at 32°C in zeroK solution (fig.28 B) ($p=0.538$, unpaired t-test, n=11, 9).
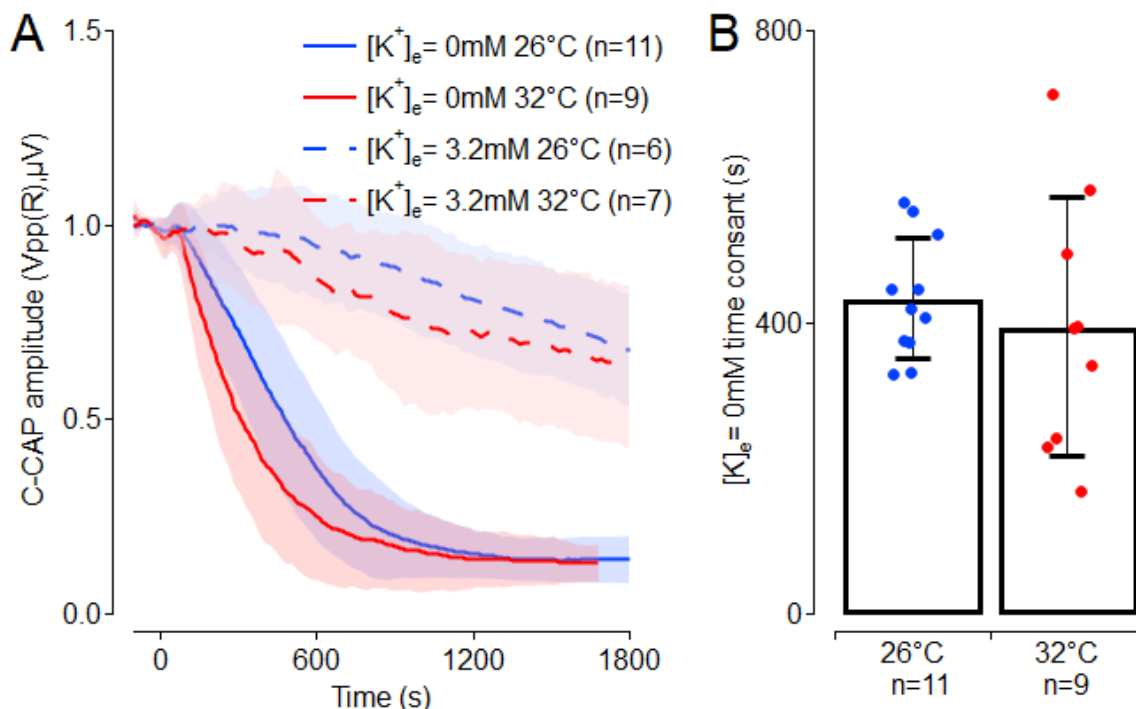
Fig. 28: C-CAP amplitude reduction by zeroK is faster at higher temperatures. Average of normalized amplitude reduction in zeroK and normal ($[K^+]_e$= 3.2mM) solution (dashed line) (A). Standard deviation is presented as light red and light blue area. Note rapid decline induced by low potassium and also faster decline at higher temperatures. In (B) time constants τ for the reduction of C-CAP amplitudes at 26 and 32°C following zeroK application are shown.

Latency of C-CAP in normal ($[K^+]_e$= 3.2mM) physiological solution was stable for 30 min (fig. 29). Upon zeroK application latency significantly increased (p<0.01, repeated measures 2-way ANOVA, n=11, 9, 6, 7), but without a significant temperature effect (p=0.977, same test).
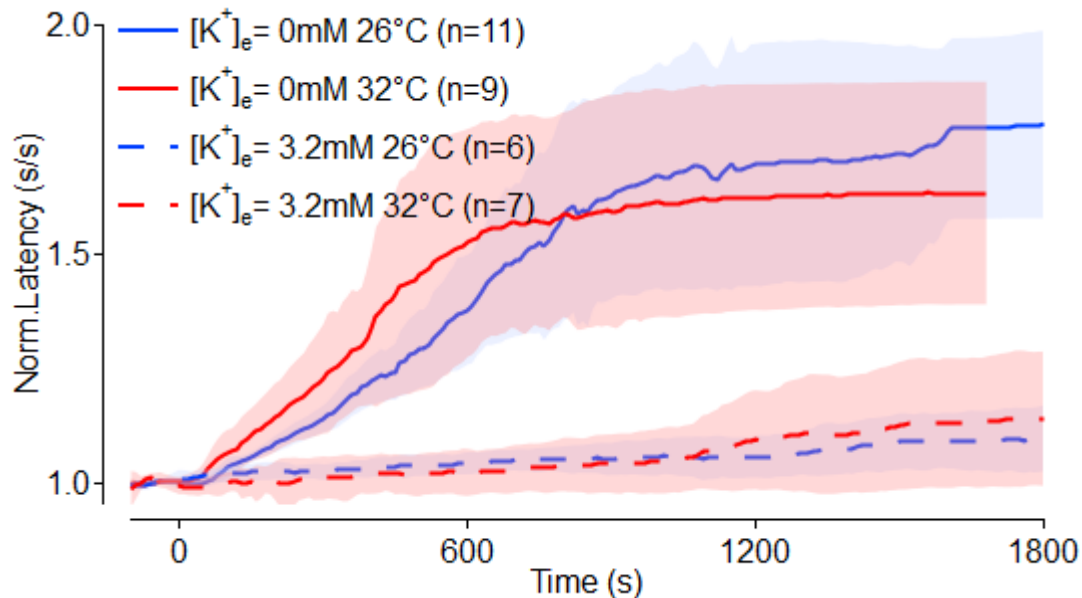
Fig. 29: Average of normalized latency of normal physiological solution (dashed line) and zeroK at 26°C (blue) and 32°C (red). Standard deviation is presented as light red and light blue area.

Zero K generated a rapid increase in excitability index, which was followed by a plateau phase (p<0.01, repeated measures 2-way ANOVA, n=11, 9, 6, 7). The initial increase was temperature independent (fig.30) (p=0.787, same test). From this plateau excitability index gradually declined again after about 10 min of application. Under control conditions the excitability index remained stable.
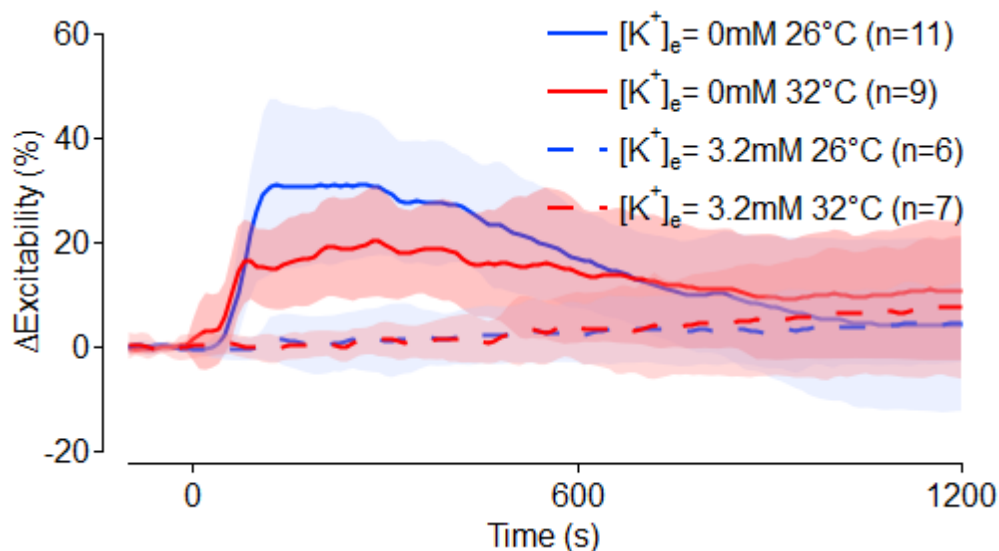
Fig. 30: Time course of excitability index for control conditions (dashed line) and zeroK at 26°C (blue) and 32°C (red) . Standard deviation is presented as light red and light blue area.

3.2.1.2 Effect of sodium potassium pump on CAP amplitude and excitability

As the Na^+/K^+-ATPase depended on extracellular potassium we compared it block by ouabain (0.1 mM) with zeroK. Ouabain reduced C-CAP amplitude (fig. 31), but much slower than zeroK did (p<0.01, repeated measures 2-way ANOVA, n=11, 9, 6, 6). Time constants of amplitude reduction were 2502.7±1072.6 s at 26°C and 1705.9±1053.4 s at 32°C in solution containing 0.1mM ouabain. This amplitude reduction was much smaller comparing to zeroK: 432.1±82.9 s at 26°C and 394.6.89±177.1 s at 32°C (p<0.01, 2-way ANOVA, n=11, 9, 6, 6). When ouabain (0.1 mM) was added to the zeroK application there was no additional effect (fig.31) (p=0.217, repeated measures 2-way ANOVA, n=11, 9, 7, 6). Time constants of amplitude reduction were 403.4±320.6 s at 26°C and 510.3±345.8 s at 32°C. These numbers were very close to zeroK solution time constants (p=0.538, 2-way ANOVA, n=11, 9, 6, 6). On other hand, there were no significant temperature effect on amplitude reduction (p=0.200, repeated measures 2-way ANOVA, n=11, 9, 6, 6, 7, 6).
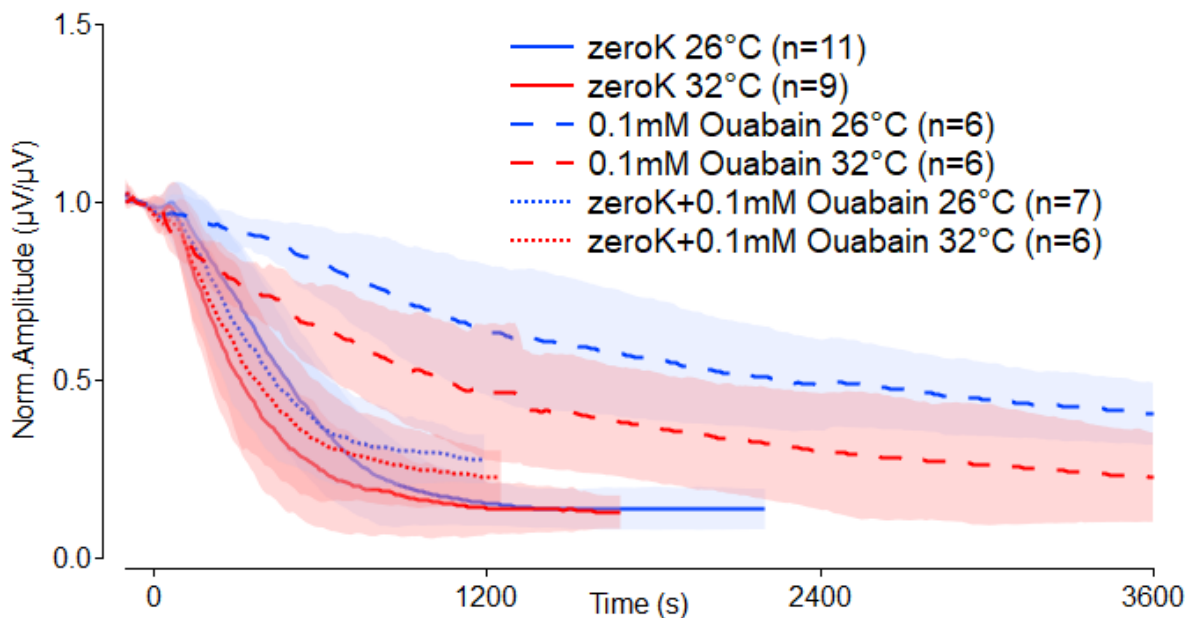
Fig. 31: Average of normalized C-CAP amplitude reduction during block of Na^+/K^+-ATPase activity using ouabain (0.1mM, dashed line), zeroK (straight line) or combination of both (pointed line) at 26°C (blue) and 32°C (red). Standard deviation is presented as light red and light blue area.

Application of ouabain (0.1mM) did not generate the initial increase in excitability as did zeroK (fig. 32) (p<0.01, repeated measures 2-way ANOVA, n=11, 9, 6, 6). When ouabain was added to zeroK stimulation the initial increase of the excitability index was unchanged (p=0.119, repeated measures 2-way ANOVA, n=11, 9, 7, 6).
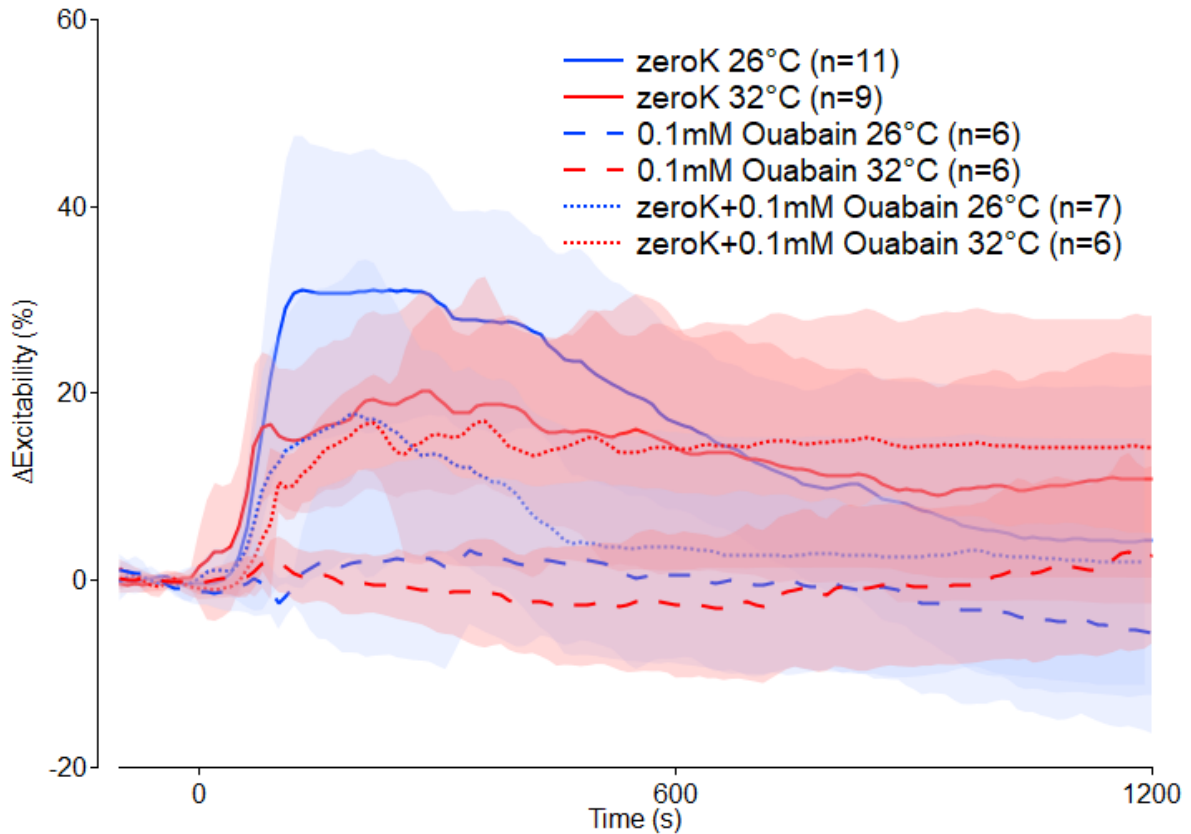
Fig. 32: Average of excitability index shift during block of Na$^+$/K$^+$-ATPase activity using ouabain (0.1mM, dashed line), zeroK or combination of both (dotted line) at 26°C (blue) and 32°C (red). Standard deviation is presented as light red and light blue area.

3.2.1.3 Effects of sodium channel NaV1.9

Mice deficient in their expression of the voltage sensitive sodium channel NaV1.9 (NaV1.9$^{-/-}$ mice) were tested to investigate the role of this sodium channel in the excitability changes. In NaV1.9$^{-/-}$ mice zeroK gradually reduced C-CAP amplitude, but this reduction was much slower than in wild type mice (fig. 33 A) (p<0.01, repeated measures 1-way ANOVA, n=11, 5). The time constant of amplitude reduction in Na$_V$1.9$^{-/-}$ animals during zeroK application was only 2264.0±652.2 s as compared to 394.6.89±177.1 s at 32°C in WT (p<0.01, unpaired t-test, n=9, 5). Interestingly, the kinetics of C-CAP reduction in NaV1.9$^{-/-}$ mice at zeroK resembled the one observed when Na$^+$/K$^+$-ATPase was blocked by ouabain (0.1 mM) in control solution and wild type mice (fig. 33 B). Time constant of amplitude reduction evoked by ouabain in WT was 2502.7±1072.6 s at 26°C and 1705.9±1053.4 s at 32°C.
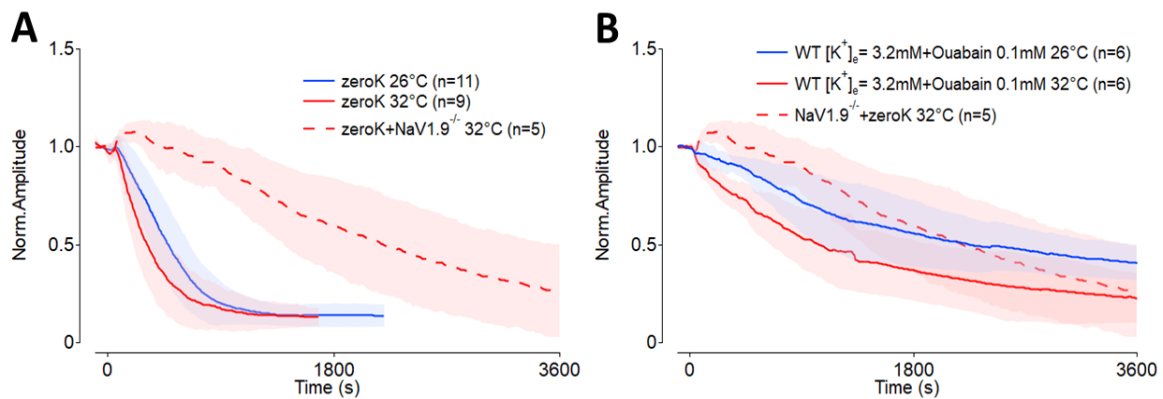
Fig. 33: Quantification of NaV1.9 influence on C-CAP amplitude during zeroK. Average of normalized C-CAP amplitude reduction during zeroK in WT (straight line, A) and NaV1.9$^{-/-}$ (dashed line, A) mice. Average of normalized C-CAP amplitude reduction during physiological solution in combination with ouabain (0.1mM, straight line, B) and NaV1.9$^{-/-}$ mice in zeroK (dashed line, B). Standard deviation is presented as light red and light blue area.

In contrast to the clearly reduced effect on amplitude, the initial changes of the excitability index were unaffected in NaV1.9$^{-/-}$ mice. The initial rapid increase of excitability index observed after zeroK application was unchanged when compared to wild type mice (fig. 34) (p=0.108, repeated measures 1-way ANOVA, n=11, 5).
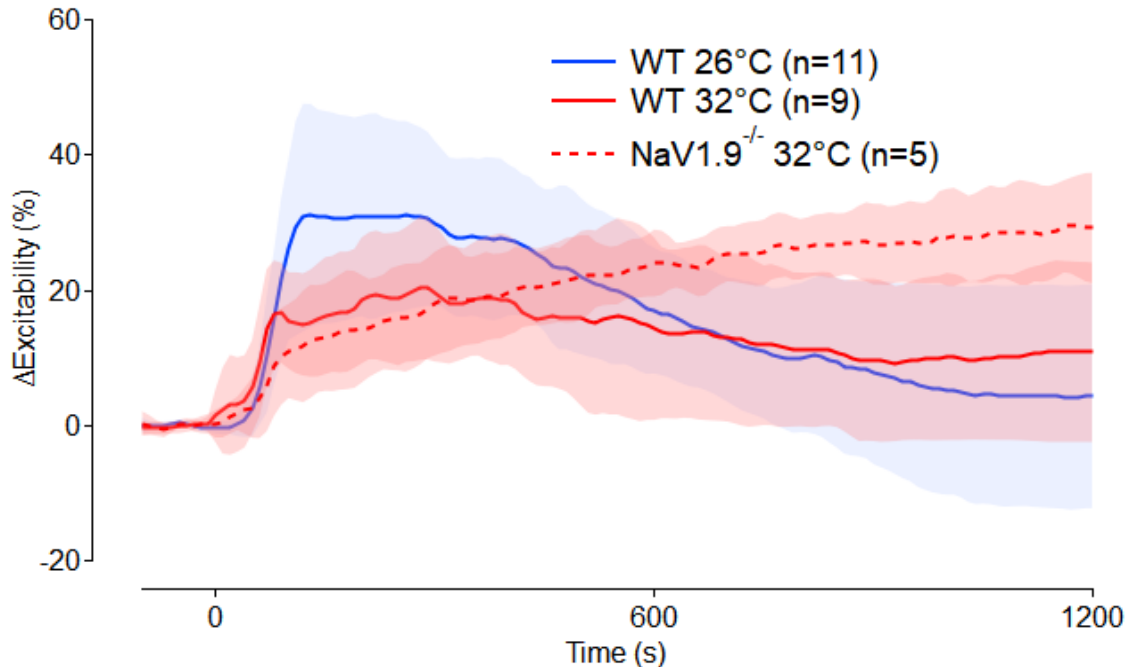
Fig. 34: Kinetics of excitability index in NaV1.9[-/-] (dashed line) mice in zeroK. Standard deviation is presented as light red and light blue area.

3.2.1.4 Effect of sodium gradient on C-CAP amplitude during zeroK

In order to test the effect of sodium concentration gradients, we exchanged 50% of extracellular sodium ions into choline or lithium thereby reducing the extracellular sodium concentration from 138 to 69 mM. At 50% of the extracellular sodium concentration C-CAP amplitude gradually declined independent to temperature (fig.35 A) (p=0.292, repeated measures 1-way ANOVA, n=6, 6). The rapid reduction of C-CAP induced by zeroK was not reduced by lower extracellular sodium concentration, both when choline (fig.35 B) (p=0.425, repeated measures 1-way ANOVA, n=11, 6) or lithium (fig.35 C) (p=0.285, repeated measures 1-way ANOVA, n=11, 8) were used. It is important to keep in mind that amplitude reduction caused by reduced sodium ion gradient (fig.35 A) was not compensated in these calculations. Observed amplitude reduction was combined effect of reduced sodium concentration gradient and accumulation. Time constants of amplitude decline were 432.1±82.9 s for zeroK, or 800.6±420.5 s in combination with choline (p=0.011, unpaired t-test, n=11, 6) or 881.2±350.8 s with lithium (p<0.01, unpaired t-test, n=11, 8).
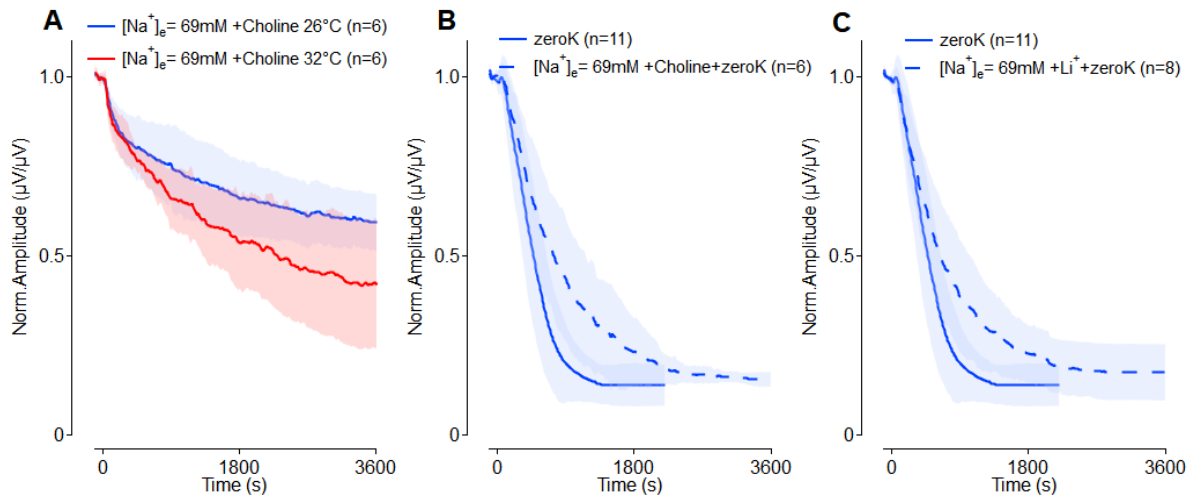
Fig. 35: Quantification of reduced sodium concentration in physiological solution effect on C-CAP amplitude. Average of normalized C-CAP amplitude reduction in physiological solution that half of sodium ions were changed into choline (A). Average of normalized C-CAP amplitude reduction in zeroK (B&C) and in zeroK solution that half of sodium ions were changed into choline (B, dashed line) or lithium (C, dashed line) Standard deviation is presented as light red and light blue area.

Reduction of extracellular sodium concentration by 50% did not generate a rapid increase in excitability index (fig.36 A) as seen after zeroK application. Adding to that, exchange of sodium with choline has not changed this increase (fig.36 B) (p=0.066, repeated measures 1-way ANOVA, n=11, 6) whereas no change was observed when lithium was used (fig.36 C) (p=0.372, repeated measures 1-way ANOVA, n=11, 6).
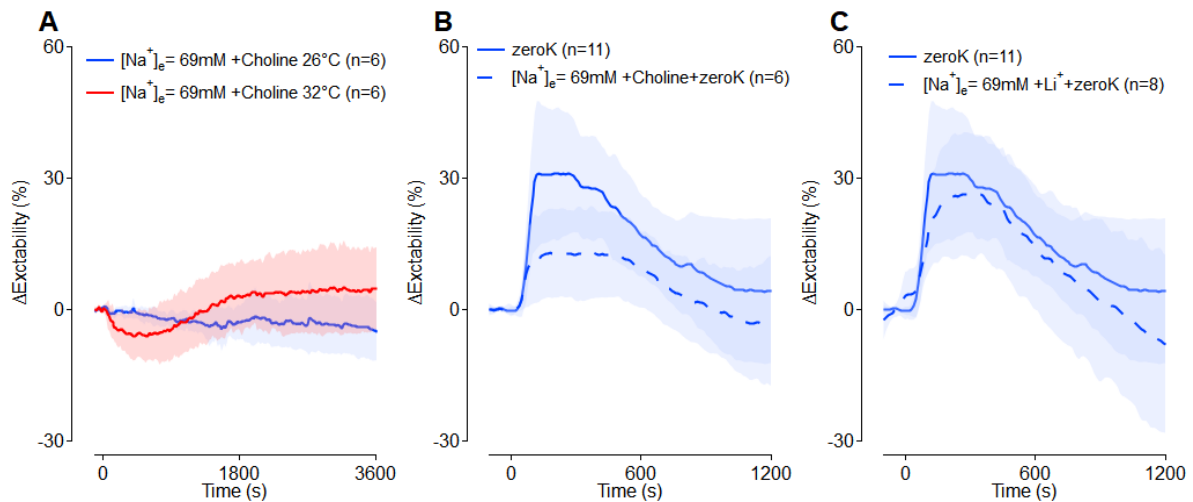
Fig. 36: Effects on excitability index. Reducing extracellular sodium concentration by 50% did not induce major changes in excitability index (A) and did not abolish the rapid increase induced by zeroK when choline (B, dashed line) or lithium (C, dashed line) was used for the exchange. Standard deviation is presented as light red and light blue area.

3.2.1.5 Low potassium vs. zero K

Different potassium concentrations between 0 and 3 mM were used in experiments to check if there is a gradual effect of potassium concentration on amplitude reduction. All experiments that had potassium concentration lower than 3.2 mM supressed C-CAP amplitude, but to smaller extent as compared to zeroK (fig. 37). Time constants of amplitude reduction were used for comparison (fig.37 A). All 1 mM or less

potassium concentrations showed rapid amplitude reduction (smaller time constants) as compared to normal $[K^+]_e$=3.2 mM concentration.
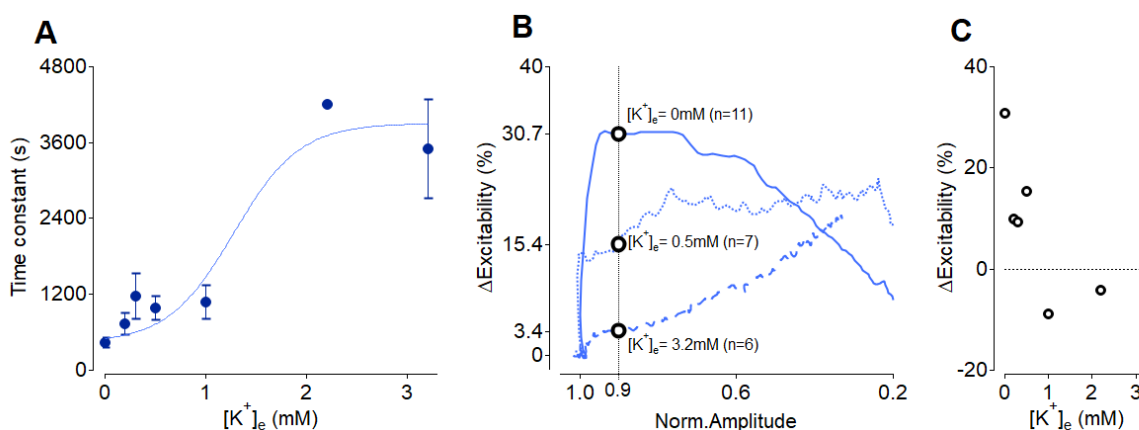
Fig. 37: Different potassium concentration solution effect on C-CAP amplitude and excitability index. C-CAP amplitude reduction was fitted to exponential drop and time constant was used for comparisons (A). Shift of excitability index was plotted against normalized C-CAP amplitude (B) to find excitability jump value at 0.9 of C-CAP amplitude at different potassium concentration solutions (C).

Rapid increase in excitability index was still observed at low potassium concentrations (data not shown). Interestingly, excitability index changes were independent of amplitude reduction (fig.37 B). Quantification of the rapid increase in excitability index (start unit C-CAP amplitude was reduced by 10%; fig.37 B) showed a non-linear correlation with potassium concentration (fig.37 C). Solutions containing less than 1 mM potassium generated a rapid increase in excitability index.

3.2.1.6 Wash out of potassium ions from cell
Assuming that application of zeroK solution will lead to increased leak of intracellular potassium ions from the axons we measured their extracellular concentration. Sciatic nerves of for mice were put into zeroK solution (200 µl) for one hour. After this stimulation sodium and potassium ion concentration of the bath solution was measured using a blood gas analyser. An increase of potassium concentration was detected in one of six experiments only (Table 4)

Experiment	Sodium conc. mM	Potassium conc. mM
Control nominal conc.	141.2	0
Control measured	136.5	-
Exp. No 1	140	-
Exp. No 2	139	0.7
Exp. No 3	139	-
Exp. No 4	139	-
Exp. No 5	140	-
Exp. No 6	140	-

Table 4: Nominal and detected sodium and potassium concentration in zeroK solution after stimulation with zeroK for one hour.

3.2.1.7 Low potassium effect on rectangular vs sinusoidal stimulus

The effects of lowering the extracellular potassium concentration to 50% ($[K^+]_e$=1.6 mM) of the normal level on axonal excitability were investigated for sine wave and regular rectangular stimulation profiles (fig. 38). There was no obvious difference in neuronal excitability between normal and reduce potassium concentration.
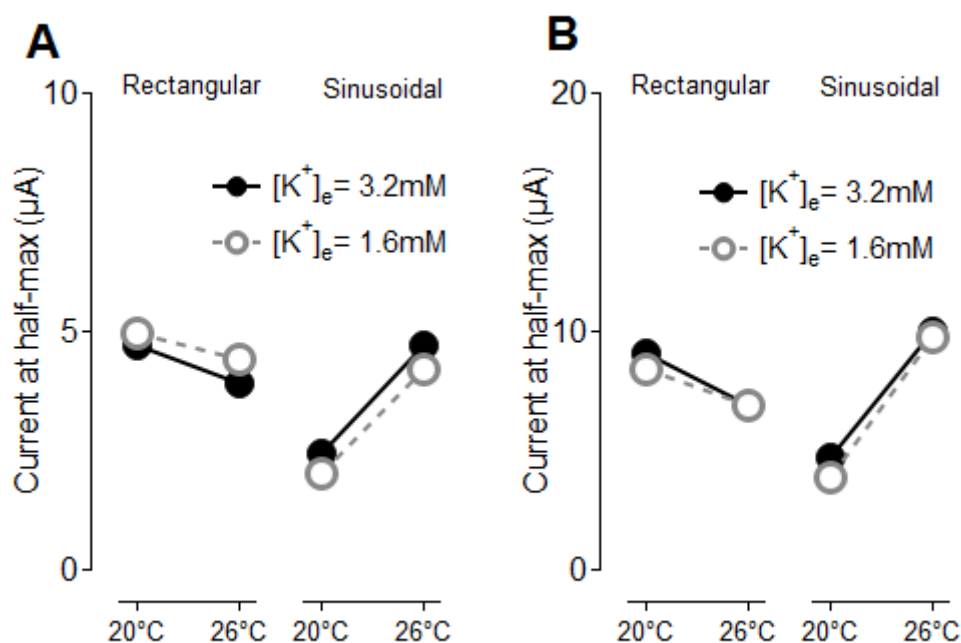
Fig. 38: Excitability testing of rectangular and sine wave electrical stimulus in two different potassium concentration solutions. Current to induce half-maximal C-CAP amplitude by rectangular (A&B, left panels) and sinusoidal (A&B, right panels) stimuli. Data showed from two different experiments (A&B panels) at 3.2mM potassium concentration physiological solution (black markers) and 1.6mM low potassium concentration solution (grey markers).

3.2.2 Effect of zeroK solution on discharge of sensory neurons in cornea

Five successful single fibre recordings from sensory neurons terminals in the cornea of guinea pigs were performed from cold sensitive A-fibres. All recordings showed ongoing activity in single fibres and spiking frequency modulation by temperature.
zeroK was applied for one hour and changes of discharge patterns was analysed. Two basic types of discharge profiles were found: cells firing at a largely constant frequency (fig.39 A, non-bursting) and cells that also showed discharge at a distinctly higher frequency (fig.39 B, bursting). Spiking probability showed that for both impulse generation profiles zeroK solution reduced the high frequency discharge.
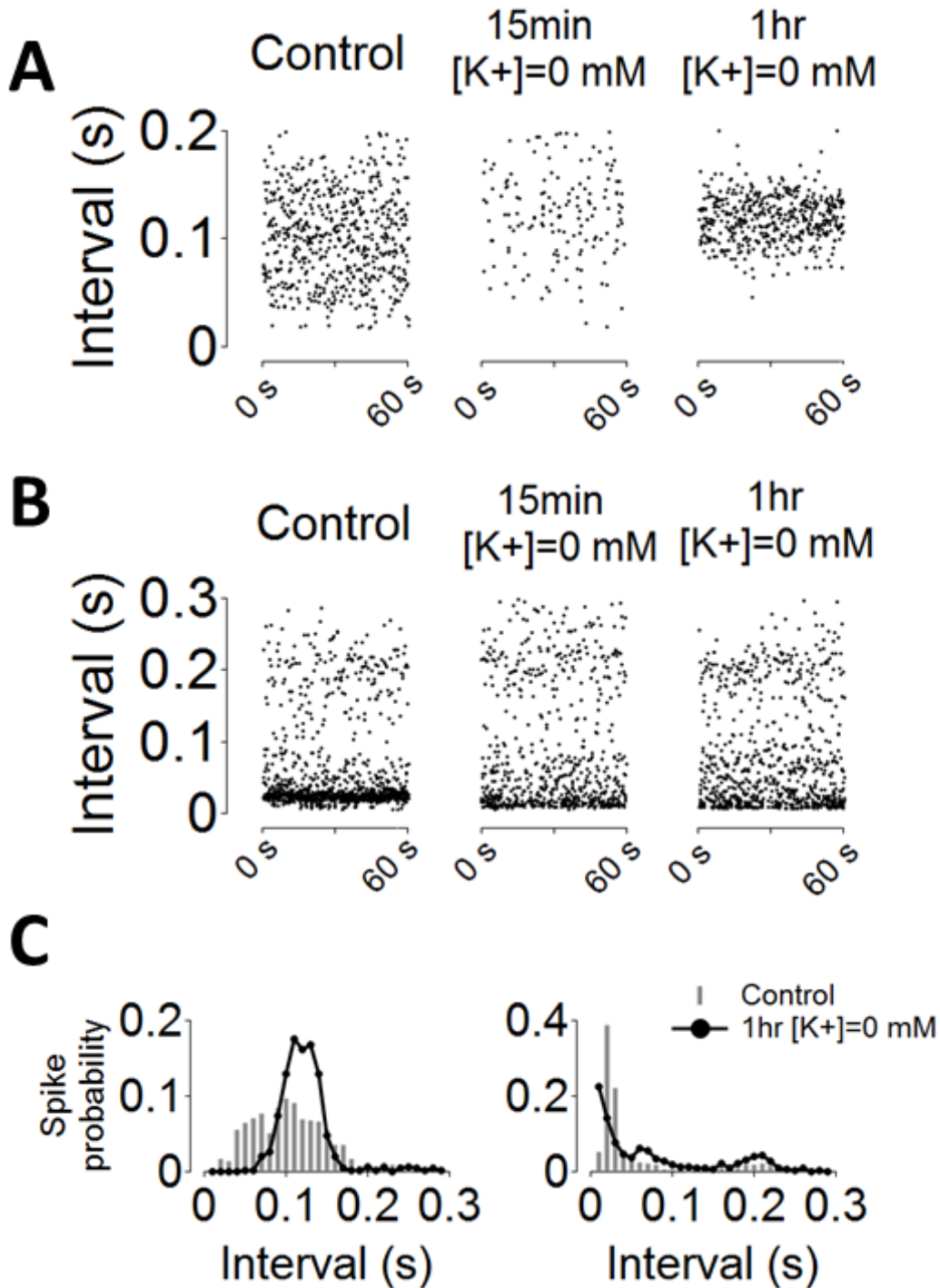
Fig. 39: Description of two different profile of sensory fibre terminal activity. Impulse generation profiles in 1min duration were taken in three different time moments: before switching solutions, 15min and 1hr after solutions were switched. Two different type of sensory fibres activity was observed: cells producing one highly expressed impulse generation period (A) and two periods (B). Quantification of impulse generation profiles (C).

In all 5 experiments there was spontaneous activity after 15min and in 4 experiments also after 1hr in physiological solution (fig. 40). In 3 of 5 experiments discharge was reduced during zeroK stimulation. In 4 out of 5 experiments amount of bursts and spikes per burst was reduced.
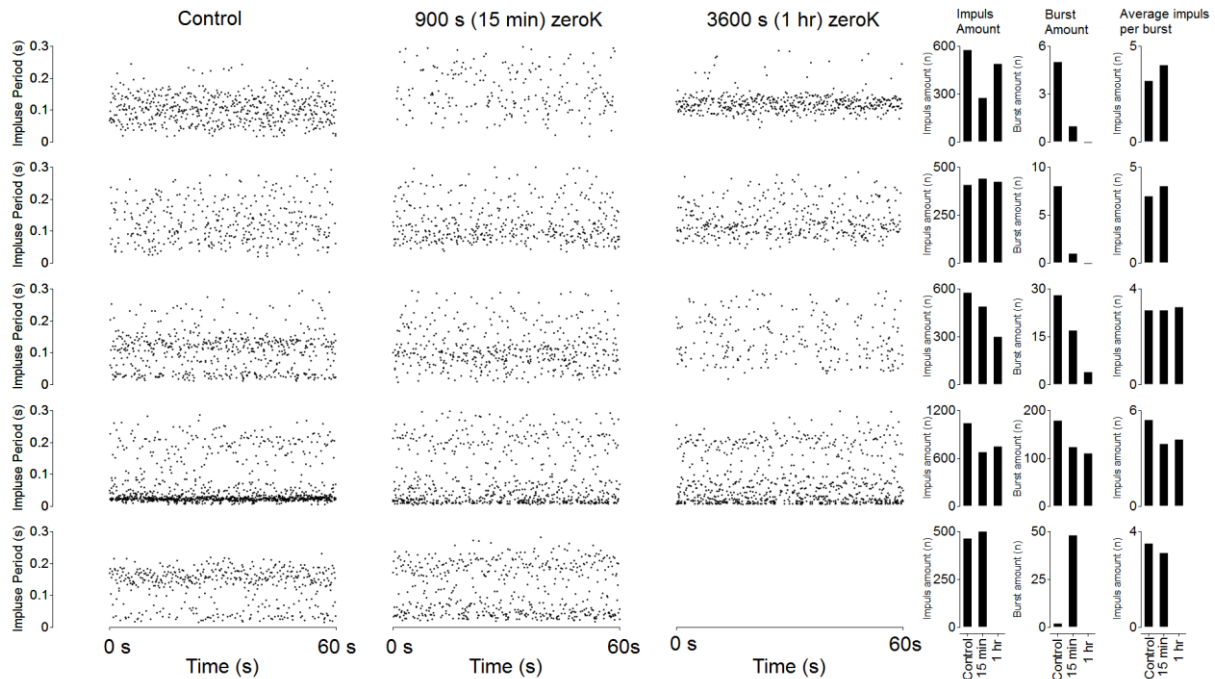
Fig. 40: Quantification of zeroK solution effect on discharge pattern. Specimens of five sensory fibres responding to zeroK are shown (left side). Quantification of number of action potentials, number of bursts and average number of action potentials per burst are depicted on the right side.

Pooled data analysis showed that zeroK is reducing action potential discharge to 0.83±0.27 per minute after 15min and to 0.62±0.40 after 60 min of zeroK (fig. 41).
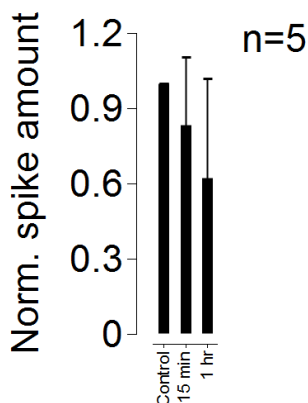
Fig. 41: Quantification of action potentials ("spike") per minute before, after 15min and 1 h of stimulation with zeroK.

3.3 Excitability testing on cisplatin-induced neuropathy

3.3.1 Effect of temperature on excitability index in cisplatin model animals

Excitability index was measured at 26°C and 32°C in healthy (n=3) and cisplatin (n=7) rats. Heating increased excitability index for both groups (fig. 42). The average excitability index was 4.6±3.8% at 26°C and 7.6±3.1% at 32°C in healthy animals, but 0.9±8.8% at 26°C and 9.9±6.4% at 32°C in cisplatin rats. The shift of excitability upon heating did not differ significantly between healthy and cisplatin rats (unpaired t-test, n=3, 7, p=0.12).
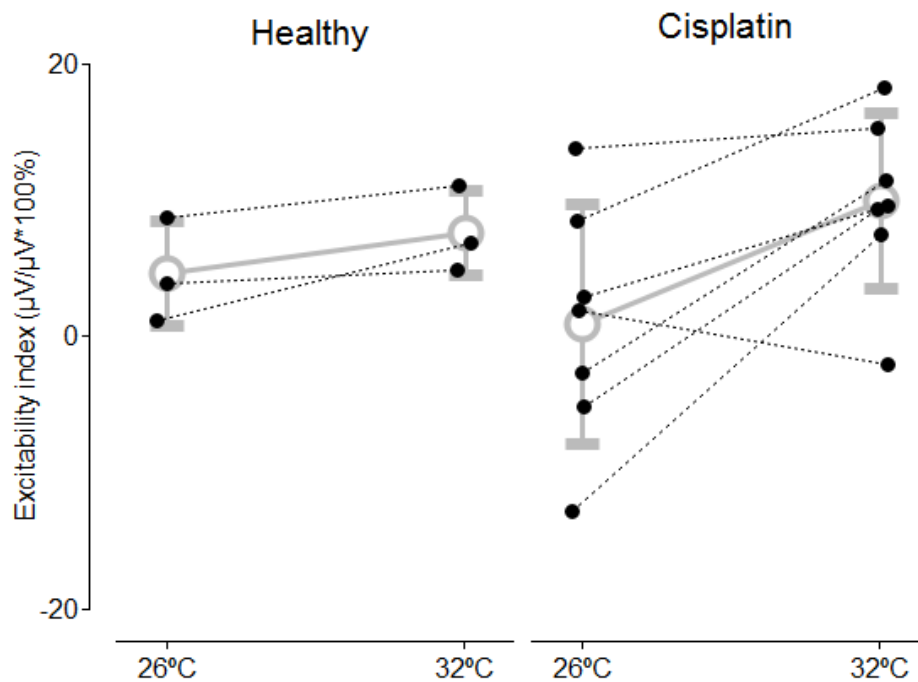
Fig. 42: Quantification of excitability index changes for two temperatures in control animals and cisplatin-treated rats.

3.3.2 Slow ramp and sine wave testing in cisplatin rats

Sinusoidal excitability testing was successful only in one healthy rat. Temperature effect on stimulus current to evoke half-maximal C-CAP amplitude was opposite for rectangular and sine wave stimulus rats as already found in mice (fig. 43).
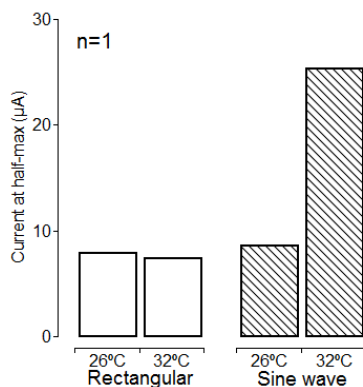
Fig. 43: Quantification of current to induce half-maximal C-CAP amplitude in healthy rat.

The same differential temperature effects described above for the mouse were observed in the cisplatin rat model (fig. 44). Warming reduced current the half-max current for rectangular stimuli from 14.8±1.8 µA at 26ºC to 11.8±1.8 µA at 32ºC. In contrast, half-max current for sine wave stimulation was increased by warming resulting in half-max current of 4.6±1.6 µA at 26ºC and 14.2±6.0 µA at 32ºC.
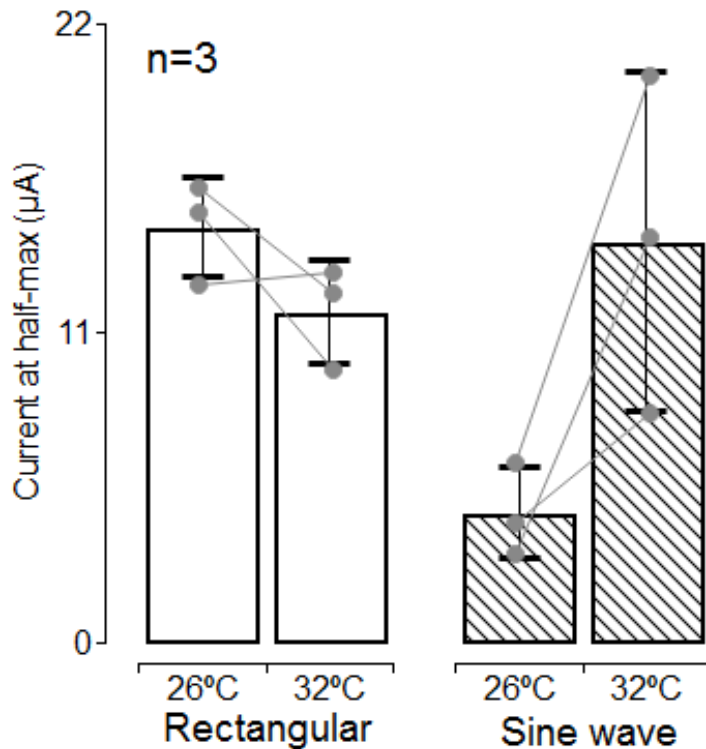
Fig. 44: Quantification of current to induce half-maximal C-CAP amplitude in rat that got cisplatin injection.

In summary, warming was decreasing current to evoke half-maximal C-CAP amplitude for constant current rectangular in healthy rats and animals that received cisplatin, and increased for sine wave stimulus. Unfortunately, the number of observation was not sufficiently large to analyse for potential effects of cisplatin on axonal excitability. Rather our results can be regarded as proof of concept that axonal excitability can be measured in this neuropathy model.

4 <u>DISCUSSION</u>

Considering neuronal excitability in the context of sensory physiology and pain it is often the case that sensory, axonal and synaptic mechanisms are investigated separately with the least attention devoted to axonal conduction (Obreja, 2013). However, in light of the key complaint of chronic pain patients, i.e. non-evoked ongoing pain, it is obvious that both the generation of spontaneous activity and the ability of axons to generate bursts of discharges is crucial to the underlying clinical problem and the suffering of patients. Thus, this thesis focused on models that mimic the generation of aberrant activity in unmyelinated afferent fibres using slow depolarizing electrical stimulation and low extracellular potassium as new experimental paradigms.

4.1 Sine wave vs rectangular and ramp shape stimuli

Traditionally, rectangular electrical stimuli of short duration have been used to induce action potentials in neurons. The main advantage of this stimulus is the synchronicity of activation as voltage sensitive channels of the stimulated neurons are recruited at the same time. This approach minimised activation thresholds and facilitated analysis of compound action potentials (Gasser and Grundfest, 1939). Moreover, the fast onset of stimulation is also the most appropriate profile for studying the physiological time course of axonal conduction. Other stimulation profiles, such as charge balanced bipolar pulses have been mainly investigated in terms of safety aspects comparing effectivity versus. tissue damage and corrosion of the electrodes (Merrill et al., 2005). Short depolarizing pulses are also the most appropriate stimulus profile to activate the crucial voltage gated sodium channel in myelinated axons in adults, i.e. $Na_V1.6$ (Israel et al., 2019). $Na_V1.6$ has a fast time constant for its transition into closed state inactivation and this feature impedes action potential generation during longer lasting depolarizing stimuli.

In contrast, $Na_V1.7$ and $Na_V1.3$ are more resistant to inactivation and can amplify weak and slow depolarization by the generation of ramp currents (Cummins et al., 1998; Estacion and Waxman, 2013). Functionally, this response pattern to slow depolarization is linked to the initiation of action potentials at sensory nerve endings. Since $Na_V1.7$ is expressed mainly in unmyelinated nociceptive primary afferents, a slow depolarizing stimulation profile can be expected to activate this fibre class. Slow depolarizing stimuli are therefore being used to probe mechanisms that are not directly related to action potential conduction, but to action potential generation, in particular in nociceptors. The initiation of action potentials is of basic interest for sensory physiology, but it is also the key mechanism underlying the generation of spontaneous activity under pathophysiological conditions, in particular in chronic pain. In summary, the *initiation* of action potentials in unmyelinated axons by slow depolarizing stimuli was investigated to complement the traditional approach of excitability testing focusing on action potential *conduction* and thereby provide new information relevant for the generation of ongoing activity in nociceptors. We confirmed that slow depolarizing stimuli initiate a C-CAP in isolated peripheral nerves as already published for human, pig and mouse nerves (Jonas et al., 2018b) and demonstrated that the initiation of the C-CAP is dependent upon charge accumulation.

4.1.1 Temperature effect on C-CAP amplitude and electrical threshold

It is well known that cooling increases the amplitude of compound action potentials (Ritchie and Straub, 1956). Our data confirmed that C-CAP amplitude and area under the curve (AUC) increased for both, rectangular and sinusoidal electrical stimuli at lower temperatures (Fig. 14, 16, 24). Higher C-CAP amplitudes upon cooling might appear counter-intuitive as colder temperatures will slow down sodium channel activation kinetics, thereby slowing conduction and increasing dispersion of the compound action potential. However, cooling also slows the kinetics of fast inactivation of sodium channels and this effect is more pronounced than the slowing of activation (Schwarz et al, 1979). The net result is a prolongation of sodium channel opening time and an increase in the sodium current. This shift in action potential duration is thought to compensate for the decrease in conduction speed at lower temperatures (Ritchie and Straub, 1956) and leads to higher C-CAP amplitudes. Indeed, this increase in CAP amplitude in unmyelinated fibres upon cooling has been experimentally verified (Hodgkin and Katz, 1949).

4.1.1.1 Differential effects of cooling on rectangular vs. sine wave stimulation

The data confirm that cooling increased C-CAP amplitude both in response to rectangular and sinusoidal stimuli (Figure XX). At warmer temperatures of 26°C and 32°C, the AUC and amplitude of the C-CAP were clearly lower for sinusoidal stimulation. However, at 20°C sine wave stimulation evoked a C-CAP with the same area under the curve as compared to rectangular stimulation and only a slightly reduced amplitude suggesting reduced synchronization. Comparing the ratio of C-CAP amplitudes for the different temperatures across the two stimulation profiles implied that cooling had differential effects with sine wave evoked C-CAP being facilitated rather than impaired by cooling.

The acute analgesic effect of cooling is well known (Bugaj, 1975) and there are many mechanisms by which cooling modulates excitability, including changes in Nernst potential, modulation of steady state activation and inactivation, time constants of activation and inactivation, and recovery from inactivation (Korogod and Demianenko, 2017). Temperature dependence of voltage-gated ion channels has been described for calcium- (Cav3.1-3.3, 1.2,1.3), sodium- (Na$_V$1.1-1.9), hyperpolarization activated cyclic nucleotide modulated- (HCN1,2), but also hyperpolarizing channels such as potassium (K$_V$2.1, 4.3, TREK1,2, TRAAK) and chloride (ANO1) channels (Korogod and Demianenko, 2017). During cooling, TTX-sensitive sodium channels exhibit a cold-induced leftward shift of steady state inactivation (Sarria et al., 2012; Zimmermann et al., 2007) resulting in reduced neuronal excitability.

Our data confirmed that cooling increased the stimulus current required to evoke half-maximal C-CAP amplitudes, but only for traditional rectangular stimulation. Unexpectedly, the efficacy of sinusoidal stimulation increased at colder temperatures. Importantly, electrical threshold for sine wave stimuli were lower than for rectangular stimuli at 20°C.

When considering the result of lower thresholds for sinusoidal stimulation at lower temperatures it might appear unclear how thermodynamics could allow for such an effect since opening voltage-gated sodium channels should require more energy at lower temperatures based on the temperature dependence of the rate constants of state transitions (Balbi et al., 2017). For rectangular current stimuli, the duration of stimulation was fixed and therefore the calculation of charge applied at C-CAP

threshold and for the half-maximal C-CAP amplitude reflected the stimulation amplitude. Consequently, the charge levels at threshold and at half-maximum C-CAP amplitude matched the stimulus amplitudes and were higher at colder temperatures. However, current amplitude thresholds do not sufficiently reflect the energy of the stimulus for the sinusoidal profiles. Indeed, lower thresholds were found to coincide with longer stimulus durations. Most interestingly, an increase in stimulus intensity reduced the duration of the sinusoidal stimulus required to elicit a response, such that the transferred charge remained constant at a given temperature. This result suggests that the C-fibre axons can integrate charge over several tens of milliseconds in order to initiate an action potential. This result is in-line with historic studies by Weiss in 1901 that already suggested that the electrical threshold of neurons is based on charge (Bostock, 1983). Importantly, the current amplitude required to elicit a C-CAP for sinusoidal stimulation decreased at lower temperature but the time until from stimulus begin to action potential initiation increased such that the required charge levels also increased. Thus, the energy required to activate sodium channels at lower temperatures increased in line with the laws of thermodynamics.

The differential dependence of stimulus intensity on temperature for rectangular vs. sinusoidal profiles have implications for the use of such stimulation profiles in humans. It was shown that transcutaneous sine wave stimulation preferentially activates C-fibres (Jonas et al., 2018b). Mechanistically, it was suggested that the kinetics of sodium channels (especially $Na_V1.7$) and the spatial position of epidermal unmyelinated axons would lead to preferential activation of C-fibres over A-fibres. Our results add another aspect to this differential activation profile, namely surface temperature. At room temperatures of around 21°C, skin temperature in the volar forearm is about 32°C, but can be considerably lower in the periphery (Schick et al., 2003). Our results predict that for lower skin temperatures prefential activation of unmyelinated fibres is favoured and may be achieved at even lower stimulus intensities.

4.1.1.2 Potential contribution of cold sensitive TRP channels TRPM8 and TRPA1

When investigating temperature effects in primary afferent fibres it is also important to investigate whether the activation of cold sensitive receptors contribute to the observed effect. The cold sensitive transduction protein TRPM8 is expressed in primary afferent neurons (Facer et al., 2007; Peier et al., 2002) and its activation threshold is in the range of 18-23°C (Brauchi et al., 2004; Madrid et al., 2006; Zakharian et al., 2010). Thus, it can be assumed that TRPM8 was activated in experiments using bath temperatures of 20°C. We therefore tested the influence of the chemical TRPM8 agonists –(-)-menthol and icilin (Peier et al., 2002) for potential effects on excitability. There are eight different menthol isoforms and most common in nature is –(-)-menthol. Menthol is widely used in the food and cosmetic industry to evoke sensations of cooling, while icilin is more known in pharmacology. Icilin has an affinity for TRPM8 that is more than 2.5 times higher than menthol (McKemy et al., 2002; Wei and Seid, 1983). A crucial difference between icilin and menthol is their effect on the cold sensitive channel TRPA1 that has a broad sensitivity to chemical mediators (Bautista et al., 2006; Kichko et al., 2015; Viana, 2016), but has also be suggested to mediate noxious cold (Miyake et al., 2016; Moparthi et al., 2016; Viana, 2016). Icilin activates TRPA1 while menthol does not. We applied each of these agonists separately to mouse nerves and assessed excitability changes. The temperature dependent changes in C-CAP amplitude and electrical threshold of rectangular and sine wave stimuli persisted despite the presence of either menthol or icilin. This might have been expected to some extent for TRPM8 agonist activity since

only a small percentage of C-fibres are cold sensitive (Wang et al., 2018). In summary, TRPM8 activation through cooling cannot explain the differential effect of cooling on electrical threshold reduction for sine wave stimuli.

4.1.2 Mechanisms of action potential generation by sinusoidal stimulation

Induction of action potentials by tonic mild depolarization has been mainly linked to "ramp currents" that amplify weak depolarizing stimuli and can be generated in particular by $Na_V1.7$ and $Na_V1.3$ (Cummins et al., 2001; Cummins et al., 1998). $Na_V1.3$ is expressed in primary afferent neurons during foetal development and following injury (Cummins et al., 2001; He et al., 2010; Lampert et al., 2006; Osteen et al., 2016; Waxman et al., 1994) and therefore for our experiments $Na_V1.7$ might appear to be the primary target. $Na_V1.7$ is more resistant to slow inactivation and has a less depolarized activation threshold than $Na_V1.8$ (Akopian et al., 1996; Cummins et al., 1998; Elliott and Elliott, 1993; Herzog et al., 2003). However, our results clearly indicate, that the sine wave stimulus could evoke C-CAP with long latency at colder temperature and that it could still be elicited in the presence of TTX (1 µM) a concentration sufficient to block $Na_V1.7$ completely. Thus, as $Na_V1.7$ is TTX sensitive and strongly temperature dependent (Zimmermann et al., 2007) it cannot be the main contributor. Application of TTX did not remove ability of C-fibres to generate long latency C-CAP suggesting that TTXr channels such as $Na_V1.8$ could be underlying to late C-CAP generation by sine wave stimulus at cold temperatures. From the other voltage-sensitive sodium channels expressed in C-fibres such as $Na_V1.1$, $Na_V1.3$, $Na_V1.6$ and $Na_V1.9$ (Bennett et al., 2019) only NaV1.9 is TTXr. $Na_V1.9$ is generating a persistent current, which contributes to the resting membrane potential, but not electrical threshold (Cummins et al., 1999). $Na_V1.6$ is expressed in C-fibres, but after blocking these channels using µ-conotoxin PIIIA (Wilson et al., 2011) no major changes in electrical threshold or shapes of C-CAP were detected in this study. Thus, we conclude that characteristics of sodium channel subtypes are not sufficient to explain the temperature dependence of the late C-CAP upon slow depolarization.

4.1.2.1 Impact of membrane resistance, capacitance and potassium channels
The passive electrical properties of biological membranes include resistance (R), capacitance (C) and inductance (L) with resistance and capacitance being crucial for excitability (Hille, 1992). Resistance is described as ion permeability via the membrane and is determined by the conductance of ion channels. The resting membrane potential of cells is determined primarily by two-pore potassium channel (K_{2P}) potassium channels (Kang and Kim, 2006; Plant, 2012). Other ion channels can also be open at resting membrane potential and therefore contribute to setting its level such as $Na_V1.9$ or HCN channels, but two-pore potassium channels dominate.
Some K_{2P} channels are sensitive to temperature and close upon cooling (de la Pena et al., 2012). This exerts a depolarizing effect on membrane potential and the closure of K_{2P} will increase membrane resistance (Esquibel et al., 1980). It was found that K_{2P} channels are fully open around 40°C and closed at 14°C (Kang and Kim, 2006).
The electrical properties of the lipid bilayer of the cell membrane can be regarded as a capacitor in parallel with a resistor. Capacitance describes the ability of the membrane to store charge over a certain voltage (membrane potential). The capacitance is proportional to cell surface area. Capacitance is only slightly reduced upon cooling, but this change is minute compared to the temperature dependent change of membrane resistance (Esquibel et al., 1980).
Membrane resistance and capacitance are combined in the biophysical passive membrane model arranged in a parallel electrical chain, also called RC circuit (fig.

46) (Hille, 1992). The combination of resistive and capacitive elements of the membrane give rise to a membrane time constant (t=RC) that quantifies the rate of change of membrane potential. Under warm conditions, membrane resistance is fairly low such that the time constant is short (red arrows, fig. 46). Upon cooling K_{2P} channels will close and the time constant increases (blue arrows, fig. 46).

C

Current passing RC circuit: $$I(t) = i_R + i_C = \frac{U}{R} + C\frac{dU}{dt}; \quad (1)$$

Voltage changed over time: $$U(t) = IR \cdot e^{\frac{-t}{RC}} = U_0 \cdot e^{\frac{-t}{\tau}}; \quad (2)$$
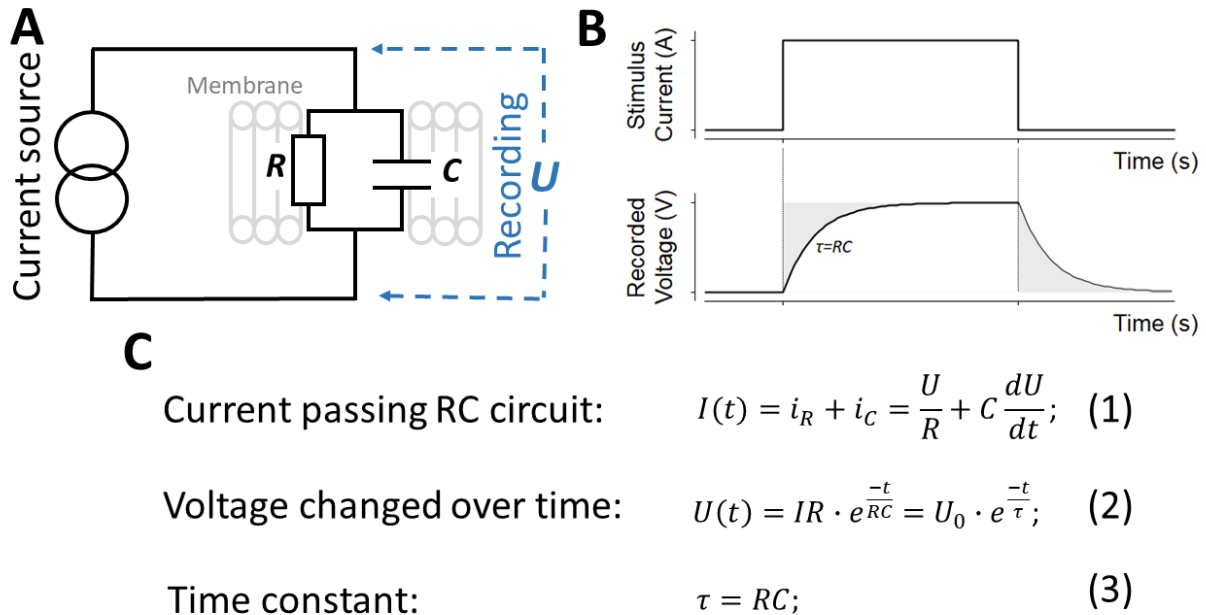
Time constant: $$\tau = RC; \quad (3)$$

Fig. 46: Artificial cell membrane electrical RC chain model. Cell membrane model has resistor (R) and capacitor (C) connected in parallel (A). Rectangular shape stimulus (B top) is responding by exponential change (B bottom) with time constant tau (τ). This RC chain response to rectangular stimulus can be described mathematical formulation by summation of all current passing chain (C formula 1) or voltage difference (C formula 2). Time constant of voltage changed over time is limited only by resistor and capacitor (C formula 3).

One key finding in our studies was the differential effect of cooling on electrical threshold to induce a C-CAP. Current amplitude thresholds increased for rectangular, but decreased for sinusoidal stimulation. For the short rectangular pulses the change in membrane resistance is not expected to be crucial for threshold changes as the rapid onset of the pulse that is triggering the action potential will be mainly channelled into a capacitive current. Thus, the expected increase in threshold upon cooling can be attributed to the slower opening kinetics of sodium channels (Zimmermann et al., 2007). For longer lasting stimuli such as our sinusoidal profile, the increase in membrane resistance will increase the membrane time constant improving charge integration (fig. 46). Indeed, cold-induced closure of 2 pore domain potassium channels has been assumed to contribute to cold-induced reduction of rheobase in small trigeminal ganglion neurons (Kanda and Gu, 2017). At a higher membrane resistance, the same transmembrane current will induce larger changes of membrane potential, which could explain lower rheobase levels (Kanda and Gu, 2017). Moreover, these neurons show an increase their sensitivity to depolarizing stimuli upon cooling that can be reversed by potassium channel (M-current) openers (Kanda and Gu, 2017). A cold-induced increase in excitability linked to closure of 2 pore domain potassium channels has also been shown for central hippocampal neurons (de la Pena et al., 2012).

In summary, it is important to note that cold-induced excitability changes in responses to slow depolarization observed in our data on C-CAP assess mechanisms that determine action potential generation in nociceptors. The ability to convert prolonged depolarization into discharge under cold conditions might well contribute to cold-induced pain in patients suffering from neuropathic pain (Gonzalez et al., 2017). There is already evidence for a clinical role of K_{2P} channels in hyper-excitability of nociceptive neurons (Haskins et al., 2017; Li and Toyoda, 2015; Mao et al., 2017) and K_{2P} channel openers have been shown to reduce nociceptor excitability (Dadi et al., 2017) suggesting that they represent a potential therapeutic target (Li and Toyoda, 2015; Mathie and Veale, 2015).

4.2 zeroK – new model for ongoing activity in nociceptors

In previous studies, we found that C-nociceptors develop ongoing activity when their sensory endings are treated with physiological solution without potassium ions (zeroK). Nominally, zero extracellular potassium is an unconventional stimulus. We used it here not to emulate any clinical conditions associated with hypokalemia ([K] <3.5mM), which at its most extreme may reach plasma potassium levels below 1 mM (Ten Bos et al., 2016), but rather as a stimulus to generate ongoing activity in somatosensory C-fibres. The value and utility of zero potassium as an experimental paradigm resides in the long time course over which ongoing activity can be sustained and the ability to readily reverse the effect. In this respect, zero potassium surpasses previous attempts to generate ongoing activity using a variety of algogens including capsaicin (Kenins, 1982; Schmelz et al., 2000), bradykinin (Beck and Handwerker, 1974), leukotrienes (Martin et al., 1987) PGE2 (Lang et al., 1990) and cytokines (Binshtok et al., 2008) all of which typically produce an initial high firing frequency in C-fibres with subsequent quiescence during which C-fibres are often refractory to any stimuli for tens of minutes. In contrast, ongoing non-bursting activity in single C-fibres can be sustained over longer periods through exposure to combinations of inflammatory mediators (Davis et al., 1993; Kessler et al., 1992) and physiochemical changes, such as lowered pH (Steen and Reeh, 1993) or reduced extracellular calcium (Lang et al., 1990). Consistent with this, in people. low pH evokes maintained pain upon sustained injection into human skin (Steen et al., 1995a). However, low pH results in a progressive change in sensitivity to mechanical stimuli (Steen and Reeh, 1993) while changes in thermal responsiveness accompany inflammation (Lang et al., 1990). The zero potassium paradigm circumvents the need for prior tissue injury and in our hands is fully reversible. Zero potassium thus serves as an adequate model to examine the molecular components contributing to ongoing firing in C-fibres.

It is of particular value as the standard approach that investigates sensitized induced activity of nociceptors will not include the mechanisms of ongoing activity (Bennett, 2012; Mogil, 2012). Thus, rather than investigating extracellular low potassium as a pathophysiological process we were focusing on the excitability changes it induced in order to extract a pattern of changes that enables spontaneous activity in nociceptors.

4.2.1 Low extracellular potassium decreases CAP amplitude

Basic parameters that determine the amplitude of C-CAP are in particular:
- Number of axons/action potentials
- Kinetics and amplitude of the sodium current in each axon

While these parameters are obviously based on the profile of action potentials in each single axon the amplitude of compound action potentials, also depend on the synchronicity of the single action potentials superimposing in the CAP. Thus, longer recording distances will increase dispersion of the action potentials of C-fibres and thereby the amplitude will drop. On the other hand, longer duration of a single action potential will increase the probability of summation and thereby increase amplitude (Kiernan et al., 2001).

One key result of the application of zeroK was a reduction of C-CAP amplitude. Our experiments indicated that an increase of intracellular sodium concentration was the primary factor underlying this reduction.

Under the conditions of zeroK, a lack of extracellular substrate is likely to reduce Na^+/K^+-ATPase activity (Nakamura et al., 1999; Pivovarov et al., 2018). Indeed, application of zeroK to sheep cardiomyocytes at voltage clamp conditions (-80 mV) caused an increase of intracellular sodium from about to about 30 mM by 10 minutes (January and Fozzard, 1984). Our compound action potential recordings are consistent with a reduced Na^+/K^+-ATPase activity during zero potassium contributing to accumulation of intra-axonal sodium. Reducing Na^+/K^+-ATPase activity either by lower temperature or by pharmacological block with ouabain reduced C-CAP amplitude but the magnitude of this effect was small in comparison to the effects of zeroK.

Low extracellular potassium concentrations will change the equilibrium potential of potassium towards hyperpolarization. Among the protection mechanisms of a neuron against hyperpolarization there is a family of hyperpolarization activated ion channels (HCN) that open upon hyperpolarization and are involved in setting the resting membrane potential (Doan et al., 2004). Thus, HCN channels could have been a major source for the intracellular accumulation of sodium. However, blocking HCN channels with ZD7288 did not change the C-CAP amplitude reduction to a major extent indicating that HCN is of minor importance for this effect.

4.2.1.1 Crucial role of $Na_V1.9$

The particular role of $Na_V1.9$ for intracellular accumulation of sodium was confirmed using transgenic mice globally lacking $Na_V1.9$- mice that were partly protected from the zeroK effects. The reduction of C-CAP amplitude reduction upon zeroK stimulation in wild type mice is not apparent in $Na_V1.9$-/- mice suggesting that $Na_V1.9$ plays a crucial role in the C-CAP amplitude reduction. The crucial role of sodium influx via $Na_V1.9$ in the zeroK model provides interesting links to mechanistic studies in animal pain models in which this channel has been implicated in increased nociception and pain following injury (Erickson et al., 2018; Hockley et al., 2014; Hoffmann et al., 2017; Zhang et al., 2019). Moreover, there is also clinical evidence that mutations of $Na_V1.9$ can cause chronic pain in humans (Bennett et al., 2019; Han et al., 2016; Kabata et al., 2018; Kleggetveit et al., 2016; Park and Baker, 2017). Thus, it appears that although the experimental condition of low extracellular potassium concentration does not have a pathophysiological correlate, its implications may provide important and clinically relevant mechanistic insight into the generation of spontaneous activity in nociceptors.

4.2.1.2 Control experiments

Several control experiments confirmed that the reduction of C-CAP amplitude was linked to an accumulation of intracellular sodium. When 50% of the extracellular sodium was exchanged for choline or lithium, zeroK application still led to a reduction of C-CAP amplitude, but at a significantly reduced rate. Thus, reduced extracellular sodium concentration limited C-CAP amplitude reduction during zeroK suggesting

consistent with a slower rate of accumulation of intracellular sodium ion concentration.

We also tried to combine slow depolarizing stimuli with the zeroK model. However, the rapid decline of the C-CAP amplitude upon zeroK precluded this direct approach. Sinusoidal stimulation was therefore tested at 50% potassium concentration. Unfortunately, no significant changes were observed in the threshold currents (rectangular vs. sinusoidal stimulation) that evoke half-maximal C-CAP amplitudes after switching from control solution to 50% potassium concentration.

4.2.2 Rapid excitability changes upon zeroK application

ZeroK solution generated a rapid increase in the excitability index, which was more pronounced at 26°C than at 32°C. This increase of excitability was mainly caused by the instantaneous increase of the threshold of the conditioned stimulus whereas the threshold for the non-conditioned current remained fairly constant initially. The excitability index is the ratio of conditioned vs. unconditioned threshold current. At low stimulation frequencies, the threshold for the conditioned C-CAP is higher than the unconditioned as the axon is slightly hypo-excitable immediately after an action potential (Bostock et al., 2003; Moalem-Taylor et al., 2007; Tigerholm et al., 2015). However, upon hyperpolarization a "supernormal period" can arise directly following an action potential in which activation thresholds are reduced (Bostock and Bergmans, 1994; Bowe et al., 1987; Kiernan et al., 1997). Such a reduction of the threshold of the conditioned stimulus will lead to a decrease of the excitability index. In contrast, depolarization will primarily reduce the threshold for the unconditioned stimulus and thereby increase the excitability index. Thus, an increase of the excitability index is an indirect sign of depolarization. Our data would thus suggest an initial depolarization induced by zeroK application. However, lowering extracellular potassium is expected to hyperpolarize the potassium equilibrium potential. Thus, accepting the hyperpolarizing shift of the potassium equilibrium potential we have to assume another mechanism that is induced by zeroK that might explain depolarization. Low extracellular potassium concentrations have been shown to alter ion selectivity of two-pore domain potassium channels such that become permeable to sodium and provide a leak current (Ma et al, 2011) (Goldstein, 2017). This leads to a paradoxical depolarization in the presence of low extracellular potassium via the TWIK-1 two-pore domain potassium channel in human, but interestingly not in rodent cardiomyocytes (Ma et al., 2011). TWIK-1 mRNA has been reported in adult dorsal root ganglion neurons (Zhu and Oxford, 2011) and functional evidence also implicates a role for TWIK channels in primary afferent fibres (Cooper et al, 2004). Our test of different potassium concentrations between 0 and 1 mM revealed that the initial depolarization occurred in a concentration dependent manner, being most apparent at potassium concentrations below 1 mM.

4.3 Effect of zeroK on activity in corneal cold fibres

Signal fibre recordings were obtained from cold sensitive, spontaneously active nerve terminals in the corneal. After application of zeroK on the cornea even for more than two hours recordings were found to be stable in 4 out of 5 experiments. This is in contrast to the C-CAP in peripheral sural nerves that was abolished after less than 20 minutes of zeroK. There are different factors that can explain this difference: Cold – sensitive endings in the cornea have A-fibre axons and do not express $Na_V1.9$ that we showed to be primarily responsible for the accumulation of intracellular sodium during zeroK. Detailed analysis revealed that corneal cold fibres showed a reduction

in their high frequency impulse generation in zeroK without an overt reduction of number of action potentials over time. Another main difference was the ability of the corneal tissue to buffer changes in extracellular potassium: while minute filaments of the peripheral nerve were completely immersed in zeroK solution, the cornea was stimulated by exposure fothe epithelium to low potassium. The corneal epithelium comprises cells bound by tight junctions, whereby affecting changes in ionic concentrations is difficult. In addition, the corneal stroma is rich in potassium ions. The stroma of the cornea will hold large amounts of potassium ions that can act a sink to slow down the reduction of extracellular potassium around the sensory endings. Moreover, recordings from unmyelinated corneal nociceptors have to be conducted to directly compare the results obtained in the C-CAP recordings.

4.4 Cisplatin rat model

Cisplatin is a chemotherapeutic drug that is in clinical use against various forms of cancer (Makhija et al., 2000; Riddell, 2018) and is characterized by side effects including nephropathy (Holditch et al., 2019) and neuropathy (Peltier and Russell, 2002; Quasthoff and Hartung, 2002). Based on these observations animal models of platinum salt-induced nephropathy (Daugaard, 1990; Stein and Fried, 1985) and neuropathy (Attal et al., 2009; Authier et al., 2003; Quasthoff and Hartung, 2002) have been developed. In our studies, we included rats that had received single cisplatin injections (7 mg/kg) two weeks before sacrifice for the induction of a acute kidney injury. In these animals, we assessed excitability index, using non-conditioned and conditioned threshold currents and sine wave stimuli tested in peroneal nerves taken immediately after sacrificing the animals.

Cisplatin and control rats showed the expected increase of excitability index upon warming without any significant difference between them. In addition, excitability and temperature-dependence upon sine wave stimulation was tested. In control rats, the temperature effects on rectangular and sinusoidal thresholds did not differ from those observed in control mice. Rectangular stimulus current to evoke half-maximal C-CAP amplitude in healthy rats increased upon cooling and decreased for sine wave as it did in healthy mice. These temperature effects did not significantly differ in nerves obtained from the cisplatin rats. However, in the control rats higher thresholds for sine wave stimulation were observed when compared to the rectangular stimulation. In the cisplatin group, however, nerves were more sensitive to sine wave stimuli. This difference might indicate that cisplatin induced a small fibre neuropathy with hyper-excitable C-fibres. Such hyper-excitable C-fibres could contribute to the hypersensitivity observed in cisplatin-treated animals (Authier et al., 2003). Unfortunately, our sample size was limiting the impact of this observation.

5 <u>SUMMARY</u>

The main underlying mechanisms of chronic pain are still unclear. In this thesis, two new approaches targeting the excitability of peripheral nociceptive neurons were employed to examine processes leading to ongoing nociceptive discharge. Thereby we aimed to contribute to the understanding of peripherally driven spontaneous pain that leads to suffering in many patients with chronic pain. We used a new model of low extracellular potassium application that induces ongoing nociceptor activity at the sensory endings of skin nociceptors and a slow depolarizing ramp stimulus that preferentially activates C-fibres and is more closely related to the physiologic induction of action potentials in primary afferent neurons.

Low potassium solution unexpectedly led to a rapid and transient depolarisation that is probably mediated by a loss of ion selectivity in 2 pore domain potassium channels. However, the dominant effect of low potassium was a massive increase of intracellular sodium mediated primarily by an influx of sodium ions via NaV1.9 channels. Moreover, primary afferents lacking $Na_V1.9$ such as cold sensitive A-fibres of the cornea did not increase their discharge upon stimulation with low potassium.

Slow depolarizing ramp stimuli (4 Hz sinusoidal) were found to be more effective at activating C-fibres during cooling whereas traditional rectangular stimulation became less effective. This differential effect could be explained by cold-induced closure of two pore domain potassium channels leading to increased membrane resistance. The increased membrane resistance increases the membrane time constant whereby the same transmembrane current will more effectively change membrane potential. This mechanism has major clinical importance for cold-induced pain.

The voltage-sensitive sodium channel $Na_V1.7$ would have the ideal characteristics to mediate the activation upon slow depolarizing ramps as it is known to amplify such stimuli via a "ramp current". Activation of C-fibres by sinusoidal stimuli was not blocked by TTX suggesting that $Na_V1.7$ is not the only Na_V that can respond to slow depolarizing changes in membrane potential.

Innovative excitability tests were used to investigate peripheral nerve fibres of rats that had received cisplatin to induce an acute nephropathy and potentially a peripheral neuropathy. In treated animals, unmyelinated fibres were found to be more sensitive to slow depolarizing stimuli suggesting hyper-excitability. However, the number of animals was low and it remains unclear how robust this effect is.

In summary, the model of potassium free extracellular solution was used to identify $Na_V1.9$ and 2 pore domain potassium channels as major determinants of small fibre excitability that have already been linked to clinical chronic pain states. Moreover, the cold-induced hyper-excitability of unmyelinated fibres in response to slow depolarizing ramp stimuli found in our study has important mechanistic implications for the generation of cold-induced pain and hypersensitivity in patients with neuropathic pain. It will be of major interest to use the newly developed tests for axonal excitability in pathophysiologic conditions and ultimately in human tissue in order to specify promising molecular targets that can lead to innovative analgesic treatment options in the future.

6 <u>REFERENCES</u>

Ackerley, R., and Watkins, R.H. (2018). Microneurography as a tool to study the function of individual C-fibre afferents in humans: responses from nociceptors, thermoreceptors, and mechanoreceptors. J Neurophysiol *120*, 2834-2846.

Acosta, C., McMullan, S., Djouhri, L., Gao, L., Watkins, R., Berry, C., Dempsey, K., and Lawson, S.N. (2012). HCN1 and HCN2 in Rat DRG neurons: levels in nociceptors and non-nociceptors, NT3-dependence and influence of CFA-induced skin inflammation on HCN2 and NT3 expression. PLoS One *7*, e50442.

Adriaensen, H., Gybels, J., Handwerker, H.O., and Van Hees, J. (1983). Response properties of thin myelinated (A-delta) fibres in human skin nerves. J Neurophysiol *49*, 111-122.

Akopian, A.N., Sivilotti, L., and Wood, J.N. (1996). A tetrodotoxin-resistant voltage-gated sodium channel expressed by sensory neurons. Nature *379*, 257-262.

Andrasik, F., Flor, H., and Turk, D.C. (2005). An expanded view of psychological aspects in head pain: the biopsychosocial model. NeurolSci *26 Suppl 2:s87-91.*, s87-s91.

Armstrong, C.M. (2006). Na channel inactivation from open and closed states. Proc Natl Acad Sci U S A *103*, 17991-17996.

Attal, N., Bouhassira, D., Gautron, M., Vaillant, J.N., Mitry, E., Lepere, C., Rougier, P., and Guirimand, F. (2009). Thermal hyperalgesia as a marker of oxaliplatin neurotoxicity: a prospective quantified sensory assessment study. Pain *144*, 245-252.

Authier, N., Gillet, J.P., Fialip, J., Eschalier, A., and Coudore, F. (2003). An animal model of nociceptive peripheral neuropathy following repeated cisplatin injections. ExpNeurol *182*, 12-20.

Balbi, P., Massobrio, P., and Hellgren Kotaleski, J. (2017). A single Markov-type kinetic model accounting for the macroscopic currents of all human voltage-gated sodium channel isoforms. PLoS Comput Biol *13*, e1005737.

Bautista, D.M., Jordt, S.E., Nikai, T., Tsuruda, P.R., Read, A.J., Poblete, J., Yamoah, E.N., Basbaum, A.I., and Julius, D. (2006). TRPA1 mediates the inflammatory actions of environmental irritants and proalgesic agents. Cell *124*, 1269-1282.

Beck, P.W., and Handwerker, H.O. (1974). Bradykinin and serotonin effects on various types of cutaneous nerve fibres. Pflugers Arch *347*, 209-222.

Bennett, D.L., Clark, A.J., Huang, J., Waxman, S.G., and Dib-Hajj, S.D. (2019). The Role of Voltage-Gated Sodium Channels in Pain Signaling. Physiol Rev *99*, 1079-1151.

Bennett, G.J. (2010). Pathophysiology and animal models of cancer-related painful peripheral neuropathy. Oncologist *15 Suppl 2:9-12. doi: 10.1634/theoncologist.2009-S503.*, 9-12.

Bennett, G.J. (2012). What is spontaneous pain and who has it? JPain *13*, 921-929.

Bennett, G.J., Chung, J.M., Honore, M., and Seltzer, Z. (2003). Models of neuropathic pain in the rat. CurrProtocPharmacol *Chapter 5:Unit5.32. doi: 10.1002/0471141755.ph0532s21.*, Unit5.

Binshtok, A.M., Wang, H., Zimmermann, K., Amaya, F., Vardeh, D., Shi, L., Brenner, G.J., Ji, R.R., Bean, B.P., Woolf, C.J*., et al.* (2008). Nociceptors are interleukin-1beta sensors. J Neurosci *28*, 14062-14073.

Black, J.A., Dib-Hajj, S., McNabola, K., Jeste, S., Rizzo, M.A., Kocsis, J.D., and Waxman, S.G. (1996). Spinal sensory neurons express multiple sodium channel alpha-subunit mRNAs. Brain Res Mol Brain Res *43*, 117-131.

Blair, N.T., and Bean, B.P. (2003). Role of tetrodotoxin-resistant Na+ current slow inactivation in adaptation of action potential firing in small-diameter dorsal root ganglion neurons. J Neurosci *23*, 10338-10350.

Bostock, H. (1983). The Strength Duration Relationship for Excitation of Myelinated Nerve - Computed Dependence on Membrane Parameters. J Physiol-London *341*, 59-74.

Bostock, H., and Bergmans, J. (1994). Post-tetanic excitability changes and ectopic discharges in a human motor axon. Brain *117*, 913-928.

Bostock, H., Campero, M., Serra, J., and Ochoa, J. (2003). Velocity recovery cycles of C fibres innervating human skin. JPhysiol *553*, 649-663.

Bostock, H., Campero, M., Serra, J., and Ochoa, J.L. (2005). Temperature-dependent double spikes in C-nociceptors of neuropathic pain patients. Brain *128*, 2154-2163.

Bowe, C.M., Kocsis, J.D., and Waxman, S.G. (1987). The association of the supernormal period and the depolarizing afterpotential in myelinated frog and rat sciatic nerve. Neuroscience *21*, 585-593.

Brauchi, S., Orio, P., and Latorre, R. (2004). Clues to understanding cold sensation: thermodynamics and electrophysiological analysis of the cold receptor TRPM8. Proc Natl Acad Sci U S A *101*, 15494-15499.

Brock, J.A., and Cunnane, T.C. (1995). Effects of Ca2+ and K+ channel blockers on nerve impulses recorded from guinea-pig postganglionic sympathetic nerve terminals. J Physiol-London *489*, 389-402.

Bugaj, R. (1975). The cooling, analgesic, and rewarming effects of ice massage on localized skin. Phys Ther *55*, 11-19.

Burchiel, K.J., and Baumann, T.K. (2004). Pathophysiology of trigeminal neuralgia: new evidence from a trigeminal ganglion intraoperative microneurographic recording. Case report. J Neurosurg *101*, 872-873.

Cai, T., Jen, H.I., Kang, H., Klisch, T.J., Zoghbi, H.Y., and Groves, A.K. (2015). Characterization of the transcriptome of nascent hair cells and identification of direct targets of the Atoh1 transcription factor. J Neurosci *35*, 5870-5883.

Caldwell, J.H., Schaller, K.L., Lasher, R.S., Peles, E., and Levinson, S.R. (2000). Sodium channel Na(v)1.6 is localized at nodes of Ranvier, dendrites, and synapses. P Natl Acad Sci USA *97*, 5616-5620.

Campero, M., Baumann, T.K., Bostock, H., and Ochoa, J.L. (2009). Human cutaneous C fibres activated by cooling, heating and menthol. J Physiol *587*, 5633-5652.

Campero, M., Bostock, H., Baumann, T.K., and Ochoa, J.L. (2010). A search for activation of C nociceptors by sympathetic fibres in complex regional pain syndrome. Clin Neurophysiol *121*, 1072-1079.

Campero, M., Serra, J., Bostock, H., and Ochoa, J.L. (2001). Slowly conducting afferents activated by innocuous low temperature in human skin. J Physiol *535*, 855-865.

Campero, M., Serra, J., Marchettini, P., and Ochoa, J.L. (1998). Ectopic impulse generation and autoexcitation in single myelinated afferent fibres in patients with peripheral neuropathy and positive sensory symptoms. Muscle Nerve *21*, 1661-1667.

Campero, M., Serra, J., and Ochoa, J.L. (1996). C-polymodal nociceptors activated by noxious low temperature in human skin. JPhysiol *497*, 565-572.

Campos, S.A., Sanada, L.S., Sato, K.L., and Fazan, V.P. (2008). Morphometry of saphenous nerve in young rats. J Neurosci Methods *168*, 8-14.

Catterall, W.A. (2000). From ionic currents to molecular mechanisms: The structure and function of voltage-gated sodium channels. Neuron *26*, 13-25.

Cesare, P., and McNaughton, P. (1996). A novel heat-activated current in nociceptive neurons and its sensitization by bradykinin. ProcNatlAcadSciUSA *93*, 15435-15439.

Choi, J.S., Boralevi, F., Brissaud, O., Sanchez-Martin, J., te Morsche, R.H., Dib-Hajj, S.D., Drenth, J.P., and Waxman, S.G. (2011). Paroxysmal extreme pain disorder: a molecular lesion of peripheral neurons. NatRevNeurol *7*, 51-55.

Cline, M.A., Ochoa, J., and Torebjörk, H.E. (1989). Chronic hyperalgesia and skin warming caused by sensitized C nociceptors. Brain *112*, 621-647.

Costigan, M., Scholz, J., and Woolf, C.J. (2009). Neuropathic Pain: A Maladaptive Response of the Nervous System to Damage. AnnuRevNeurosci.

Cox, J.J., Reimann, F., Nicholas, A.K., Thornton, G., Roberts, E., Springell, K., Karbani, G., Jafri, H., Mannan, J., Raashid, Y*., et al.* (2006). An SCN9A channelopathy causes congenital inability to experience pain. Nature *444*, 894-898.

Cox, J.J., Sheynin, J., Shorer, Z., Reimann, F., Nicholas, A.K., Zubovic, L., Baralle, M., Wraige, E., Manor, E., Levy, J*., et al.* (2010). Congenital insensitivity to pain: novel SCN9A missense and in-frame deletion mutations. Human mutation *31*, E1670-1686.

Cummins, T.R., Aglieco, F., Renganathan, M., Herzog, R.I., Dib-Hajj, S.D., and Waxman, S.G. (2001). Nav1.3 sodium channels: rapid repriming and slow closed-state inactivation display quantitative differences after expression in a mammalian cell line and in spinal sensory neurons. JNeurosci *21*, 5952-5961.

Cummins, T.R., Dib-Hajj, S.D., Black, J.A., Akopian, A.N., Wood, J.N., and Waxman, S.G. (1999). A novel persistent tetrodotoxin-resistant sodium current in SNS-null and wild-type small primary sensory neurons. J Neurosci *19*, RC43.

Cummins, T.R., Howe, J.R., and Waxman, S.G. (1998). Slow closed-state inactivation: a novel mechanism underlying ramp currents in cells expressing the hNE/PN1 sodium channel. JNeurosci *18*, 9607-9619.

Dadi, P.K., Vierra, N.C., Days, E., Dickerson, M.T., Vinson, P.N., Weaver, C.D., and Jacobson, D.A. (2017). Selective Small Molecule Activators of TREK-2 Channels Stimulate Dorsal Root Ganglion c-fibre Nociceptor Two-Pore-Domain Potassium Channel Currents and Limit Calcium Influx. ACS Chem Neurosci *8*, 558-568.

Daugaard, G. (1990). Cisplatin nephrotoxicity: experimental and clinical studies. Dan Med Bull *37*, 1-12.

Davis, K.D., Meyer, R.A., and Campbell, J.N. (1993). Chemosensitivity and sensitization of nociceptive afferents that innervate the hairy skin of monkey. J Neurophysiol *69*, 1071-1081.

de la Pena, E., Malkia, A., Vara, H., Caires, R., Ballesta, J.J., Belmonte, C., and Viana, F. (2012). The influence of cold temperature on cellular excitability of hippocampal networks. PLoS One *7*, e52475.

Dib-Hajj, S.D., Yang, Y., Black, J.A., and Waxman, S.G. (2013). The Na(V)1.7 sodium channel: from molecule to man. Nat Rev Neurosci *14*, 49-62.

Dib-Hajj, S.D., Yang, Y., and Waxman, S.G. (2008). Genetics and molecular pathophysiology of Na(v)1.7-related pain syndromes. AdvGenet *63:85-110.*, 85-110.

Djouhri, L., Fang, X., Okuse, K., Wood, J.N., Berry, C.M., and Lawson, S.N. (2003a). The TTX-resistant sodium channel Nav1.8 (SNS/PN3): expression and correlation with membrane properties in rat nociceptive primary afferent neurons. JPhysiol *550*, 739-752.

Djouhri, L., Newton, R., Levinson, S.R., Berry, C.M., Carruthers, B., and Lawson, S.N. (2003b). Sensory and electrophysiological properties of guinea-pig sensory neurones expressing Na(v)1.7 (PN1) Na+ channel alpha subunit protein. J Physiol-London *546*, 565-576.

Doan, T.N., Stephans, K., Ramirez, A.N., Glazebrook, P.A., Andresen, M.C., and Kunze, D.L. (2004). Differential distribution and function of hyperpolarization-activated channels in sensory neurons and mechanosensitive fibres. J Neurosci *24*, 3335-3343.

Ebenezer, G.J., McArthur, J.C., Thomas, D., Murinson, B., Hauer, P., Polydefkis, M., and Griffin, J.W. (2007). Denervation of skin in neuropathies: the sequence of axonal and Schwann cell changes in skin biopsies. Brain *130*, 2703-2714.

Elliott, A.A., and Elliott, J.R. (1993). Characterization of TTX-sensitive and TTX-resistant sodium currents in small cells from adult rat dorsal root ganglia. J Physiol *463*, 39-56.

Enax-Krumova, E.K., Lenz, M., Frettloh, J., Hoffken, O., Reinersmann, A., Schwarzer, A., Westermann, A., Tegenthoff, M., and Maier, C. (2017). Changes of the Sensory Abnormalities and Cortical Excitability in Patients with Complex Regional Pain Syndrome of the Upper Extremity After 6 Months of Multimodal Treatment. Pain Med *18*, 95-106.

Erickson, A., Deiteren, A., Harrington, A.M., Garcia-Caraballo, S., Castro, J., Caldwell, A., Grundy, L., and Brierley, S.M. (2018). Voltage-gated sodium channels: (NaV)igating the field to determine their contribution to visceral nociception. J Physiol *596*, 785-807.

Esquibel, M.A., Negreiros, J., and Gawryszewski, L.G. (1980). Electrocyte physiology: I. Temperature dependence of membrane excitability. An Acad Bras Cienc *52*, 627-631.

Estacion, M., and Waxman, S.G. (2013). The response of Na(V)1.3 sodium channels to ramp stimuli: multiple components and mechanisms. JNeurophysiol *109*, 306-314.

Facer, P., Casula, M.A., Smith, G.D., Benham, C.D., Chessell, I.P., Bountra, C., Sinisi, M., Birch, R., and Anand, P. (2007). Differential expression of the capsaicin receptor TRPV1 and related novel receptors TRPV3, TRPV4 and TRPM8 in normal human tissues and changes in traumatic and diabetic neuropathy. BMC Neurol *7*, 11.

Featherstone, D.E., Richmond, J.E., and Ruben, P.C. (1996). Interaction between fast and slow inactivation in Skm1 sodium channels. Biophysical Journal *71*, 3098-3109.

Flor, H., Nikolajsen, L., and Staehelin, J.T. (2006). Phantom limb pain: a case of maladaptive CNS plasticity? NatRevNeurosci *7*, 873-881.

Gao, L.L., McMullan, S., Djouhri, L., Acosta, C., Harper, A.A., and Lawson, S.N. (2012). Expression and properties of hyperpolarization-activated current in rat dorsal root ganglion neurons with known sensory function. J Physiol *590*, 4691-4705.

Gasser, H.S., and Grundfest, H. (1939). Axon diameters in relation to the spike dimensions and the conduction velocity in mammalian A fibres. American Journal of Physiology *127*, 393-414.

Goldberg, Y.P., MacFarlane, J., MacDonald, M.L., Thompson, J., Dube, M.P., Mattice, M., Fraser, R., Young, C., Hossain, S., Pape, T.*, et al.* (2007). Loss-of-function mutations in the Nav1.7 gene underlie congenital indifference to pain in multiple human populations. ClinGenet *71*, 311-319.

Goldstein, S.A. (2017). Sodium leak through K2P potassium channels and cardiac arrhythmia, an emerging theme. EMBO Mol Med *9*, 399-402.

Gonzalez, A., Ugarte, G., Restrepo, C., Herrera, G., Pina, R., Gomez-Sanchez, J.A., Pertusa, M., Orio, P., and Madrid, R. (2017). Role of the Excitability Brake Potassium Current IKD in Cold Allodynia Induced by Chronic Peripheral Nerve Injury. J Neurosci *37*, 3109-3126.

Han, C., Yang, Y., Te Morsche, R.H., Drenth, J.P., Politei, J.M., Waxman, S.G., and Dib-Hajj, S.D. (2016). Familial gain-of-function Nav1.9 mutation in a painful channelopathy. J Neurol Neurosurg Psychiatry.

Handwerker, H.O., and Neher, K.D. (1976). Characteristics of C-fibre receptors in the cat's foot responding to stepwise increase of skin temperature ot noxious levels. Pflugers Arch *365*, 221-229.

Haring, M., Zeisel, A., Hochgerner, H., Rinwa, P., Jakobsson, J.E.T., Lonnerberg, P., La Manno, G., Sharma, N., Borgius, L., Kiehn, O.*, et al.* (2018). Neuronal atlas of the dorsal horn defines its architecture and links sensory input to transcriptional cell types. Nat Neurosci.

Haroutounian, S., Ford, A.L., Frey, K., Nikolajsen, L., Finnerup, N.B., Neiner, A., Kharasch, E.D., Karlsson, P., and Bottros, M.M. (2018). How central is central poststroke pain? The role of afferent input in poststroke neuropathic pain: a prospective, open-label pilot study. Pain *159*, 1317-1324.

Haskins, W., Benitez, S., Mercado, J.M., and Acosta, C.G. (2017). Cutaneous inflammation regulates THIK1 expression in small C-like nociceptor dorsal root ganglion neurons. Mol Cell Neurosci *83*, 13-26.

He, X.H., Zang, Y., Chen, X., Pang, R.P., Xu, J.T., Zhou, X., Wei, X.H., Li, Y.Y., Xin, W.J., Qin, Z.H.*, et al.* (2010). TNF-alpha contributes to up-regulation of Nav1.3 and Nav1.8 in DRG neurons following motor fibre injury. Pain *151*, 266-279.

Herzog, R.I., Cummins, T.R., Ghassemi, F., Dib-Hajj, S.D., and Waxman, S.G. (2003). Distinct repriming and closed-state inactivation kinetics of Nav1.6 and Nav1.7 sodium channels in mouse spinal sensory neurons. J Physiol *551*, 741-750.

Hille, B. (1992). Ionic Channels of Excitable Membranes, Second Edition.

Hockley, J.R., Boundouki, G., Cibert-Goton, V., McGuire, C., Yip, P.K., Chan, C., Tranter, M., Wood, J.N., Nassar, M.A., Blackshaw, L.A.*, et al.* (2014). Multiple roles for NaV1.9 in the activation of visceral afferents by noxious inflammatory, mechanical, and human disease-derived stimuli. Pain *155*, 1962-1975.

Hodgkin, A.L., and Huxley, A.F. (1952). A Quantitative Description of Membrane Current and Its Application to Conduction and Excitation in Nerve. J Physiol-London *117*, 500-544.

Hodgkin, A.L., and Katz, B. (1949). The effect of temperature on the electrical activity of the giant axon of the squid. J Physiol *109*, 240-249.

Hoffmann, T., Kistner, K., Carr, R.W., Nassar, M.A., Reeh, P.W., and Weidner, C. (2017). Reduced excitability and impaired nociception in peripheral unmyelinated fibres from Nav1.9-null mice. Pain *158*, 58-67.

Holditch, S.J., Brown, C.N., Lombardi, A.M., Nguyen, K.N., and Edelstein, C.L. (2019). Recent Advances in Models, Mechanisms, Biomarkers, and Interventions in Cisplatin-Induced Acute Kidney Injury. Int J Mol Sci *20*.

Huang, J., Han, C., Estacion, M., Vasylyev, D., Hoeijmakers, J.G., Gerrits, M.M., Tyrrell, L., Lauria, G., Faber, C.G., Dib-Hajj, S.D.*, et al.* (2014). Gain-of-function mutations in sodium channel Na(v)1.9 in painful neuropathy. Brain *137*, 1627-1642.

Huang, J., Vanoye, C.G., Cutts, A., Goldberg, Y.P., Dib-Hajj, S.D., Cohen, C.J., Waxman, S.G., and George, A.L., Jr. (2017). Sodium channel NaV1.9 mutations associated with insensitivity to pain dampen neuronal excitability. J Clin Invest *127*, 2805-2814.

Ilfeld, B.M., Preciado, J., and Trescot, A.M. (2016). Novel cryoneurolysis device for the treatment of sensory and motor peripheral nerves. Expert Rev Med Devices *13*, 713-725.

Israel, M.R., Tanaka, B.S., Castro, J., Thongyoo, P., Robinson, S.D., Zhao, P., Deuis, J.R., Craik, D.J., Durek, T., Brierley, S.M.*, et al.* (2019). NaV 1.6 regulates excitability of mechanosensitive sensory neurons. J Physiol *597*, 3751-3768.

January, C.T., and Fozzard, H.A. (1984). The effects of membrane potential, extracellular potassium, and tetrodotoxin on the intracellular sodium ion activity of sheep cardiac muscle. Circ Res *54*, 652-665.

Jonas, R., Namer, B., Stockinger, L., Chisholm, K., Schnakenberg, M., Landmann, G., Kucharczyk, M., Konrad, C., Schmidt, R., Carr, R.*, et al.* (2018a). Tuning in C-nociceptors to reveal mechanisms in chronic neuropathic pain. Ann Neurol *83*, 945-957.

Jonas, R., Namer, B., Stockinger, L., Chisholm, K., Schnakenberg, M., Landmann, G., Kucharczyk, M., Konrad, C., Schmidt, R., Carr, R.*, et al.* (2018b). Tuning in C-nociceptors to reveal mechanisms in chronic neuropathic pain. Ann Neurol *83*, 945-957.

Jorum, E., Orstavik, K., Schmidt, R., Namer, B., Carr, R.W., Kvarstein, G., Hilliges, M., Handwerker, H., Torebjork, E., and Schmelz, M. (2007). Catecholamine-induced excitation of nociceptors in sympathetically maintained pain. Pain *127*, 296-301.

Jurcakova, D., Ru, F., Kollarik, M., Sun, H., Krajewski, J., and Undem, B.J. (2018). Voltage-Gated Sodium Channels Regulating Action Potential Generation in Itch-, Nociceptive-, and Low-Threshold Mechanosensitive Cutaneous C-fibres. Mol Pharmacol *94*, 1047-1056.

Kabata, R., Okuda, H., Noguchi, A., Kondo, D., Fujiwara, M., Hata, K., Kato, Y., Ishikawa, K., Tanaka, M., Sekine, Y.*, et al.* (2018). Familial episodic limb pain in kindreds with novel Nav1.9 mutations. PLoS One *13*, e0208516.

Kanda, H., and Gu, J.G. (2017). Effects of cold temperatures on the excitability of rat trigeminal ganglion neurons that are not for cold sensing. J Neurochem *141*, 532-543.

Kandel, E.R., Schwartz, J.H., Jessell, T.M., Siegelbaum, S.A., and Hudspeth, A.J. (2013). Principles of neural science, fifth edition.

Kang, D., and Kim, D. (2006). TREK-2 (K2P10.1) and TRESK (K2P18.1) are major background K+ channels in dorsal root ganglion neurons. Am J Physiol Cell Physiol *291*, C138-146.

Kellenberger, S., West, J.W., Scheuer, T., and Catterall, W.A. (1997). Molecular analysis of the putative inactivation particle in the inactivation gate of brain type IIA Na+ channels. Journal of General Physiology *109*, 589-605.

Kenins, P. (1982). Responses of single nerve fibres to capsaicin applied to the skin. NeurosciLett *29*, 83-88.

Kessler, W., Kirchhoff, C., Reeh, P.W., and Handwerker, H.O. (1992). Excitation of cutaneous afferent nerve endings in vitro by a combination of inflammatory mediators and conditioning effect of substance P. ExpBrain Res *91*, 467-476.

Kichko, T.I., Kobal, G., and Reeh, P.W. (2015). Cigarette smoke has sensory effects through nicotinic and TRPA1 but not TRPV1 receptors on the isolated mouse trachea and larynx. Am J Physiol Lung Cell Mol Physiol *309*, L812-820.

Kiernan, M.C., Cikurel, K., and Bostock, H. (2001). Effects of temperature on the excitability properties of human motor axons. Brain *124*, 816-825.

Kiernan, M.C., Mogyoros, I., Hales, J.P., Gracies, J.M., and Burke, D. (1997). Excitability changes in human cutaneous afferents induced by prolonged repetitive axonal activity. JPhysiol(Lond) *500*, 255-264.

Kleggetveit, I.P., Namer, B., Schmidt, R., Helas, T., Ruckel, M., Orstavik, K., Schmelz, M., and Jorum, E. (2012). High spontaneous activity of C-nociceptors in painful polyneuropathy. Pain *153*, 2040-2047.

Kleggetveit, I.P., Schmidt, R., Namer, B., Salter, H., Helas, T., Schmelz, M., and Jorum, E. (2016). Pathological nociceptors in two patients with erythromelalgia-like symptoms and rare genetic Nav 1.9 variants. Brain Behav *6*, e00528.

Klein, A.H., Vyshnevska, A., Hartke, T.V., De Col, R., Mankowski, J.L., Turnquist, B., Bosmans, F., Reeh, P.W., Schmelz, M., Carr, R.W.*, et al.* (2017). Sodium Channel Nav1.8 Underlies TTX-Resistant Axonal Action Potential Conduction in Somatosensory C-fibres of Distal Cutaneous Nerves. J Neurosci *37*, 5204-5214.

Koltzenburg, M. (2000). Neural mechanisms of cutaneous nociceptive pain. Clin J Pain *16*, S131-S138.

Korogod, S.M., and Demianenko, L.E. (2017). Temperature effects on non-TRP ion channels and neuronal excitability. Opera Mecica et Physiologica *3*, 84-92.

LaMotte, R.H. (1984). Can the sensitization of nociceptors account for hyperalgesia after skin injury? HumNeurobiol *3*, 47-52.

LaMotte, R.H., and Thalhammer, J.G. (1982). Response properties of high-threshold cutaneous cold receptors in the primate. Brain Res *244*, 279-287.

Lampert, A., Hains, B.C., and Waxman, S.G. (2006). Upregulation of persistent and ramp sodium current in dorsal horn neurons after spinal cord injury. ExpBrain Res*.*

Lang, E., Novak, A., Reeh, P.W., and Handwerker, H.O. (1990). Chemosensitivity of fine afferents from rat skin in vitro. JNeurophysiol *63*, 887-901.

Leipold, E., Liebmann, L., Korenke, G.C., Heinrich, T., Giesselmann, S., Baets, J., Ebbinghaus, M., Goral, R.O., Stodberg, T., Hennings, J.C.*, et al.* (2013). A de novo gain-of-function mutation in SCN11A causes loss of pain perception. Nat Genet *45*, 1399-1404.

Li, C., Wang, S., Chen, Y., and Zhang, X. (2018). Somatosensory Neuron Typing with High-Coverage Single-Cell RNA Sequencing and Functional Analysis. Neurosci Bull *34*, 200-207.

Li, C.L., Li, K.C., Wu, D., Chen, Y., Luo, H., Zhao, J.R., Wang, S.S., Sun, M.M., Lu, Y.J., Zhong, Y.Q.*, et al.* (2016). Somatosensory neuron types identified by high-coverage single-cell RNA-sequencing and functional heterogeneity. Cell Res *26*, 967.

Li, X.Y., and Toyoda, H. (2015). Role of leak potassium channels in pain signaling. Brain Res Bull *119*, 73-79.

Ma, L., Zhang, X., and Chen, H. (2011). TWIK-1 two-pore domain potassium channels change ion selectivity and conduct inward leak sodium currents in hypokalemia. Sci Signal *4*, ra37.

Mackel, R., Brink, E., Jorum, E., and Aisen, M. (1994). Properties of cutaneous afferents during recovery from Guillain- Barre syndrome. Brain *117*, 169-183.

Madrid, R., Donovan-Rodriguez, T., Meseguer, V., Acosta, M.C., Belmonte, C., and Viana, F. (2006). Contribution of TRPM8 channels to cold transduction in primary sensory neurons and peripheral nerve terminals. Journal of Neuroscience *26*, 12512-12525.

Makhija, S., Sabbatini, P., Aghajanian, C., Venkatraman, E., Spriggs, D.R., and Barakat, R. (2000). Intraperitoneal cisplatin and intravenous paclitaxel in the treatment of epithelial ovarian cancer patients with a positive second look. GynecolOncol *79*, 28-32.

Mantyh, P.W. (2018). Mechanisms that drive bone pain across the lifespan. Br J Clin Pharmacol.

Mao, Q., Yuan, J., Ming, X., Wu, S., Chen, L., Bekker, A., Yang, T., and Tao, Y.X. (2017). Role of dorsal root ganglion K2p1.1 in peripheral nerve injury-induced neuropathic pain. Mol Pain *13*, 1744806917701135.

Martin, H.A., Basbaum, A.I., Goetzl, E.J., and Levine, J.D. (1988). Leukotriene B4 decreases the mechanical and thermal thresholds of C-fibre nociceptors in the hairy skin of the rat. JNeurophysiol *60*, 438-445.

Martin, H.A., Basbaum, A.I., Kwiat, G.C., Goetzl, E.J., and Levine, J.D. (1987). Leukotriene and prostaglandin sensitization of cutaneous high-threshold C- and A-delta mechanonociceptors in the hairy skin of rat hindlimbs. Neuroscience *22*, 651-659.

Mathie, A., and Veale, E.L. (2015). Two-pore domain potassium channels: potential therapeutic targets for the treatment of pain. Pflugers Arch *467*, 931-943.

McKemy, D.D., Neuhausser, W.M., and Julius, D. (2002). Identification of a cold receptor reveals a general role for TRP channels in thermosensation. Nature *416*, 52-58.

Meacham, K., Shepherd, A., Mohapatra, D.P., and Haroutounian, S. (2017). Neuropathic Pain: Central vs. Peripheral Mechanisms. Curr Pain Headache Rep *21*, 28.

Merrill, D.R., Bikson, M., and Jefferys, J.G. (2005). Electrical stimulation of excitable tissue: design of efficacious and safe protocols. J Neurosci Methods *141*, 171-198.

Meyer, R.A. (1995). Cutaneous hyperalgesia and primary afferent sensitization. PulmPharmacol *8*, 187-193.

Meyer, R.A., Davis, K.D., Cohen, R.H., Treede, R.D., and Campbell, J.N. (1991). Mechanically insensitive afferents (MIAs) in cutaneous nerves of monkey. Brain Res *561*, 252-261.

Millan, M.J. (1999). The induction of pain: an integrative review. ProgNeurobiol *57*, 1-164.

Miyake, T., Nakamura, S., Zhao, M., So, K., Inoue, K., Numata, T., Takahashi, N., Shirakawa, H., Mori, Y., Nakagawa, T*., et al.* (2016). Cold sensitivity of TRPA1 is unveiled by the prolyl hydroxylation blockade-induced sensitization to ROS. Nature communications *7*, 12840.

Moalem-Taylor, G., Lang, P.M., Tracey, D.J., and Grafe, P. (2007). Post-spike excitability indicates changes in membrane potential of isolated C-fibres. Muscle Nerve *36*, 172-182.

Mogil, J.S. (2009). Animal models of pain: progress and challenges. NatRevNeurosci *10*, 283-294.

Mogil, J.S. (2012). The etiology and symptomatology of spontaneous pain. JPain *13*, 932-933.

Moparthi, L., Kichko, T.I., Eberhardt, M., Hogestatt, E.D., Kjellbom, P., Johanson, U., Reeh, P.W., Leffler, A., Filipovic, M.R., and Zygmunt, P.M. (2016). Human TRPA1 is a heat sensor displaying intrinsic U-shaped thermosensitivity. Sci Rep *6*, 28763.

Murinson, B.B., and Griffin, J.W. (2004). C-fibre structure varies with location in peripheral nerve. J Neuropathol Exp Neurol *63*, 246-254.

Nagi, S.S., Marshall, A.G., Makdani, A., Jarocka, E., Liljencrantz, J., Ridderstrom, M., Shaikh, S., O'Neill, F., Saade, D., Donkervoort, S*., et al.* (2019). An ultrafast system for signaling mechanical pain in human skin. Sci Adv *5*, eaaw1297.

Nakamura, Y., Ohya, Y., Abe, I., and Fujishima, M. (1999). Sodium-potassium pump current in smooth muscle cells from mesenteric resistance arteries of the guinea-pig. J Physiol *519 Pt 1*, 203-212.

Nordin, M., Nystrom, B., Wallin, U., and Hagbarth, K.E. (1984). Ectopic sensory discharges and paresthesiae in patients with disorders of peripheral nerves, dorsal roots and dorsal columns. Pain *20*, 231-245.

Nystrom, B., and Hagbarth, K.E. (1981). Microelectrode recordings from transected nerves in amputees with phantom limb pain. NeurosciLett *27*, 211-216.

Obreja, O. (2013). Erregbarkeitsänderungen von Nozizeptoren - sensorische und axonale Mechanismen. In Inst für Anästhesiologie und Operative Intensivmedizin (Mannheim: Heidelberg), pp. 118.

Ochoa, J.L., Campero, M., Serra, J., and Bostock, H. (2005). Hyperexcitable polymodal and insensitive nociceptors in painful human neuropathy. Muscle Nerve *32*, 459-472.

Orstavik, K., Norheim, I., and Jorum, E. (2006). Pain and small-fibre neuropathy in patients with hypothyroidism. Neurology *67*, 786-791.

Orstavik, K., Weidner, C., Schmidt, R., Schmelz, M., Hilliges, M., Jorum, E., Handwerker, H., and Torebjork, E. (2003). Pathological C-fibres in patients with a chronic painful condition. Brain *126*, 567-578.

Osteen, J.D., Herzig, V., Gilchrist, J., Emrick, J.J., Zhang, C., Wang, X., Castro, J., Garcia-Caraballo, S., Grundy, L., Rychkov, G.Y.*, et al.* (2016). Selective spider toxins reveal a role for the Nav1.1 channel in mechanical pain. Nature *534*, 494-499.

Pace, M.C., Passavanti, M.B., De Nardis, L., Bosco, F., Sansone, P., Pota, V., Barbarisi, M., Palagiano, A., Iannotti, F.A., Panza, E.*, et al.* (2018). Nociceptor plasticity: A closer look. J Cell Physiol *233*, 2824-2838.

Park, S.B., and Baker, M.D. (2017). Too fast: rare neuropathic pain state associated with easy activation of NaV1.9. J Neurol Neurosurg Psychiatry *88*, 194.

Patton, D.E., West, J.W., Catterall, W.A., and Goldin, A.L. (1992). Amino acid residues required for fast Na(+)-channel inactivation: charge neutralizations and deletions in the III-IV linker. Proc Natl Acad Sci U S A *89*, 10905-10909.

Peier, A.M., Moqrich, A., Hergarden, A.C., Reeve, A.J., Andersson, D.A., Story, G.M., Earley, T.J., Dragoni, I., McIntyre, P., Bevan, S.*, et al.* (2002). A TRP channel that senses cold stimuli and menthol. Cell *108*, 705-715.

Peltier, A.C., and Russell, J.W. (2002). Recent advances in drug-induced neuropathies. CurrOpinNeurol *15*, 633-638.

Perl, E.R. (1996). Cutaneous polymodal receptors: characteristics and plasticity. ProgBrain Res *113*, 21-37.

Perl, E.R., Kumazawa, T., Lynn, B., and Kenins, P. (1976). Sensitization of high threshold receptors with unmyelinated (C) afferent fibres. ProgBrain Res *43*, 263-277.

Pivovarov, A.S., Calahorro, F., and Walker, R.J. (2018). Na(+)/K(+)-pump and neurotransmitter membrane receptors. Invert Neurosci *19*, 1.

Plant, L.D. (2012). A Role for K2P Channels in the Operation of Somatosensory Nociceptors. Front Mol Neurosci *5*, 21.

Prato, V., Taberner, F.J., Hockley, J.R.F., Callejo, G., Arcourt, A., Tazir, B., Hammer, L., Schad, P., Heppenstall, P.A., Smith, E.S.*, et al.* (2017). Functional and Molecular Characterization of Mechanoinsensitive "Silent" Nociceptors. Cell Rep *21*, 3102-3115.

Price, T.J., and Inyang, K.E. (2015). Commonalities between pain and memory mechanisms and their meaning for understanding chronic pain. Prog Mol Biol Transl Sci *131*, 409-434.

Quasthoff, S., and Hartung, H.P. (2002). Chemotherapy-induced peripheral neuropathy. J Neurol *249*, 9-17.

Reeh, P.W. (1988). Sensory receptors in a mammalian skin-nerve in vitro preparation. ProgBrain Res *74:271-6.*, 271-276.

Reichling, D.B., and Levine, J.D. (2009). Critical role of nociceptor plasticity in chronic pain. Trends Neurosci *32*, 611-618.

Renganathan, M., Cummins, T.R., and Waxman, S.G. (2001). Contribution of Na(v)1.8 sodium channels to action potential electrogenesis in DRG neurons. J Neurophysiol *86*, 629-640.

Renganathan, M., Dib-Hajj, S., and Waxman, S.G. (2002). Na-v 1.5 underlies the 'third TTX-R sodium current' in rat small DRG neurons. Mol Brain Res *106*, 70-82.

Riddell, I.A. (2018). Cisplatin and Oxaliplatin: Our Current Understanding of Their Actions. Met Ions Life Sci *18*.

Rigaud, M., Gemes, G., Barabas, M.E., Chernoff, D.I., Abram, S.E., Stucky, C.L., and Hogan, Q.H. (2008). Species and strain differences in rodent sciatic nerve anatomy: implications for studies of neuropathic pain. Pain *136*, 188-201.

Ringkamp, M., Peng, Y.B., Wu, G., Hartke, T.V., Campbell, J.N., and Meyer, R.A. (2001). Capsaicin responses in heat-sensitive and heat-insensitive A-fibre nociceptors. J Neurosci *21*, 4460-4468.

Ringkamp, M., Schepers, R.J., Shimada, S.G., Johanek, L.M., Hartke, T.V., Borzan, J., Shim, B., LaMotte, R.H., and Meyer, R.A. (2011). A role for nociceptive, myelinated nerve fibres in itch sensation. J NEUROSCI *31*, 14841-14849.

Ritchie, J.M., and Straub, R.W. (1956). The effect of cooling on the size of the action potential of mammalian non-medullated fibres. J Physiol *134*, 712-717.

Rukwied, B., Weinkauf, B., Main, M., Obreja, O., and Schmelz, M. (2014). Axonal hyper-excitability after combined NGF sensitization and UV-B inflammation in humans. European journal of pain *18*, 785-793.

Rukwied, R., Weinkauf, B., Main, M., Obreja, O., and Schmelz, M. (2013). Inflammation meets sensitization--an explanation for spontaneous nociceptor activity? Pain *154*, 2707-2714.

Salvatierra, J., Diaz-Bustamante, M., Meixiong, J., Tierney, E., Dong, X.Z., and Bosmans, F. (2018). A disease mutation reveals a role for Na(V)1.9 in acute itch. J Clin Invest *128*, 5434-5447.

Sarria, I., Ling, J., and Gu, J.G. (2012). Thermal sensitivity of voltage-gated Na+ channels and A-type K+ channels contributes to somatosensory neuron excitability at cooling temperatures. J Neurochem *122*, 1145-1154.

Scadding, J.W., and Koltzenburg, M. (2006). Painful peripheral neuropathies. In Walls and Melzack´s Textbook of pain, S.B. McMahon, and M. Koltzenburg, eds. (Philadelphia: Elsevier Limited), pp. 973-999.

Schaefer, I., Prato, V., Arcourt, A., Taberner, F.J., and Lechner, S.G. (2018). Differential modulation of voltage-gated sodium channels by nerve growth factor in three major subsets of TrkA-expressing nociceptors. Mol Pain *14*, 1744806918814640.

Schick, C.H., Fronek, K., Held, A., Birklein, F., Hohenberger, W., and Schmelz, M. (2003). Differential effects of surgical sympathetic block on sudomotor and vasoconstrictor function. Neurology *60*, 1770-1776.

Schmelz, M., Schmidt, R., Handwerker, H.O., and Torebjörk, H.E. (2000). Encoding of burning pain from capsaicin-treated human skin in two categories of unmyelinated nerve fibres. Brain *123*, 560-571.

Schmelz, M., Schmidt, R., Ringkamp, M., Forster, C., Handwerker, H.O., and Torebjörk, H.E. (1996). Limitation of sensitization to injured parts of receptive fields in human skin C-nociceptors. ExpBrain Res *109*, 141-147.

Schmidt, R., Schmelz, M., Forster, C., Ringkamp, M., Torebjörk, H.E., and Handwerker, H.O. (1995). Novel classes of responsive and unresponsive C nociceptors in human skin. JNeurosci *15*, 333-341.

Serra, J. (2010). Sensory profiles: the cliche and the challenge. Pain *150*, 384-385.

Serra, J., Campero, M., Bostock, H., and Ochoa, J. (2004). Two types of C nociceptors in human skin and their behavior in areas of capsaicin-induced secondary hyperalgesia. J Neurophysiol *91*, 2770-2781.

Serra, J., Campero, M., Ochoa, J., and Bostock, H. (1999). Activity-dependent slowing of conduction differentiates functional subtypes of C fibres innervating human skin. J Physiol *515 (Pt 3)*, 799-811.

Serra, J., Sola, R., Quiles, C., Casanova-Molla, J., Pascual, V., Bostock, H., and Valls-Sole, J. (2009). C-nociceptors sensitized to cold in a patient with small-fibre neuropathy and cold allodynia. Pain *147*, 46-53.

Shen, H.Z., Liu, D.L., Wu, K., Lei, J.L., and Yan, N. (2019). Structures of human Na(v)1.7 channel in complex with auxiliary subunits and animal toxins. Science *363*, 1303-+.

Sherrington, C.S. (1906). The integrative action of the nervous system (New York).

Shields, S.D., Ahn, H.S., Yang, Y., Han, C., Seal, R.P., Wood, J.N., Waxman, S.G., and Dib-Hajj, S.D. (2012). Nav1.8 expression is not restricted to nociceptors in mouse peripheral nervous system. Pain *153*, 2017-2030.

Shim, B., Kim, D.W., Kim, B.H., Nam, T.S., Leem, J.W., and Chung, J.M. (2005). Mechanical and heat sensitization of cutaneous nociceptors in rats with experimental peripheral neuropathy. Neuroscience *132*, 193-201.

Steen, K.H., Issberner, U., and Reeh, P.W. (1995a). Pain Due to Experimental Acidosis in Human Skin Evidence for Non Adapting Nociceptor Excitation. NeurosciLett *199*, 29-32.

Steen, K.H., and Reeh, P.W. (1993). Sustained graded pain and hyperalgesia from harmless experimental tissue acidosis in human skin. Neurosci Lett *154*, 113-116.

Steen, K.H., Steen, A.E., and Reeh, P.W. (1995b). A dominant role of acid pH in inflammatory excitation and sensitization of nociceptors in rat skin, in vitro. J Neurosci *15*, 3982-3989.

Stein, J.H., and Fried, T.A. (1985). Experimental models of nephrotoxic acute renal failure. Transplant Proc *17*, 72-80.

Szolcsanyi, J. (1977). A pharmacological approach to elucidation of the role of different nerve fibres and receptor endings in mediation of pain. J Physiol (Paris) *73*, 251-259.

Tan, Z.Y., Piekarz, A.D., Priest, B.T., Knopp, K.L., Krajewski, J.L., McDermott, J.S., Nisenbaum, E.S., and Cummins, T.R. (2014). Tetrodotoxin-resistant sodium channels in sensory neurons generate slow resurgent currents that are enhanced by inflammatory mediators. J Neurosci *34*, 7190-7197.

Ten Bos, L.M., Veenstra, T.C., Westerhof, B.D., and Bosch, F.H. (2016). A case of extreme hypokalaemia. Neth J Med *74*, 406-409.

Tigerholm, J., Petersson, M.E., Obreja, O., Eberhardt, E., Namer, B., Weidner, C., Lampert, A., Carr, R.W., Schmelz, M., and Fransen, E. (2015). C-fibre recovery cycle supernormality depends on ion concentration and ion channel permeability. Biophys J *108*, 1057-1071.

Tikhonov, D.B., and Zhorov, B.S. (2007). Sodium channels: ionic model of slow inactivation and state-dependent drug binding. Biophys J *93*, 1557-1570.

Treede, R.D., Meyer, R.A., and Campbell, J.N. (1998). Myelinated mechanically insensitive afferents from monkey hairy skin: heat-response properties. J Neurophysiol *80*, 1082-1093.

Treede, R.D., Meyer, R.A., Raja, S.N., and Campbell, J.N. (1995). Evidence for two different heat transduction mechanisms in nociceptive primary afferents innervating monkey skin. J Physiol *483 (Pt 3)*, 747-758.

Ulbricht, W. (2005). Sodium channel inactivation: Molecular determinants and modulation. Physiological Reviews *85*, 1271-1301.

Usoskin, D., Furlan, A., Islam, S., Abdo, H., Lonnerberg, P., Lou, D., Hjerling-Leffler, J., Haeggstrom, J., Kharchenko, O., Kharchenko, P.V.*, et al.* (2015). Unbiased classification of sensory neuron types by large-scale single-cell RNA sequencing. Nat Neurosci *18*, 145-153.

Vassilev, P.M., Scheuer, T., and Catterall, W.A. (1988). Identification of an intracellular peptide segment involved in sodium channel inactivation. Science *241*, 1658-1661.

Vedantham, V., and Cannon, S.C. (1998). Slow inactivation does not affect movement of the fast inactivation gate in voltage-gated Na+ channels. J Gen Physiol.

Viana, F. (2016). TRPA1 channels: molecular sentinels of cellular stress and tissue damage. J Physiol *594*, 4151-4169.

Wallace, V.C., Segerdahl, A.R., Lambert, D.M., Vandevoorde, S., Blackbeard, J., Pheby, T., Hasnie, F., and Rice, A.S. (2007). The effect of the palmitoylethanolamide analogue, palmitoylallylamide (L-29) on pain behaviour in rodent models of neuropathy. Br J Pharmacol *151*, 1117-1128.

Wang, F., Belanger, E., Cote, S.L., Desrosiers, P., Prescott, S.A., Cote, D.C., and De Koninck, Y. (2018). Sensory Afferents Use Different Coding Strategies for Heat and Cold. Cell Rep *23*, 2001-2013.

Wang, S., Davis, B.M., Zwick, M., Waxman, S.G., and Albers, K.M. (2006). Reduced thermal sensitivity and Nav1.8 and TRPV1 channel expression in sensory neurons of aged mice. Neurobiol Aging *27*, 895-903.

Waxman, S.G., and Dib-Hajj, S. (2005). Erythermalgia: molecular basis for an inherited pain syndrome. Trends MolMed *11*, 555-562.

Waxman, S.G., Kocsis, J.D., and Black, J.A. (1994). Type III sodium channel mRNA is expressed in embryonic but not adult spinal sensory neurons, and is reexpressed following axotomy. Journal of Neurophysiology *72*.

Wei, E.T., and Seid, D.A. (1983). AG-3-5: a chemical producing sensations of cold. J Pharm Pharmacol *35*, 110-112.

Weidner, C., Schmelz, M., Schmidt, R., Hansson, B., Handwerker, H.O., and Torebjork, H.E. (1999). Functional attributes discriminating mechano-insensitive and mechano-responsive C nociceptors in human skin. J Neurosci *19*, 10184-10190.

West, J.W., Patton, D.E., Scheuer, T., Wang, Y., Goldin, A.L., and Catterall, W.A. (1992). A cluster of hydrophobic amino acid residues required for fast Na(+)-channel inactivation. Proc Natl Acad Sci U S A *89*, 10910-10914.

Wilson, M.J., Yoshikami, D., Azam, L., Gajewiak, J., Olivera, B.M., Bulaj, G., and Zhang, M.-M. (2011). μ-Conotoxins that differentially block sodium channels NaV1.1 through 1.8 identify those responsible for action potentials in sciatic nerve. PNAS *108*, 10302-10307.

Woolf, C.J., and Ma, Q.F. (2007). Nociceptors-noxious stimulus detectors. Neuron *55*, 353-364.

Wooten, M., Weng, H.J., Hartke, T.V., Borzan, J., Klein, A.H., Turnquist, B., Dong, X., Meyer, R.A., and Ringkamp, M. (2014). Three functionally distinct classes of C-fibre nociceptors in primates. Nature communications *5*, 4122.

Xiao, Y., Barbosa, C., Pei, Z., Xie, W., Strong, J.A., Zhang, J.M., and Cummins, T.R. (2019). Increased Resurgent Sodium Currents in Nav1.8 Contribute to Nociceptive Sensory Neuron Hyper-excitability Associated with Peripheral Neuropathies. J Neurosci *39*, 1539-1550.

Yan, Z., Zhou, Q., Wang, L., Wu, J., Zhao, Y., Huang, G., Peng, W., Shen, H., Lei, J., and Yan, N. (2017). Structure of the Nav1.4-beta1 Complex from Electric Eel. Cell *170*, 470-482 e411.

Yang, Y., Wang, Y., Li, S., Xu, Z., Li, H., Ma, L., Fan, J., Bu, D., Liu, B., Fan, Z.*, et al.* (2004). Mutations in SCN9A, encoding a sodium channel alpha subunit, in patients with primary erythermalgia. JMedGenet *41*, 171-174.

Yarnitsky, D., and Ochoa, J.L. (1991). Warm and cold specific somatosensory systems. Psychophysical thresholds, reaction times and peripheral conduction velocities. Brain *114 (Pt 4)*, 1819-1826.

Zakharian, E., Cao, C., and Rohacs, T. (2010). Gating of transient receptor potential melastatin 8 (TRPM8) channels activated by cold and chemical agonists in planar lipid bilayers. J Neurosci *30*, 12526-12534.

Zeisel, A., Hochgerner, H., Lonnerberg, P., Johnsson, A., Memic, F., van der Zwan, J., Haring, M., Braun, E., Borm, L.E., La Manno, G.*, et al.* (2018). Molecular Architecture of the Mouse Nervous System. Cell *174*, 999-1014 e1022.

Zhang, F., Wang, Y., Liu, Y., Han, H., Zhang, D., Fan, X., Du, X., Gamper, N., and Zhang, H. (2019). Transcriptional Regulation of Voltage-Gated Sodium Channels Contributes to GM-CSF-Induced Pain. J Neurosci *39*, 5222-5233.

Zhou, X., Xiao, Z., Xu, Y., Zhang, Y., Tang, D., Wu, X., Tang, C., Chen, M., Shi, X., Chen, P.*, et al.* (2017). Electrophysiological and Pharmacological Analyses of Nav1.9 Voltage-Gated Sodium Channel by Establishing a Heterologous Expression System. Front Pharmacol *8*, 852.

Zhu, W., and Oxford, G.S. (2011). Differential gene expression of neonatal and adult DRG neurons correlates with the differential sensitization of TRPV1 responses to nerve growth factor. Neurosci Lett *500*, 192-196.

Zimmermann, K., Leffler, A., Babes, A., Cendan, C.M., Carr, R.W., Kobayashi, J., Nau, C., Wood, J.N., and Reeh, P.W. (2007). Sensory neuron sodium channel Nav1.8 is essential for pain at low temperatures. Nature *447*, 855-858.

7   <u>CURRICULUM VITAE AND PUBLICATIONS</u>

PERSONAL INFORMATION

JULIUS PAKALNIŠKIS

Sex: Male
Data of birth: 15/02/1990
Nationality: Lithuanian

EDUCATION

- 04 2016 – 2019   **PHD IN NEUROPHYSIOLOGY**
  Ruprecht-Karls-University of Heidelberg, Germany

"**Modulation of neuronal excitability in *ex vivo* and *in vitro* systems**"

- 09 2013 – 06 2015 **MASTER OF BIOPHYSICS**
  Vilnius University, Lithuania

"**Subjective Colours Perception Influenced by Temporal Modulation in Retina**"

- 09 2010 – 06 2012 **INTERNSHIP**
  Institute of Oncology, Vilnius University, Lithuania

Research focus: **Investigation of quantum dots' photostability**

- 09 2009 – 06 2013 **BACHELOR OF BIOPHYSICS**
  Vilnius University, Lithuania

"**Adaptation of methods for intracellular recordings from snail neurons**"

8   <u>ACKNOWLEDGEMENTS</u>